Alma Mater Studiorum · Università di Bologna

SCUOLA DI SCIENZE
Corso di Laurea Magistrale in Fisica del Sistema Terra

MECHANICAL SIMULATION OF SHALLOW DIKE PROPAGATION IN VOLCANIC EDIFICES

Relatrice:
Prof.ssa
ELEONORA RIVALTA

Correlatore:
Dott.
LORENZO MANTILONI

Presentata da:
GRETA BELLAGAMBA

Sessione straordinaria, maggio 2023

Anno Accademico: 2021/2022

Contents

Abstract (Eng)

Volcanic eruptions are complex events that can have significant impacts on human populations and infrastructure. In this thesis, I investigate stresses induced by gravity in volcanic edifices. In particular, I study the orientation of principal stress axes, as these control the direction of magma propagation by diking. I construct simple axisymmetric volcano topographies inspired by volcanoes in nature and then I test widely used assumptions on the state of stress, to discuss which of these assumptions might be more appropriate for volcano edifices. I also use a simple, recently developed, dike propagation model (Simplified Analytical model, or SAM) to predict dike trajectories in a progressively more realistic edifice stress field. The results of this study provide new insights into the factors that influence dike propagation and vent opening, highlighting the importance of considering the topographic loading and other stress-modifying processes in the modelling of volcanic eruptions. The study also demonstrates the potential of the SAM model for investigating dike propagation behaviour in volcanic areas.

Abstract (Ita)

Le eruzioni vulcaniche sono eventi complessi che possono avere un impatto significativo sulla popolazione e sulle infrastrutture. In questa tesi analizzo gli sforzi elastici generati dalla gravità negli edifici vulcanici. In particolare, studio l'orientamento degli assi principali di sforzo, i quali controllano la direzione di propagazione dei dicchi. Costruendo semplici topografie di vulcani assisimmetrici ispirati ai vulcani in natura, metto alla prova le principali ipotesi utilizzate nella modellaizone dello stato di sforzo, per discutere quale, tra esse, potrebbe essere più appropriata per rappresentare lo stato di sforzo di edifici vulcanici. Utilizzo inoltre un semplice modello di propagazione di dicchi (Simplified Analytical model, o SAM), sviluppato recentemente, per simulare le traiettorie dei dicchi in un campo di sforzo dell'edificio via via più realistico. I risultati di questo studio forniscono nuove conoscenze sui fattori che influenzano la propagazione dei dicchi e l'apertura dei vent, evidenziando l'importanza di considerare il carico topografico e altri processi che modificano lo sforzo nella modellazione delle eruzioni vulcaniche. Lo studio dimostra inoltre il potenziale del modello SAM per studiare il comportamento della propagazione dei dicchi nelle aree vulcaniche.

Introduction

Volcanic eruptions are complex processes involving the opening of an eruptive vent and the effusive or explosive ejection of magma along with gas and rock fragments. Some eruptions occur from already established vents; others, perhaps counterintuitively, occur from newly opened vents at the summit, on the flanks of the volcano or even far from the volcanic edifice. Examples are the 2018 eruption at Kilauea (Hawaii), the 2014-2015 eruption at Bardarbunga (Iceland) and the 1669 historical eruption at Etna. In all these cases the eruptive vent opened at tens of km distance from the volcano summit. These complex scenarios illustrates why a better understanding of magma transport in the volcano edifice is necessary. In particular, we need to study the mechanisms controlling the location where magma will breach the Earth's surface to erupt, in order to develop effective long-term land planning and emergency response.

In the elastic brittle crust, magma is transported by diking, which is a mechanism similar to hydraulic fracturing: dikes are sheet-like magma intrusions which break the rock ahead of their tip to propagate. We know from both field and theoretical studies that the trajectories of propagating dikes are rarely perfectly vertical: they can tilt when crossing interfaces between rock layers with different densities, be attracted towards topographic loading, or change their direction when encountering faults or other intrusions in their path. This happens because the orientation of dikes is controlled by the principal axes of the stress field: In particular, dikes will tend to orient perpendicularly to the axis of minimum compressive stress (σ_3 in the convention of this thesis). Numerous studies have addressed the stress field at volcanoes. This has helped establishing that the dominant influence comes from topographic loads and regional stresses, and in minor amount by the pressurization of a magma reservoir. However, the state of stress of volcanoes is not static, and is continuously modified by a range of processes, such as the injection of new intrusions, which tend to homogenize the underground stress; by new eruptions, which impose new stress on the preexisting layers; by flank slides or collapses. The complexity and diversity of these processes makes it a challenge to quantify their influence on the stress state of a volcanic area.

In this thesis, I lay the groundwork to clarify the role of topographic loading, together with other causes of stress changing, in influencing dike propagation and new vent opening. I calculate the stress according to different assumptions proposed by pre-

vious studies and test the outcome in terms of dike propagation trajectories through a recently published dike propagation simulator, the Simplified Analytical Model for dike propagation (Mantiloni, Eleonora Rivalta, and Davis, 2023). In Chapter 1, I introduce some observations of dike propagation in volcanic edifices; this will clarify the motivation and ultimate goals of the study, as well as the main sources of constraints for my models.

In Chapter 2, I analyze the main factors that modify underground stress, and illustrate the state of the art in terms of modelling techniques, with particular focus on the techniques that I will use in the following chapters.

In Chapter 3, I present my modelling results in terms of volcanic topography approximation and underground stress computing, and show the results obtained with the SAM model for the propagation of dikes.

In Chapter 4, I discuss the results obtained, analyzing the potential and limitations of my work.

In Chapter 5, I present a conclusion to my work, expanding to future research directions.

Chapter 1

Dikes, volcanoes, vent opening: an overview

1.1 Magma transport through diking

Dikes are sheet-like, low-viscosity magma intrusions, which force their way into the crust by fracturing the rock they propagate into. They generally have a thickness of around 1-10 m and a lateral extent of about 1-100 km, and are acknowledged as the principal mean of magma transport in the elastic brittle crust, and possibly in the lithosphere. Dikes propagate with a velocity in the order of meters per second, which allows them to cover large distances without significant solidification due to cooling (Gonnermann and Taisne, 2015). They are modelled in different ways depending on the need: 2D dislocations with constant opening, 2D cracks, 3D rectangular dislocations, penny-shaped cracks, etc, whereby most of these models consider purely tensile, or mixed mode (tensile + shear), dislocations.

Dike tend to orient perpendicularly to the direction of the least compressive principal stress axis (σ_3), and to propagate, as theorized by Griffith (1921) for all types of cracks, only if the released strain energy, combined with the potential energy, is large enough to match or overcome the surface energy needed for the creation of the two new increments of crack surfaces. The surface energy increases linearly with crack length; on the other hand, the mechanical energy decreases quadratically with length. This leads to the existence of a *critical crack length*: once the crack reaches that length, it will propagate unstably. In practice, the crack will propagate when the released energy is sufficient to overcome the resistance of the material, because other factors act to stabilize the propagation. Indeed, dikes are fluid-filled cracks. As such, dikes will never achieve unstable propagation, first because this would require an infinite supply of injectable fluid, and second because the fluid itself requires time to flow, according to its rheology. Therefore, fluid-filled cracks, like dikes, will achieve their own typical propagation speed

(determined by the fluid viscosity, density and by the properties of the encasing rock) rather than propagating unsteadily.

The stress in a region near the crack tip for a crack subject to uniform stress decrease, in an r-coordinate system with origin at the crack tip, is given by:

$$\sigma_{ij}(r,\theta) = \frac{K}{\sqrt{2\pi r}} f_{ij}(\theta) + higher\, order\, terms \tag{1.1}$$

where σ_{ij} is the elastic stress tensor, K is the *Stress Intensity Factor*, and $f_{ij}(\theta)$ are functions of the angular distance from the crack plane; there is a different $f_{ij}(\theta)$ for any crack mode. Crack mode I corresponds to opening; crack mode 2 is in-plane shear; crack mode 3 is anti-plane shear. For the purpose of modelling dikes, we will only consider mode I (opening).

Equation 1.1 defines the Stress Intensity Factor, K. We can say that the crack will propagate when K at the crack tip overcomes the Rock *Fracture Toughness*, K_c, which is defined as the capacity of the material to resist fracturing when stressed (Gonnermann and Taisne, 2015).

As mentioned above, likewise to other predominantly tensile fractures, dikes tend to propagate perpendicularly to the plane of the least compressive stress. Dike trajectories, however, can be far more complex. The shape of tensile fractures is altered by stress gradients (Pollard and O. H. Muller, 1976). Even in purely compressional conditions, like those in the lithosphere, tensile crack propagation may occur, as long as the magma is buoyant or stress gradients are present. Among other studies, this was demonstrated by Dahm (2000) through a numerical method developed to compute trajectories for fluid-filled fractures. A tear-drop-shaped fracture results from the equilibrium of elastic stresses and internal pressure. To better explain the concept, in fig. 1.1 a dike is represented as an opening fracture, undergoing a pressurization exerted by the intruding magma on its walls. In this scenario, magma is provided by a pressurized magma chamber. If the overpressure (sum of the external stress and magma pressure) on the dike plane is uniform, the dike opening is elliptical. If, on the other hand, the overpressure is not uniform, e.g. because of a stress gradient in the rock, the crack will pinch closed at the tip undergoing the strongest compression, and the stress intensity factor at the other end will be larger. The dike is now enabled to break the rock at one tip, propagating toward the direction of decreasing compression. As shown in the last panel, the dike can become detahced from the fluid-injecting magma chamber, maintaining a nearly constant length and fluid volume while propagating even for large distances. Strictly, this can only occur if all the magma is extracted from the tail and flows into the mose region of the dike, which happens if magma viscosity is comparatively low.

If the rock density is different from the fluid density, an apparent stress gradient can occur along the vertical extent of the fracture. This is the so-called *Buoyancy effect* (See fig. 1.2). Specifically, when the rock density is larger than the fluid density ($\rho^{Rock} > \rho^{Fluid}$), there is a larger overpressure at the top of a vertical fracture, because

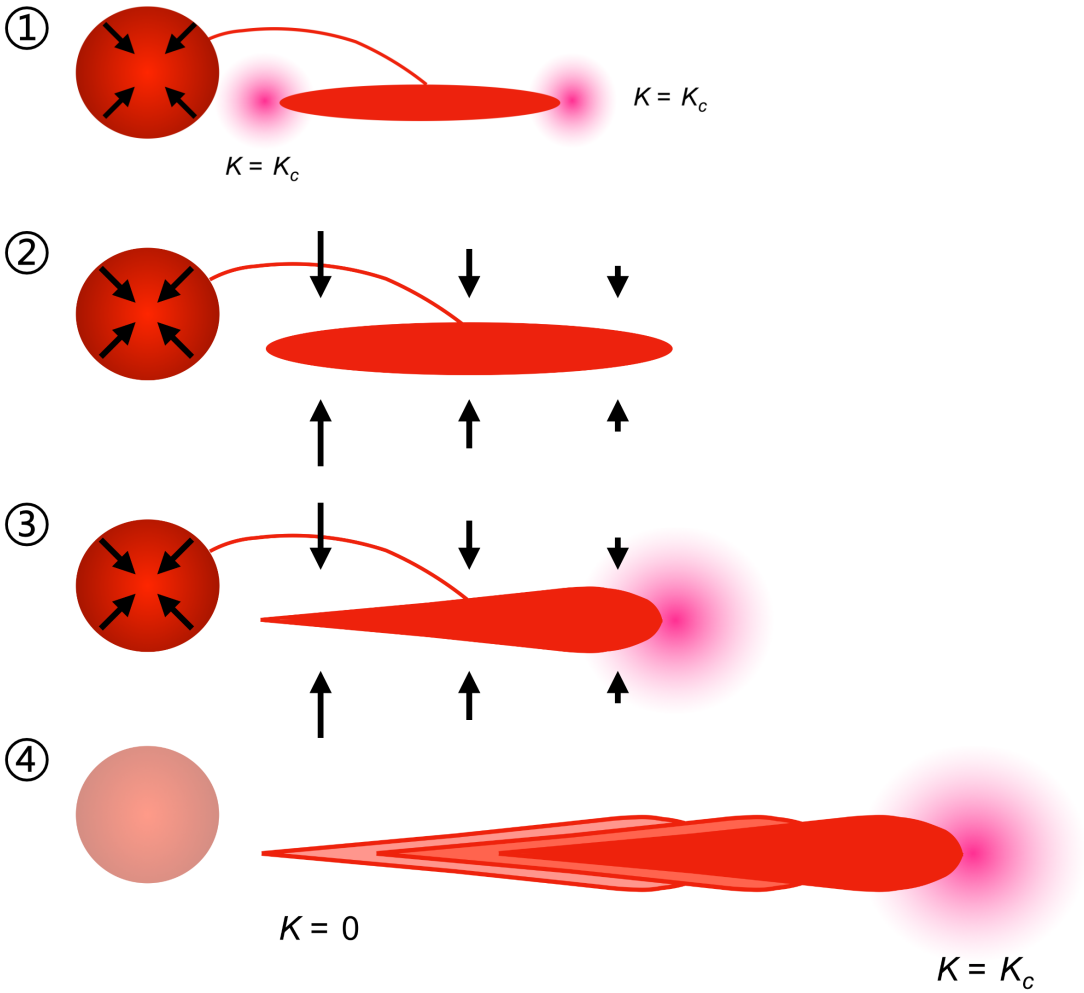

Figure 1.1: Stress gradient effect on dike propagation. (1): Magma chamber feeding a dike. If the overpressure (sum of external stress and magma pressure) on the dike plane is uniform, the dike opening is elliptical. (The opening is exaggerated in the figure) (2): The dike may undergo a pressure gradient due to external factors. (3): The dike seals at the end undergoing the greater stress. (4): The stress intensity factor at the dike tip overcomes the fracture toughness; the dike begins to propagate autonomously, without further injection of magma from the magma chamber. (Modified from a figure by E. Rivalta)

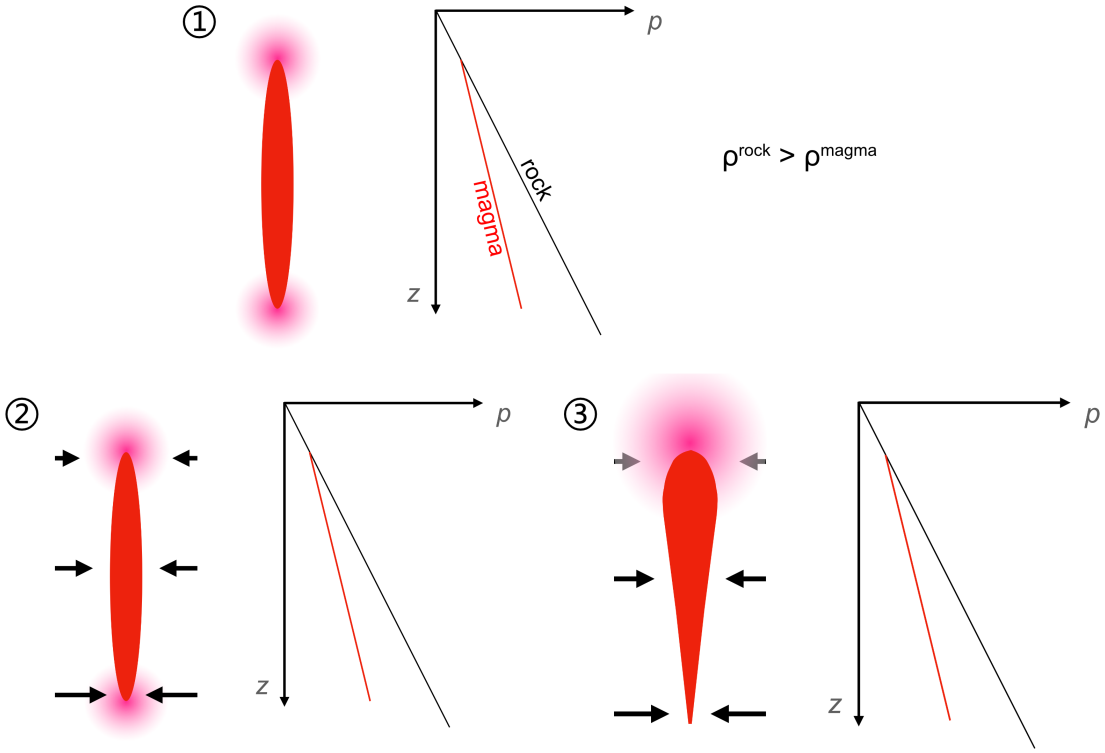

Figure 1.2: Buoyancy effect. (1): For a vertical dike, when rock density is greater than magma density, magma pressure increases more slowly than rock pressure as depth increases. (2): A pressure gradient results along the intrusion vertical line. (3): The dike seals at the bottom and rises at the top, breaking the rock above it (Modified from a figure by Eleonora Rivalta).

the lithostatic stress decrease in the rock moving towards the surface is greater than the hydrostatic stress decrease in the fluid. This leads the fracture to propagate upward (Weertman, 1971; Pollard and O. H. Muller, 1976; Dahm, 2000).

Furthermore, dikes do not undergo sudden, abrupt turns along their path: they bend over a finite distance, comparable to the dimension of the crack itself. All things considered, the dike will not be strictly perpendicular to the plane of minimum compressive stress at each point in its trajectory (Rivalta et al., 2015).

The orientation of the principal stress axes is strongly influenced by surface topography, which, thus, affects the fluid-filled crack propagation pathways even on a large scale. Through a boundary-element approach, Dahm (2000) found dikes to be attracted to gravitational loads such as those due to volcano edifice sources. Maccaferri, Bonafede, and Eleonora Rivalta (2011) computed dike trajectories for various initial angles and

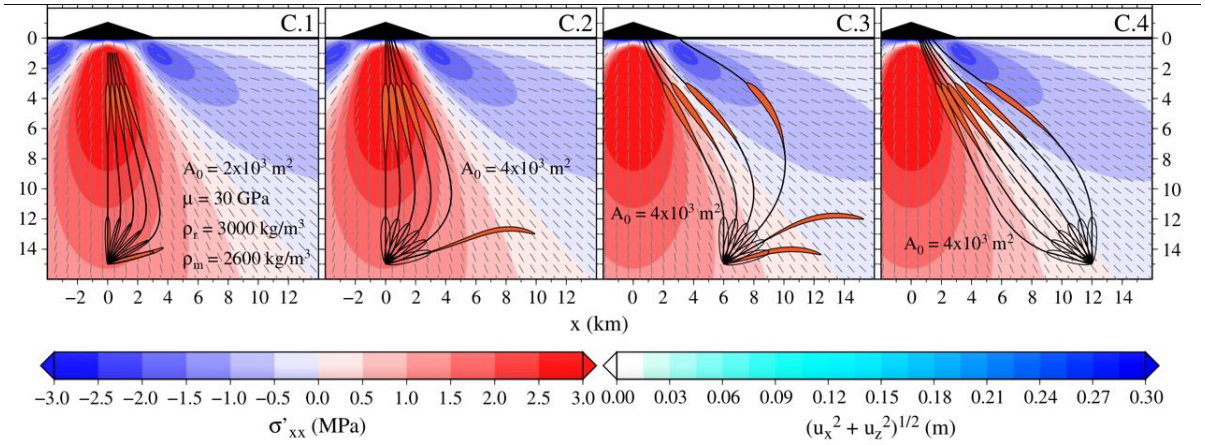

Figure 1.3: Effect on dike propagation induced by a triangular load applied on the surface. In panel C2 the volume of the intrusion is double than in panel C1. In panel C3 the starting point of the intrusions is shifted horizontally by 6 km and in C4 by 12 km (in this last configuration the initial dip angles of the dikes are opposite with respect to the previous configurations.) Here σ is plotted in background (the horizontal component of the deviatoric stress tensor induced by the load), the short grey lines indicate the direction of the maximum compressive axis. From: Maccaferri, Bonafede, and Eleonora Rivalta (2011)

different starting position with respect to the volcanic edifice. They observed that the majority of the paths flow into the volcanic structure's base, but on rare occasions a dike may escape and erupt at a significant distance from it. The dikes will get arrested just below the base of the load if the buoyancy is insufficient (when their volume is not big enough), expanding laterally and erupting, or creating/feeding a shallow crustal magma reservoir (fig. 1.3)

1.2 The shape of volcanoes

The shape of volcanoes is a key factor in determining dike emplacement. In fact, gravity deforms and stresses volcanic edifices and exerts a load onto the underlying rocks. Dikes will be affected by this and so will be the location of the eruptive vents. Due to the everchanging stresses in a volcano edifice, eruptions do not always occur from the same fissure. In contrast, magma propagating below the surface usually break the volcano flanks along a new pathway and create new vents. This creates a feedback effect between dikes and the effect of eruptions, with new loading by deposition of eruptive products affecting areas where dikes breach the surface. In turn, deposition affect stresses and drives future dikes along new pathways.

Volcanoes have different morphologies depending on the magma composition and eruptive style. First, we distinguish between polygenetic and monogenetic volcanoes.

Monogenetic volcanoes are formed in just one eruption. Monogenetic volcanic fields develop in regions where magma production is scarce or eruptions are rare. At shallow depth there is no common volcanic plumbing system among the individual volcanoes in these fields. In order to reach the surface, each consecutive batch of magma from the source location creates its own conduit. With long time intervals between eruptions, monogenetic volcanic fields can contain hundreds of individual volcanoes. They can be divided into:

- **Cinder cones**: also known as scoria cones, they are built out of pieces of magma that are released into the air. They are extremely vesicular (with bubble-shaped holes), and are normally solid when they fall. They are the most prevalent kind of volcano on Earth, with the appearance of an idealized volcano, having the shape of a steep, conical hill with a prominent crater at its top.
- **Maars**: volcanic craters surrounded by low pyroclastic cones. It lays below the surrounding ground level. Maars often have lakes in their craters because they are topographic lows.
- **Tuff rings**: pyroclastic cones with craters that are elevated above the surrounding terrain. Unlike maars, their craters are often dry.
- **Eruptive Fissures**.

Polygenetic volcanoes, in contrast, experience multiple eruptions. They can be divided into:

- **Composite volcanoes** (or Stratocones);
- **Shield volcanoes**;
- **Calderas**, which are collapse landforms that form after large-scale volcanic eruptions and are created when the earth above a magma chamber partially empties and sinks into it. There are two basic types of calderas, which may develop in both mafic and silicic volcanic systems. These calderas are distinguished not only by the kind of magma that was erupted but also by whether or not the eruptions that created them were effusive or explosive.

(National Park Service, 2023).

We often find monogenetic cones on stratocones or shield volcanoes, they represent the evolution of fissure eruptions into discrete outlets for the magma.

In order to distinguish between Stratocones and shield volcanoes, magma viscosity plays a key role. High viscous magma eruptions typically result in steep-sided volcanoes

with 30-35° slopes. This is due to the fact that the viscous volcanic material does not flow very far once it is erupted; instead, it accumulates in layers to create a stratovolcano. In contrast, shield volcanoes have mild slopes of less than 10° and produce low-viscosity basaltic lavas during eruptions. An eruption from a shield volcano can cause the basalt to flow far from the vent, creating broad, gentle slopes. (British Geological Survey, 2023).

1.2.1 Stratocones, shield and shield-like volcanoes

Polygenetic shield volcanoes are generally defined as very large structures, with broad flanks primarily composed by lava flows, producing effusive eruptions of low-viscosity lavas. However, when it comes to analyze in details the actual shape of many different shield volcanoes, they significantly differ from one another. Grosse and Matthieu Kervyn (2018), identify two threshold values to distinguish a shield volcano from a stratovolcano:

- $\frac{Height}{Basal\ width} < 0.1$
- Mean slope $< 12°$

Several edifices, commonly classified as stratovolcanoes, lie within this threshold, and are considered *shield-like* for the purpose of their study: Etna (Italy) and Fuji (Japan), analyzed in this thesis, are two of these special cases.

Three factors contribute in determining the shield volcanoes shapes (Grosse and Matthieu Kervyn, 2018):

1. Proportion of lava versus pyroclasts and length versus thickness of lava flows, controlled by:
    - Magma composition;
    - Rheology;
    - Effusion rate.
2. Vent spatial distribution and their magma output, caused by the magmatic feeding system, in its turn controlled by:
    - The initial regional tectonic stress field;
    - Loading-induced stress field.
3. Summit caldera formation, shaping the edifice as truncated (and occurring at lower shield volumes in continental rift zones)

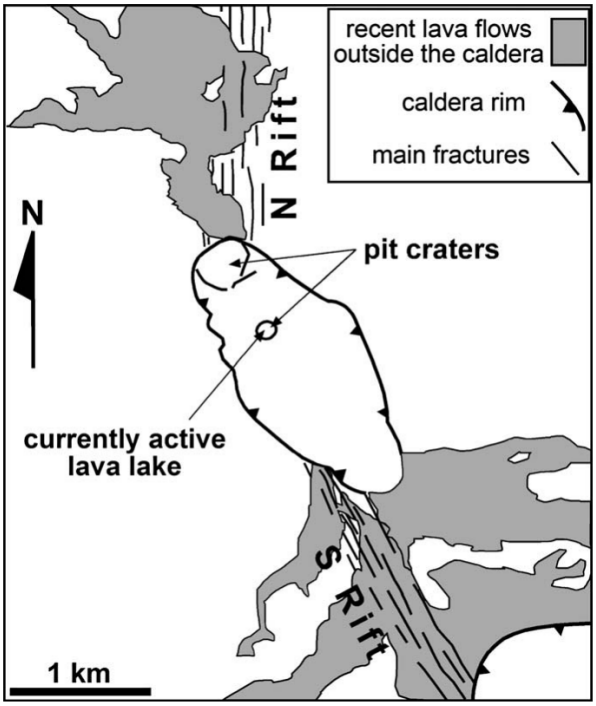

Figure 1.4: Erta Ale, Ethiopia. Example of elongated volcano edifice, with the bigger axis oriented perpendicularly to the least compressive regional stress. Dikes are shown orienting accordingly. From: (Valerio Acocella, 2006).

The shape and size of a volcano can provide insight about local stress and dike emplacement. For instance, Acocella and Neri (2009) observed that regional stress field control fades for taller edifices. Higher volcanoes promote the emplacement of radially distributed dikes, rather than intrusions aligned with the far field stress, because of the stress field generated by loading (more at 1.4). Acocella and Neri (2009) also observed a direct correlation between the maximum length of an eruptive fissure or dike and the total height of the volcano, suggesting a strong topographic control on dike propagation.

Moreover, the whole shape of a volcanic edifice can give clues about the preferential direction of emplacement of dikes. Acocella and Neri (2009) remark that a volcano with an elongated shape will always have its longest axis aligned perpendicular to the axis of minimum regional compressive stress, thereby also revealing the favored direction of propagation for its dikes. A striking example is provided in fig. 1.4, where the Erta Ale volcanic edifice is shown. The edifice is elongated in the same direction in which the dikes propagate, confirming the above.

1.3 New vent opening in a volcano edifice

Lava flow models are commonly used to understand lava pathways, and prevent catastrophes in heavily populated areas. Lava, however, starts flowing from volcanic vents: this is why a crucial, although understudied, factor in volcanic risk, is the location of new vent opening.

Vents can open throughout the whole volcano edifice, but there are areas where they tend to cluster. Up to now, in order to forecast the opening locations of future vents, maps of pre-existing vents have been used. E. Rivalta et al. (2019) and Mantiloni, Eleonora Rivalta, and Davis (2023), however, proposed that we can improve the quality of spatial forecasts of eruptive vent location by exploiting our understanding of the physical mechanisms ontrolling the trajectories of dike propagation. In practice, this requires constraining the state of stress of volcanoes.

Kervyn et al. (2009) highlighted that eruptive vents tend to cluster within a specific area, called "Break-In-Slope" (BIS). The area is centered where the flank slope abruptly changes from more than 15° to less than 10°, and extends for about one km from the base of steep upper flanks. At the BIS, not only there is a concentration of vent outbreaks, but the existing vents tend to be larger than the ones located at steeper heights. Besides, eruptions at the BIS tend to erupt larger volumes of lava. In fig. 1.5, the vent positions identifying the BIS are clearly visible for the example of Conception volcano (Nicaragua).

In fig. 2.2 is shown a simplified stress pattern under the influence of a topographic loading, created in Kervyn et al. (2009) after the works by James H Dieterich (1988), Wyk (1995), Vries and Matela (1998). This conceptual representation aims to show, through the orientation of the most compressive stress axis σ_1 in the subsurface and within a volcanic cone, how the dikes would orient in this configuration, and why they not always tend to erupt inside the volcanic cone, but migrate laterally. However, the diagram is not very effective in clarifying where the BIS is located and how dikes tend to breach in their proximity, since this model is really simplified.

The location and alignment of vents and fissures on the flanks of a volcanic edifice can help understand the history of dike emplacement. Chadwick Jr and J. Dieterich (1995), highlighted the simultaneous presence of circumferential (emplaced along circumferences around the volcano summit), and radial (radiating outward from the center of a volcano) dikes at all the six active Galapagos volcanoes on Fernandina and Isabela islands, the former arranged around the main eruptive vent, the latter arranged below its flanks at lower elevations. Despite their very different pattern, they emplaced at contemporary periods, and appear to have different orientations due to the different stress field present at distinct elevations on the edifice (See fig. 1.7, panel c). Modelling of InSAR observations of the trajectories of dikes at Fernandina by Bagnardi, Amelung, and Poland (2013) also confirmed that these two different types of intrusion, represented in 1.8, have all occurred in the last two decades. Dikes started as horizontal fractures below the caldera, propagated with circumferential orientation and gradually curved downslope transition-

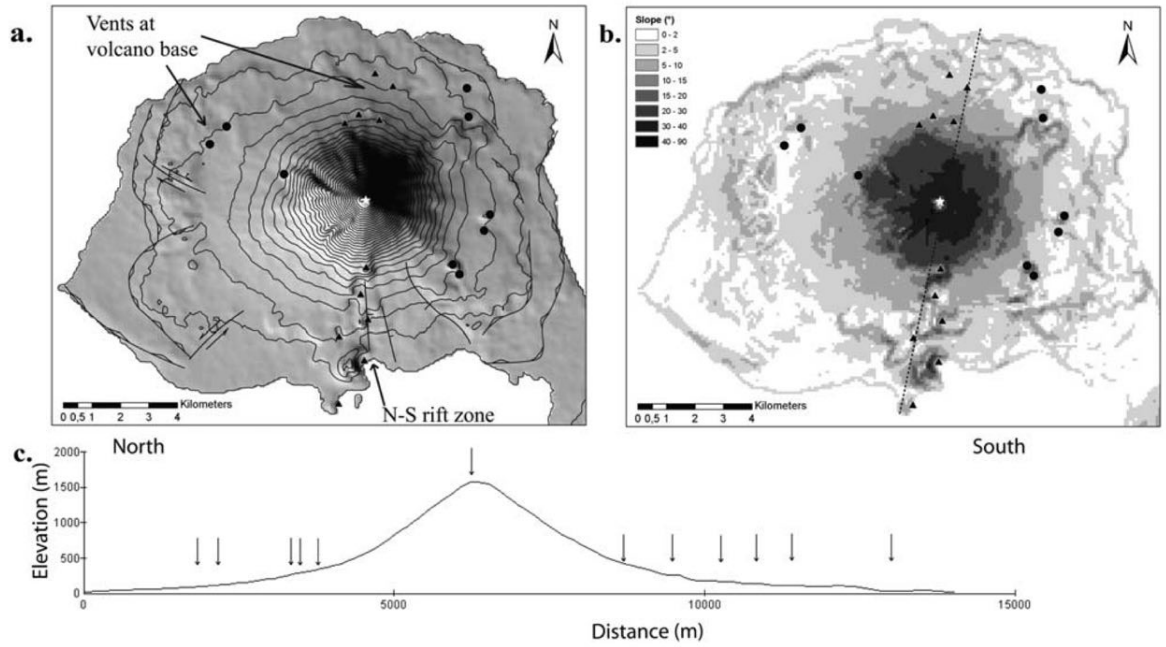

Figure 1.5: Vent distribution at Concepcion volcano, Nicaragua. (a) Shaded relief and structural features; (b) slope angle; (c) north–south topographic profile along dashed line in Figure 1b. Arrows indicate the location of vents, including several at the cone base. Old domes (circles) and Holocene cones (triangles) along a pronounced north–south rift zone are all located on the lower volcano slopes. From Kervyn et al. (2009), adapted from the works of Borgia and Wyk de Vries (2003)a and Wyk (1995).

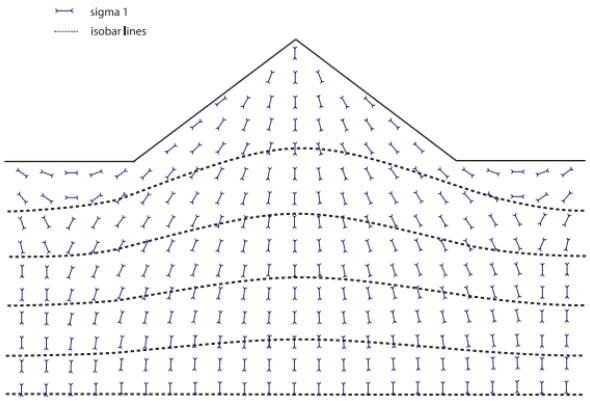

Figure 1.6: Figure showing a simple representation of the σ_1 orientation (the most compressive stress) and of the isobar lines in the substratum and in a volcanic cone based, from Kervyn et al. (2009), based on James H Dieterich (1988), Wyk (1995), Vries and Matela (1998). Dikes tend to propagate perpendicularly to the least principal stress and parallel to orientations of σ_1 and σ_2. The stress distribution within the conical edifice will focus dikes toward the central axis. On the other hand, the pressure gradient below the volcano load can favor lateral dike propagation toward lower confining pressure, so that dikes would tend to migrate out from under the volcano, and then erupt away from the center of the cone.

ing to radial. The state of stress causing this pattern is maintained, because the fissure pattern is continuously regenerated (it would be otherwise erased after new eruptions).

Chadwick Jr and J. Dieterich (1995) conclude that circumferential intrusions are sensitive to changes in stress at the caldera floor, that is why caldera unloading is addressed as the main cause of their presence. In addition, they concluded that the magma reservoir shape favouring most the presence of both circumferential and radial intrusion is the flat-topped and diapiric-shaped shown in the panel b of fig. 1.7. They conclude that, however, magma pressure alone is however not sufficient to create this pattern, and volcano growth through eruptions must play an important role in maintaining the stress pattern and allowing new dikes to intrude.

1.4 Observations on dike emplacement patterns

According to Acocella and Neri (2009), dikes tend to have three main distinctive configurations on a volcano edifice scale:

- regional dikes;
- circumferential dikes;

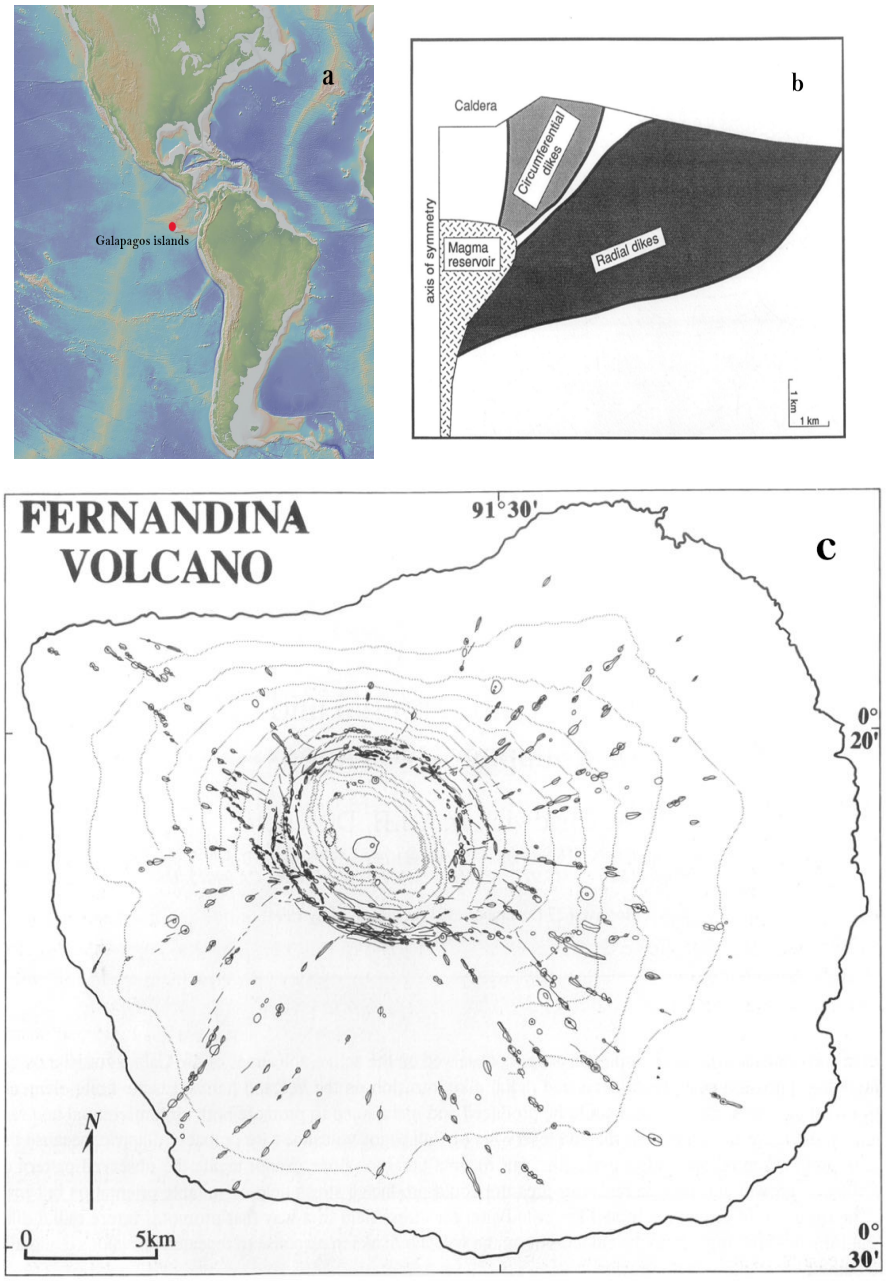

Figure 1.7: a: Geographic reference: Galapagos Islands, Ecuador (from GeomapApp Ryan (2009)) b: Idealized cross-section of a Galapagos volcano suggesting the different areas where circumferential and radial dikes should be favored in the numerical models in order to form the pattern of eruptive fissures observed at the surface. c: Maps of eruptive vents, including eruptive fissures (lines) and cones (outlines) on Fernandina. b and c from: Chadwick Jr and J. Dieterich (1995).

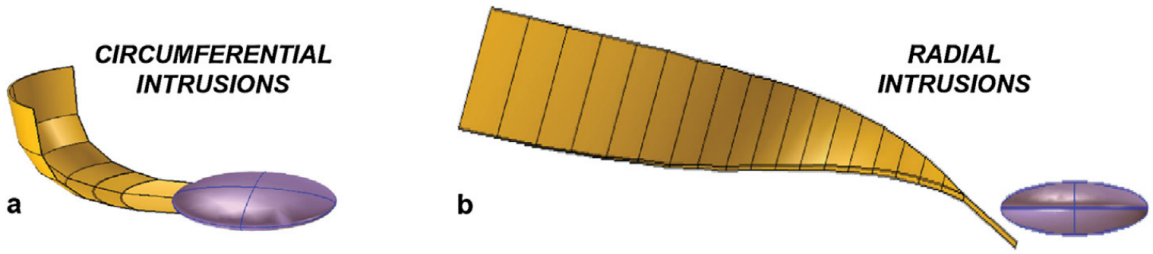

Figure 1.8: Three-dimensional representation of circumferential (a) and radial (b) intrusions; in purple the 1-km-depth magma reservoir, in yellow the intrusions feeding fissure eruptions. From Bagnardi, Amelung, and Poland (2013).

- radial dikes.

Regional dikes are defined as dikes that are oriented according to regional tectonic stress, arranging themselves perpendicular to the plane where the tensile tectonic stress is greatest. This condition is strongly present in the absence of relief; the presence of a volcanic edifice complicates this simple dependence, bringing significant deviations from expected patterns.

Circumferential dikes form arcuate patterns concentrically with the volcanic edifice, and are particularly clustered at summit craters and calderas, where they may also be connected with pre-existing faults or fractures (Acocella and Neri, 2009). An example is shown in fig. 1.7, c.

Radial dikes are vertical to subvertical dikes which radiate from a central volcanic plug (McCarthy and Rankey, 2020). This pattern might be either isotropic (as for the case of Fernandina: fig. 1.7, c) or cluster along preferred directions (as for Etna (Italy): Fig 1.9). Acocella and Neri (2009) claim that regional dikes result from the influence of a far-field (regional) stress, while circumferential and radial result from a near-field stress, due to a local factor such as a pressurized magma reservoir or the volcano load itself. The same authors point out radial dikes as the most common emplacement pattern in volcanoes at surface; circumferential dikes seem, on the other hand, more unusual. A further interesting observation is that the higher the volcano (and thus the greater the loading), the more dikes will tend to orient radially, even with the presence of tectonic stress.

The radial and circumferential patterns have in the past been attributed to the presence of a pressurized magmatic reservoir (Odé, 1957; Chadwick Jr and J. Dieterich, 1995), to caldera unloading (Corbi et al., 2015) or simply to the presence of loading; Roman and Jaupart (2014) demonstrated that stresses caused by a topographic loading dominate over stresses caused by a magma reservoir.

Topographic irregularities also play a role in dike radial emplacement. An example is dike aligned with 'Valle del Bove'at Etna (See fig. 1.9). In this case, the collapse

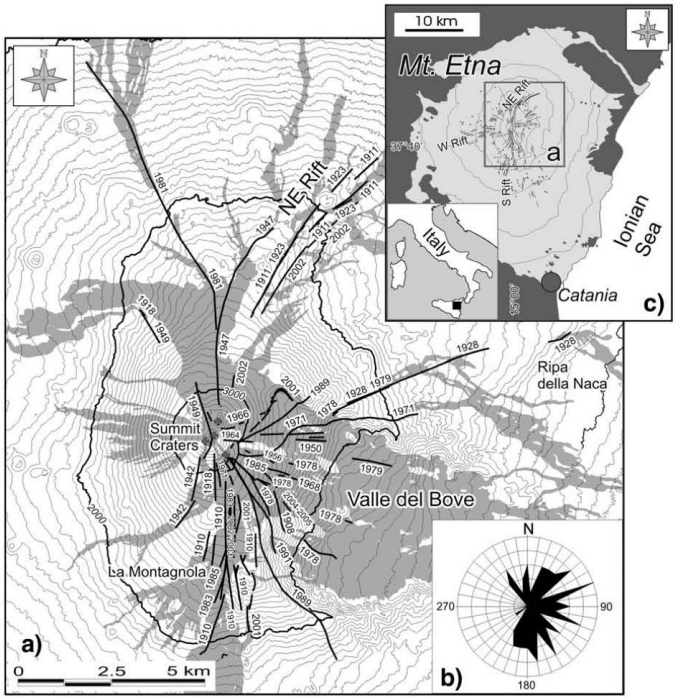

Figure 1.9: Example of radial, non-isotropic eruptive fissures. (a): Etna (Italy), period: 1900-2005. (b): Fissure orientation. Also noticeable is the peculiar arrangement of the dikes even with the "Valle del Bove," a scarp that leads the dikes to align with it. (c): inset showing the three main rift zones. From: Acocella and Neri (2009).

modified the stress field in such a way that dikes result mostly aligned with the collapse borders.

1.5 Examples of well-monitored dike intrusion and emplacement

In this section I analyse two different cases of study involving geophysical monitoring of dike emplacement, in order to showcase the geometry of magma transport within volcanic edifices, short and long-term dike emplacement behaviour in relation with local topography.

1.5.1 The May, 2021 dike propagation and eruption at Nyiragongo (DR Congo)

Nyiragongo is a volcano producing very dangerous effusive eruptions. It is located in the Congolese area of the Virunga volcanic province, on the western branch of the east African rift, and it is one of the most active volcanoes in the world, along with its neighbour Nyamuragira (fig. 1.10). Intrusions occurring at Nyiragongo tend mainly to align perpendicularly to the least regional tectonic stress, which is due to rifting (Acocella and Neri, 2009).

The May 2021 eruptive event, studied by Smittarello et al. (2022), produced no geophysical precursors, causing a heated debate on the lack of a timely alert to the population. The eruption was due to the propagation of a dike that, starting from the central lava lake on the summit of Nyiragongo, propagated laterally in a NW-SE direction for 7 km, of which 4 km to NW (towards Nyamuragira) and 3 km to SE. The dike erupted at 4 locations on the edifice, opening new vents, from where lava begun to flow, destroying buildings, infrastructures, and harming the population (See fig.1.11 for more details). The SE dike part, after partially erupting, continued to propagate underground, deviating in a southerly direction. After passing under the city of Goma, the dike headed towards the Lake Kivu stopping below the lake in the vicinity of the Nyabihu Fault, keeping to a shallow depth of about 450 m. The total volume of the dike amounts to 240 Mm^3. Though the effusive activity lasted for about 6 hours, the seismic crises due to the dike propagation lasted for about 10 days.

The fact that the dike did not erupt on its way to the lake, either in Goma or within Lake Kivu itself, is an indication that the magma was likely degassed, as analyses of the presence and dimensions of lava gas bubbles later confirmed (Delphine Smittarello et al., 2019). This is probably due to the fact that magma was sourced from a lava lake, and was therefore degassed. This resulted in a subsurface propagation of the dike, as shown in fig. 1.12.

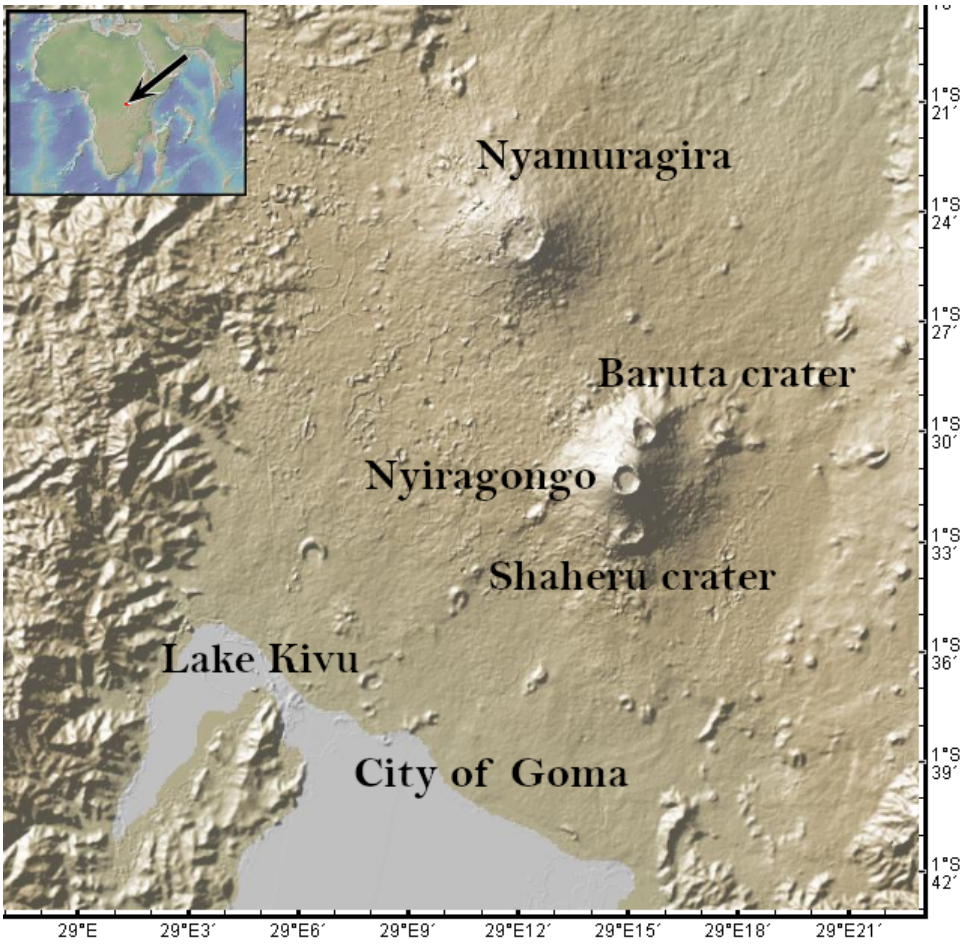

Figure 1.10: Nyiragongo and Nyamuragira, Democratic Republic of Congo. Edit of a figure made with GeomapApp (Ryan, 2009).

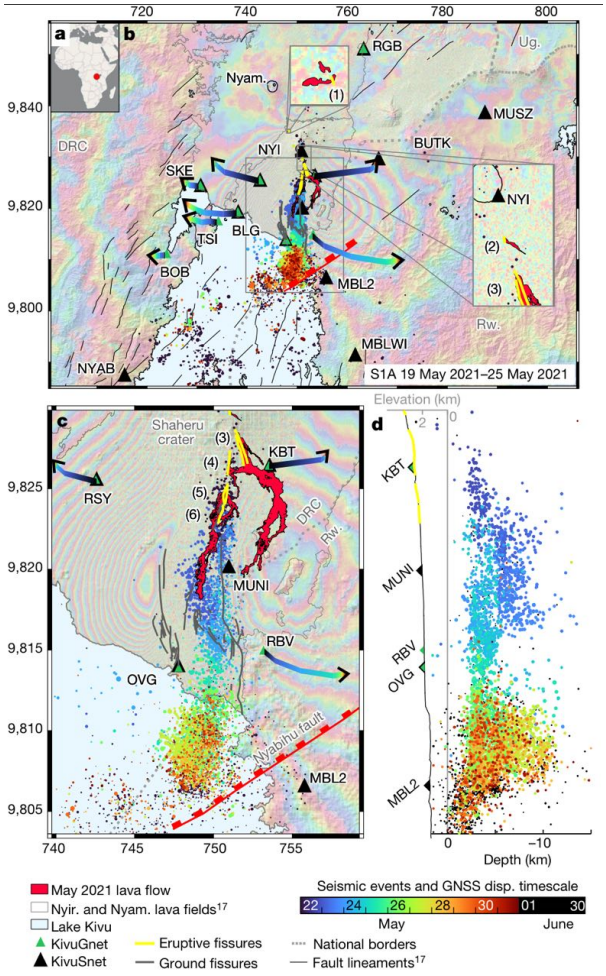

Figure 1.11: Co-eruptive geodetic signals and seismicity. a, Situation map. b,c, Sentinel-1 (S1) 19 May 2021 to 31 May 2021 ascending (A) interferogram overlaid with automatic earthquake locations and GNSS displacements (disp.) over time (blue to black colours with time from the onset of the eruption), eruptive fissures (yellow lines 1 to 6, from north to south), ground fissures detected from interferogram discontinuities (grey lines), lava flows (red area) and seismic and GNSS stations from KivuSNet18 and KivuGNet25 available during the crisis (black and green triangles, respectively). DRC, Democratic Republic of the Congo; Nyam., Nyamulagira; Rw., Rwanda; Ug., Uganda. Panel c shows a magnification of the central box in b. d, North–south transect of hypocentral depth (same symbols as in b and c). Coordinates are given in kilometres in the WGS 1984 UTM (Zone 35S) system. From: Smittarello et al. (2022).

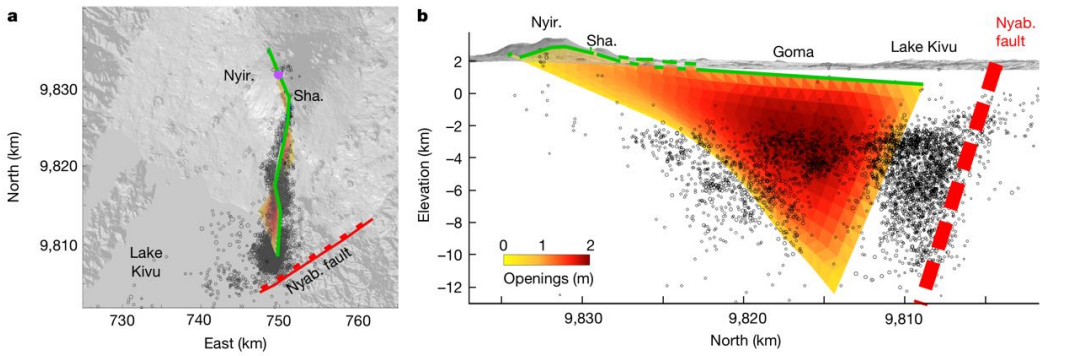

Figure 1.12: Best results of dike geometry inverted from four interferograms spanning the eruption overlaid with seismicity between 22 and 31 May in a map view (a) and along a north–south cross section (b). Colours represent the dike opening (0–2.5 m). Sha: Shaheru Crater. Nyabihu Fault is marked in red. Its 72.5°dip is estimated from seismic profiles45. Coordinates are given in kilometres in the WGS 1984 UTM (Zone 35S) system. From: Smittarello et al. (2022).

The fact that the dike propagated to such a shallow depth, however, suggests that an eruption in the city of Goma or in the lake Kivu may not be such a remote possibility. In similar circumstances, the possible consequences of a sublacustrine eruption are unknown, which is one more reason why this area needs to be studied and monitored.

This is a powerful example of how dike trajectory and vent opening predicting tools would be useful, especially if combined with lava flow models, to provide an extra prevention tool to alert the population in critical cases.

1.5.2 Long-term architecture of dike emplacement at Piton de la Fournaise (La Réunion)

Piton de la Fournaise (Réunion Island) is a shield volcano located on a hot-spot, and is one of the most active volcanoes on Earth (fig. 1.13). It stands on an intrusive gabbroic complex, formed maybe from Les Alizes, a now extint older edifice, which lies to the east of Piton de la Fournaise.

Observations highlighted an average of several intrusions per year; the fissure eruptions resulting from these magma intrusions build, on the surface, a rift system articulated in different branches (fig. 1.14). The most active one is the NE-SE one, with an arcuate shape, cutting the edges of the caldera and reaching to the shore, passing through the volcanic cone. Dumont et al. (2022) studied the deformation induced by 57 intrusions at Piton De La Fournaise, recorded by satellite interferometry. They modelled the deformation induced by dozens of these intrusions retrieving the source parameters for the dikes (location, shape, volume). Over the years, the magmatic intrusions have pieced

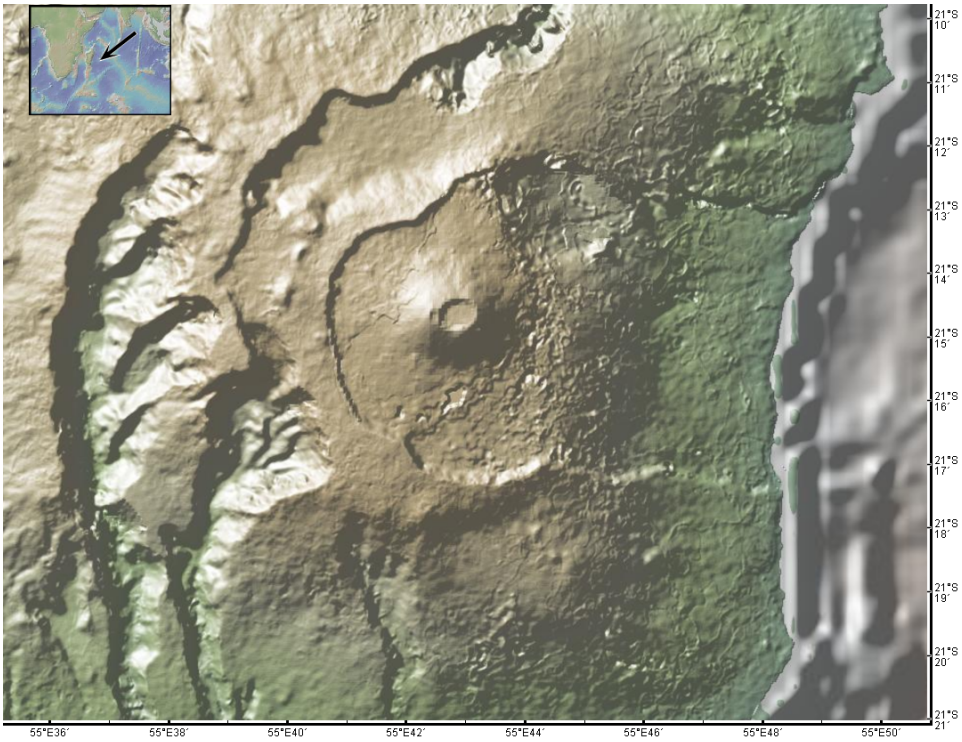

Figure 1.13: Piton de la Fournaise, Réunion Island. Figure made with GeomapApp (Ryan, 2009).

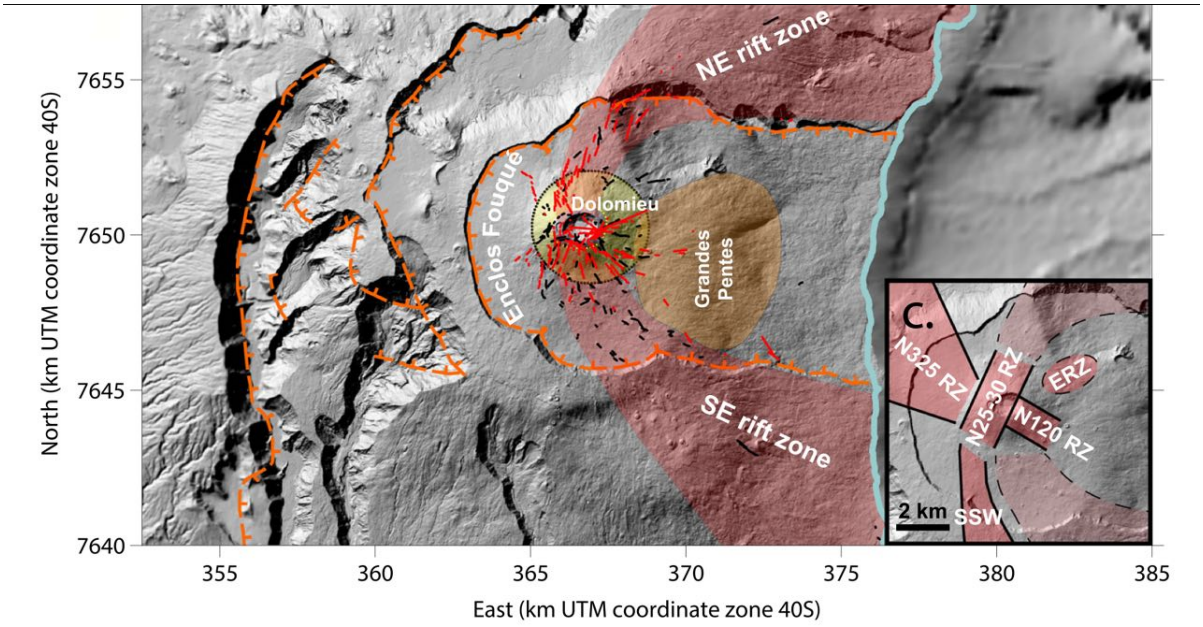

Figure 1.14: Map and structural features of Piton De La Fournaise edifice. From: Dumont et al. (2022)

together a spoon-shaped structure around the main crater (Dolomieu crater) (fig. 1.15).

From fig. 1.15, it is evident that the Dolomieu crater is the turning point for magma in its propagation. The intrusions start as sills beneath the summit, propagate laterally before turning in the vertical direction to reach the vent. At depth, the dikes meet the main NE-SE intrusion zone, extending the spoon-shaped structure to the east. The dip angles are vertical to the west of the crater, decreasing towards the east, where they follow the flank topography.

This is a unique picture of the long-term arrangement of dikes, and must reflect the stress within the edifice as produced by the edifice loading, the slow sliding to the coast of the eastern flank, and the recent 2007 caldera collapse event at the Dolomieu crater. In turn, repeating intrusions in the volcano according to such a spoon-shaped geometry may threaten the stability of the whole volcanic edifice. The scarps visible in Fig 1.13 show that huge collapse events have occurred in the past there.

Flank or sector collapse are common for many volcanic islands, due to the unconsolidated character of the fragmented eruptive products of submarine eruptions, called hyaloclastite. The major hazard at Piton de la Fournaise is the collapse of the eastern flank. Besides the apparent hazard represented by a possible slip of the whole edifice over the spoon-shaped surface delineated by the dikes, it would be important to understand the mechanisms controlling the long-term arrangement of the intrusions, as these might reveal fundamental information on the state of stress of the volcano and how such

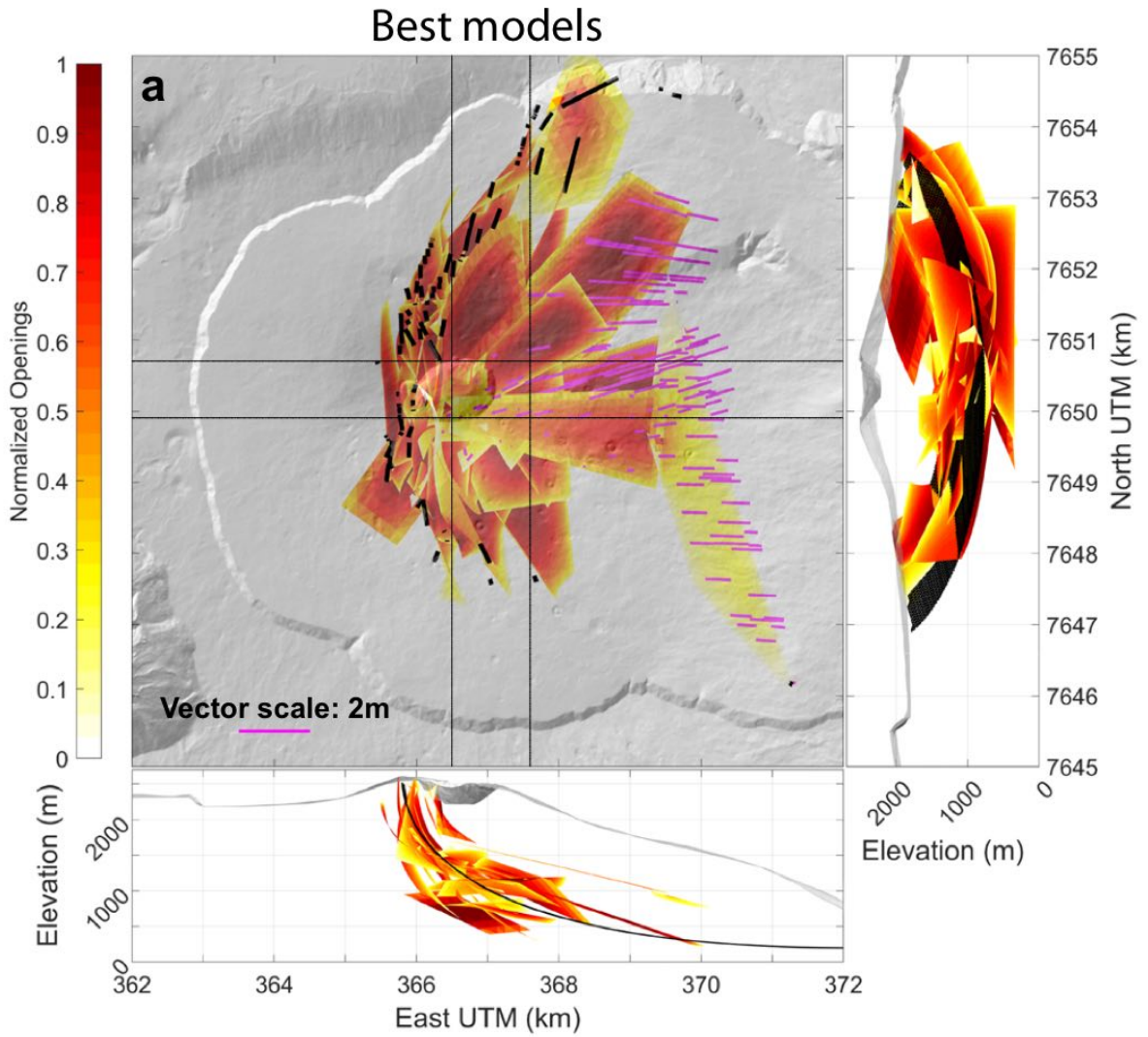

Figure 1.15: Best fit models for the 29 intrusions emplaced in the major NE-SE and sill intrusion zones. The colors show the opening of the modeled intrusions (normalized) Magenta vectors indicate displacemet of the sheared sills. From: Dumont et al. (2022).

stress has evolved over the history of the volcano and may evolve in the future, thereby controlling other processes.

1.6 Scientific questions

The aim of this work is studying the relations intercurring between topography of volcanic edifices, as sources of gravitational loadings, and dike propagation pathways; in particular:

- What arrangement do we expect within a volcanic edifice of simple shape?
- When do we observe circumferential, and when radial dikes?
- How can we understand and fairly represent the true state of local stress for volcanic areas?
- What factors related to topography affect the different propagation of dikes? (Aspect ratio of the volcano, presence of caldera, etc.).

Chapter 2

The state of stress of volcanic areas and dike propagation modelling

The state of stress underground often presents complex patterns, because it depends on a range of factors including rheological rock behaviour, topography peculiarities, geological history of the considered area. (Jaeger, Cook, and Zimmerman, 2007). Unfortunately, stress is not directly measurable and hard to infer. For these reasons, rock-disturbing techniques are often used to obtain values of local stress states. These techniques, however, such as hydraulic fracturing, are highly expensive: relying on different techniques, such as geodetic observation or earthquake features, can be preferred. The orientation of magmatic dikes, for example, is one of the main indirect indicators of near-surface stress field orientation, since they tend to propagate perpendicular to the plane of minimum compressive stress (Anderson, 1936; Chadwick Jr and J. Dieterich, 1995).

2.1 Understanding stress orientation

The local stress orientation is crucial in understanding and forecasting dike trajectories: though dikes and sills do not usually align instantly with the stress field, the alignment can still occur on a volcano-edifice spatial scale (Rivalta et al., 2015).

At volcanoes, the *in situ* state of stress is influenced by a plethora of causes, such as tectonic stress, surface loading, rock behaviour, magma chamber inflation/deflation, anthropogenic factors, and dike and sill intrusions themselves. In addition to that, all these factors are spatially heterogeneous and vary with time. Hence, the three principal stress values and directions are not easily predictable.

2.2 The state of stress of volcano edifices

Chadwick Jr and J. Dieterich (1995) investigated the stress state of Fernandina by numerical modelling. Their aim was to explain the peculiar pattern of eruptive fissures observed there: circumferential around the caldera rim and radial on the volcano flanks (fig. 1.7), as explained above. They identified five main causes that can alter the stress state:

1. geometry and pressure changes in a near-surface magma reservoir;
2. gravitational stresses;
3. loading by lava flows;
4. dike emplacement;
5. faulting or bulk yielding of the volcano edifice in response to stress changes due to processes 1-5

According to Chadwick Jr and J. Dieterich (1995), the shape of a magmatic reservoir can influence the trajectories of intrusions. With a spherical or oblate magma chamber, the stress pattern around the reservoir favours circumferential intrusions. With a prolate magma chamber, on the other hand, radial intrusions are favoured. The preferred shape for generating both types of intrusions simultaneously is a diapiric shape, with a flattened top (as the one shown in fig. 1.7, panel b). They conclude, however, that a simple change in magma pressure would not be sufficient to generate a stress field capable of generating a pattern of intrusions as complex as that seen in Galapagos volcanoes. A new point of view was introduced by Roman and Jaupart (2014), who argued that edifice loading is the main cause of the generation of a central stress pattern. Moreover, they demonstrated that edifice loading generally dominates over the stress induced by pressurized magma reservoirs, and decays spatially with a gentler slopes compared to the quadratical decay of the reservoir-induced stress (as shown in fig. 2.1). Mantiloni, Eleonora Rivalta, and Davis (2023) compared, on the basis of a numerical model, the stress field generated by a pressurized reservoir at a caldera with the stress generated by the caldera formation alone, confirming the results by Roman and Jaupart (2014).

Modelling the stress induced by topographic loading is not straightforward. Stress due to a real volcanic edifice is very different from that due to an instantly-imposed experimental load: the rheological response of the lithosphere below the volcanic load will be different than that obtained for the imposition of a whole instantaneous load. Volcanic edifices grow gradually, due to eruptive deposits that, layer by layer, build both the structure and shape of the volcanoes from which they erupt, and the underground stress. Every new layer is stress-free when added, and loads with an additional stress increment the layers underneath. The stress due to the new layers becomes available to drive further

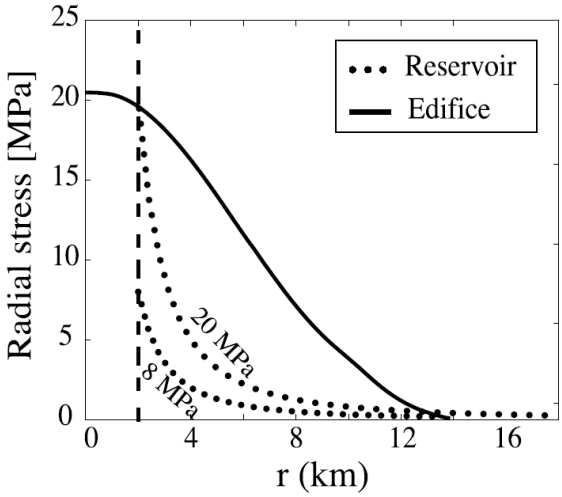

Figure 2.1: Radial stresses induced by an edifice (solid line) and a reservoir (dashed line). Edifice radius = 10 km; edifice height = 2.2 km. The reservoir radius has been set to 2 km. Results for two different values of reservoir overpressure are shown. From: Roman and Jaupart (2014)

dike emplacements. Besides dike emplacements, stresses are continuously modified by many factors, such as earthquakes and fluid transport, and this is the reason why properly including gravitational stresses in volcano modelling is a challenging problem (Chadwick Jr and J. Dieterich, 1995).

Dike and sill intrusions are known to occur perpendicular to the plane of minimum compressive stress. The same intrusions can also be the cause of the change in the orientation of that plane. Magmatic intrusions, in fact, generate an opening crack, the opening direction of which lies on the plane of minimum compressive stress. The dilatation along such plane results in an increase of compressive stress in the opening direction (lying on the least compressive stress plane), and thus in a reduction of the differential stress. After several intrusions, the value of the stress in the plane of minimum stress will get closer and closer to the value of the stress in the plane of maximum stress. Eventually, the stress pattern will change enough to stop further dike incursion, or dramatically change their orientation. This 'homogenization' effect is particularly significant for Galapagos volcanoes, which present frequent dike intrusions (Chadwick Jr and J. Dieterich, 1995).

To summarise, magma intrusions and eruptions act in competition: the firsts leading to a homogenization of stress below the edifice, and the seconds, on the other hand, contributing to an increase in differential stress, through the loading due to the deposition of eruptive products.

Several studies have quantified the stress generated by loading and inferred the sub-

sequent propagation of dikes. One of the pioneering works in this area was done by Dahm (2000); he simulated a two-dimensional topographic loading through the use of stress-free segments to which normal compressive stress was then applied. This stress was added to the lithostatic background stress (uniform and increasing with depth). Dikes were observed to bend towards the load as they ascended, in response to the stress filed imposed by the load. J. R. Muller, Ito, and S. J. Martel (2001) found similar results by using both numerical models and laboratory experiments with fluid injections in gelatin. Dahm (2000) observed that dikes were affected by loading up to a distance of four times the radius of the volcano, while J. R. Muller, Ito, and S. J. Martel (2001), through laboratory experiments, derived a scaling law to describe the maximum distance influenced by the loading they found, as:

$$x_c = 0.86\frac{P_{load}}{\Delta P_m} + 1 \tag{2.1}$$

with x_c being the maximum distance where dike undergo loading stress normalized by the load half width, P_{load} being the average load stress and ΔP_m being the dike driving pressure at the midpoint of the dike head. The equation shows how increasing surface loads will attract dikes from greater lateral distances.

These two works paved the way for new studies, such as Maccaferri, Bonafede, and Eleonora Rivalta (2011); Maccaferri, Eleonora Rivalta, Keir, et al. (2014); Maccaferri, Eleonora Rivalta, Passarelli, et al. (2016), concerning the pathways of dikes in complex scenarios, stress due to unloading in rifts, and the mechanisms causing the arrest of dikes; as Corbi et al. (2015), dealing with the unloading caused by the caldera formation, and as Maccaferri, Richter, and Walter (2017), aiming to shed light on the reasons leading to the formation of volcanic edifice cones in new areas after partial edifice collapse, and finding out that unloading due to collapse drives dike trajectories to different pathways, leading to the formation of a new area favored for eruptions, eventually resulting in establishing a new proper erupting cone.

The simulation of 3D dike propagation has only become possible recently, thanks to innovative computational models (Davis, Eleonora Rivalta, and Dahm, 2020; Mantiloni, Eleonora Rivalta, and Davis, 2023). Previously, the only way to understand dike trajectories in three dimensions was to work with stress fields resulting from loading and, obtaining the orientation of the principal stress axes, considering that dikes would propagate perpendicularly to the plane of minimum compressive stress. Many studies have investigated the stress underground in three dimensions, using Finite Element Modelling, as James H Dieterich (1988) and Chadwick Jr and J. Dieterich (1995), focusing on loading, Chestler and Grosfils (2013), dealing mainly with stress due to magma chambers, or Corbi et al. (2015), studying caldera unloading and its influence on the underground stress. Some works also focused on the interaction between different stress factors. For instance, Zhan et al. (2022) investigated, through Finite Element Modeling, the influence of various stress factors in the case of volcanic unrest at Augustine (Alaska). They

compared the influence of dike opening, tectonic stress, and edifice loading, as functions of internal dike pressure and of the intensity of the tectonic stress. It should be noted that Finite Element Modelling is a complex process requiring careful preparation of the model and with generally more complex inversion matrices than those used in boundary element modelling, which is instead used in my work.

The current understanding of stress features in the presence of edifice loading remains a topic of intense debate, as there are still uncertainties regarding the choice of background stress and the homogenization of stress due to multiple intrusions. This calls for further research to improve our understanding of these complex phenomena. To the best of our knowledge, no previous study has analyzed and compared the different factors influencing the stress. My thesis aims to lay the groundwork for future studies by providing new insights on the topic through the use of innovative 3D computational models for dike propagation. By doing so, my work contributes to the ongoing efforts to advance our understanding of the mechanics of dike propagation, and provide a more robust basis for future research in this field.

2.3 Breaking down the state of stress into separate contributions

E. Rivalta et al. (2019) expressed the stress field as the superposition of different contributions, as follows:

$$\sigma^{tot} = \sigma^{Loading} + \sigma^{Tectonic} + \sigma^{Unloading} + \sigma^{Magma\ Chamber} + \sigma^{Previous\ intrusions} + \sigma^{Previous\ large\ earthquakes} \tag{2.2}$$

where $\sigma^{Loading}$ is the stress perturbation due to edifice load; $\sigma^{Tectonic}$ is the regional tectonic stress tensor; $\sigma^{Unloading}$ is the stress perturbation due to unloading due to mass redistribution (such as flank collapse or slide, caldera collapse, icecap melting); $\sigma^{Magma\ Chamber}$ is the stress perturbation owing to magma pressurization; $\sigma^{Previous\ intrusions}$ is the stress tensor caused by previous intrusions; $\sigma^{Previous\ large\ earthquakes}$ is the term due to previous large earthquakes or slow slip events. Among these terms, the dominant ones are $\sigma^{Loading}$, $\sigma^{Tectonic}$ and $+\sigma^{Unloading}$. The stress generated by a pressurized magma chamber ($\sigma^{Magma\ Chamber}$) has been considered to be decisive in yielding dike orientations (Chadwick Jr and J. Dieterich, 1995), but other studies refute this theory, satisfactorily describing the arrangement of dikes in volcanic zones only by using tectonic stress, and that due to loading and unloading (Roman and Jaupart, 2014).

All these terms are in fact superposed to a so-called background stress ($\sigma^{Background}$) (Mantiloni, Eleonora Rivalta, and Davis, 2023), which will be discussed in more detail in the following section.

2.4 The background stress

Two simple ideal assumptions for the state of stress, often used as background states, and then overlapped by other factors, are (Jaeger, Cook, and Zimmerman, 2007):

1. Lithostatic stress (or Heim's rule);
2. Laterally constrained rock.

In the former assumption all the three principal components take the same value:

$$\tau_{xx} = \tau_{yy} = \tau_{zz} = \rho g z \tag{2.3}$$

where ρ is the rock density (considered uniform through the whole depth), g is the gravitational acceleration and z is the depth. This assumption is based on the thesis that if the rock behaves viscoelastically, then the stress state, after a proper amount of time, will meet a lithostatic condition. This assumption has its limitations: waiting a proper amount of time for the rock to meet a lithostatic stress state, for instance, neglects that tectonic force may vary over shorter timescales than the relaxation time of the rock; moreover, viscoelasticity may not be a proper description for near-surface rocks (closer to an elastic-brittle behaviour). The Heim's rule is usually considered valid for a flat or nearly flat topography; I will later question this statement, assuming that a state of stress similar to the lithostatic can be a valid stress model even in the presence of a topography loading. In the second assumption, the rock is constrained to have vanishing lateral deformation as gravity (due to the rock weight) is 'turned on'. The principal stresses are:

$$\begin{aligned} \tau_{zz} &= \rho g z; \\ \tau_{xx} = \tau_{yy} &= \frac{\nu}{1-\nu}\, \rho g z; \end{aligned} \tag{2.4}$$

This assumption is often justified by the fact that, being the Earth spherical, a rock layer is not free to extend at infinity once, for example, a load from a large topography is applied. The laterally-constrained assumption is widely used when modelling topographic loads (Savage, Swolfs, and Powers, 1985; D. F. Mc Tigue, 1987).

In general, the state of stress may be something in between lithostatic and laterally confined, so that a more general state is easily described by using a k factor:

$$\begin{aligned} \tau_{zz} &= \rho g z; \\ \tau_{xx} = \tau_{yy} &= \left[k + (1-k) \left(\frac{\nu}{1-\nu} \right) \right] \rho g z; \\ \tau_{xy} = \tau_{zy} = \tau_{xz} &= 0; \end{aligned} \tag{2.5}$$

In this way, both the two basic assumptions in eq. 2.5, and all the intermediate states, can be described by varying k:

- $k = 1$: Lithostatic assumption;
- $k = 0$: Laterally confined assumption;
- $0 < k < 1$: Intermediate stress state;

Guessing or estimating a proper value for k to be applied in 2.5, in order to obtain a realistic state of stress for a not-flat topography, is not trivial. I now discuss in more detail the processes affecting the state of stress of volcanoes.

2.5 Stress computing

2.5.1 Stress computing: Analytical approaches

Savage, Swolfs, and Powers (1985) provided one of the first analytical solution for gravity induced stress, using isolated symmetric ridges or valleys as topographic features. This method, however, will not be used in this thesis, as it assumes a plane-strain condition, which means that it is only valid for 2D problems where there is no strain variation perpendicular to the plane of analysis.

The McTigue and Mei method (D. F. Mc Tigue, 1987) uses Hankel transforms to compute stresses due to an axisymmetric Gaussian topography loading. This method requires a topography of small slope, with an Aspect Ratio (the ratio between height and half with) of a value between 0.1 and 0.2. This value may be on the small side for real volcanoes.

The stresses, in cylindrical coordinates, are then computed for a Gaussian topography of the form:

$$h = e^{-Ax^2} \tag{2.6}$$

The authors provide a general solution, which is valid at any depth, and an approximated near-surface one, valid up to a maximum depth corresponding to the height of the max topographic relief. This analytical solution was calculated with the assumption of the laterally confined background stress state (See sec. 2.4). This method can be problematic for steeper edifices shapes, preventing then to properly analyze the case of a shield-like edifice, as the ones included in the study of Grosse and Matthieu Kervyn (2018), and specifically as Fuji and Etna, included in this study. Additionally, a single Gaussian topography may be a bad approximation of some complex flank slopes, and can lead to a misrepresentation of peculiar areas of interests, such as the Break-In-Slope, found to be areas hosting vents clusters.

2.5.2 Stress computing: Boundary element numerical methods

A class of problems, known as boundary value problems, tackle applications to many significant practical issues in science and engineering. In these problems a partial differential equation models the physics of the problem in an area of interest. The area is bounded by a border, whose constraints are important for solving the partial differential equation for the whole area. Boundary Element Methods (BEM) consist in discretizing the boundary into N smaller pieces (the so called Boundary Elements), taking advantage of analytical solutions previously derived for those individual elements. For example, if we know the analytical solution for the displacements and stresses induced in the whole medium by dislocations with uniform displacement, we can find a numerical solution to the whole problem by summing the effects of all N boundary elements, appropriately scaled in such a way that our boundary conditions are satisfied. In other words, if the displacement discontinuities on the elements are unknown, we can retrieve them if stresses are given as boundary conditions at the midpoint of each element. Given the combined effect of N singularities at one element, we can write a system of N linear algebraic equations in which the unknowns are the strengths of the displacement discontinuities.

A specific case amongst the BEMs, of central importance for my study, is the Displacement Discontinuity Method (DDM). In the DDM, the boundary elements correspond to discrete approximations to a continuous distribution of displacement *along a crack*. Every crack has two opposing surfaces, which displace with respect to one another, with an arbitrary distribution of relative displacements along them. As shown in fig. 2.2, the two faces of the crack undergo displacements in each dimension; for a two-dimensional crack, result (Crouch and Starfield, 1983):

$$\begin{aligned} D_x &= u_x(x, 0_-) - u_x(x, 0_+) \\ D_y &= u_y(y, 0_-) - u_y(y, 0_+) \end{aligned} \tag{2.7}$$

This procedure is described in details for the S. Martel and J. Muller (2000) model (See paragraph 2.5.2).

The analytical solutions for individual dislocation elements are singular at their edges, so that computed displacements and stresses become less and less reliable the more we get close to the boundaries of the considered elements. The far-field solutions computed this way are then accurate, but huge oscillation are observed close to the boundary element surface. In order to obtain reliable results in applications, then, solutions must be computed at least at a distance equal to the half-length of the edge of the boundaries. The displacement discontinuity method has been extensively applied to problems of modelling faults and dikes. Some examples are Dahm (2000), S. Martel and J. Muller (2000), Maccaferri, Bonafede, and Eleonora Rivalta (2010), Maccaferri, Bonafede, and Eleonora Rivalta (2011). The DDM is now also used for 3D models, as for Xiao and Yue (2011), Davis, Eleonora Rivalta, and Dahm (2020), Davis, Bagnardi, et al. (2021)

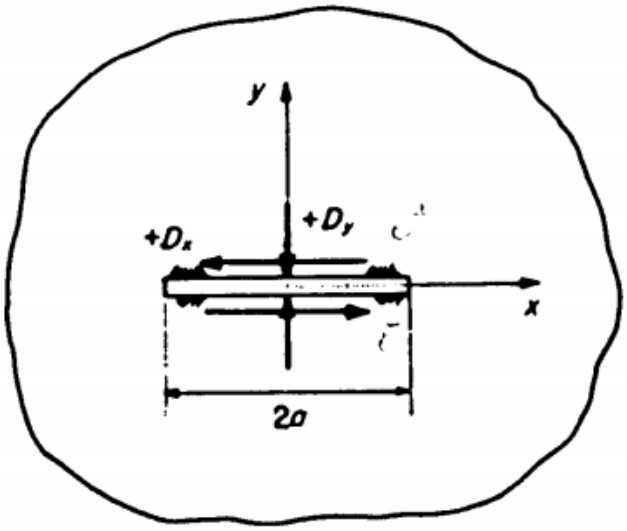

Figure 2.2: in this figure by Crouch and Starfield (1983), is shown a crack inside an elastic solid. Displacements are continuous everywhere inside the solid, except for the crack line.

Martel & Muller's numerical method for 2D stress computing

S. Martel and J. Muller (2000) proposed a method that uses displacement discontinuities to compute elastic stresses due to gravitational load. The method is built using a laterally confined elastic body, but can be adapted to a lithostatic stress state too. The elastic body undergoes the effect of gravity, under a plain strain condition. Therefore, the following stresses arise in the body as:

$$\begin{aligned} \sigma_{yy} &= \rho g y \\ \sigma_{xx} &= \frac{\nu}{1-\nu}\,\rho g y \\ \sigma_{xy} &= \sigma_{yx} = 0 \end{aligned} \tag{2.8}$$

At this point, the body is divided in two parts thanks to a crack simulating the topography, as shown in fig. 2.3. The upper part, called 'overburden', is then subtracted from the whole body, simulating an instant-erosion. The crack is then divided in small boundary elements in the form of line segments, with specific boundary conditions and constant discontinuity in displacement allowed across each segment, in order to eliminate the tractions on the boundary dislocations. In fact, we want the line crack to be free of stress to simulate a stress-free topography.

As shown in fig. 2.4, as the load is imposed on the ridge, a tensile gravitational stress will emerge. This condition, apparently meaningless in physical terms, is derived from the brute application of lithostatic stress. The vertical coordinate equation, in Eq. 2.8, is

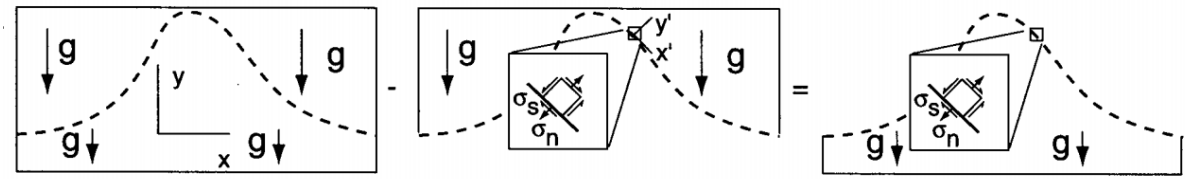

Figure 2.3: Model by S. Martel and J. Muller (2000) for an elastic body undergoing gravitational body forces. The body is separated into two pieces by a crack representing the desired topography. The upper part can be considered as an overburden: if it is subtracted from the body (like in a sudden ideal erosion episode). The segments of the dashed line are the considered boundary elements, with boundary condition and a specific reference frame for each of them. (from S. Martel and J. Muller (2000))

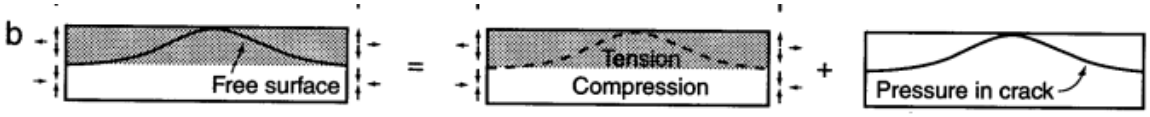

Figure 2.4: Diagram from S. Martel and J. Muller (2000) to show their construction of a boundary element solution, imposing a ridge over a flat topography with laterally constrained far-field stress. The stress undergone by the area subtended by the crack that lies above the value of z=0, is tensile. This is why pressure acting on the crack must be applied in order to nullify the value of the tensile stress on the crack and obtain a stress-free surface.

negative at depth (for $z < 0$), and positive for any $z > 0$. Hence, imposing a topography above the z=0 level, implies imposing a tensile stress within the same topography. In order for the tensile stress to be nullified on the surface of the crack, so as to obtain a free surface, the boundary elements of the crack will have to displace. The stress applied to the midpoints of each boundary element, due to the combined contribution of the displacements made by all the other boundary elements, nullifies the tensile stress on the crack, making the surface free from normal stresses.

As a consequence of the displacement discontinuity allowed on the line segments, stress is induced in the surrounding material: this effect is determined by the influence coefficient A_{ij}. Thanks to the superimposition method, we can compute the displacement discontinuity X_i as:

$$A_{ij}X_i = Bj, \tag{2.9}$$

where B_j are the boundary conditions to meet. Once the X_i are known, they can be used to compute new influence coefficients for new observation points, useful in turn to compute stresses on observation points as follows:

$$A_{ij}^{obs}X_i = \sigma_{ij}^{obs} \tag{2.10}$$

This method can be applied to any free surface loading of any tilt, thanks to the definition of a specific reference system for each boundary element, and proper transformation equations between the main reference system and the element ones.

This method can also, with some care, be extended to 3D. One example, described in detail in the section 2.6.1, is proposed by Mantiloni, Eleonora Rivalta, and Davis (2023).

2.6 Dike propagation modelling through boundary elements

Dikes can be modeled with different techniques, depending on the need. Dahm (2000), J. R. Muller, Ito, and S. J. Martel (2001) and Maccaferri, Bonafede, and Eleonora Rivalta (2011) modeled dikes as 2D Boundary Element cracks (fig. 2.5). The crack is made up of N connected dislocation elements that interact with one another, opening in a brittle elastic medium. A set of stress conditions are met at the center of each dislocation element: the combined stress produced by all the N elements calculated at the centre of each dislocation must balance the overpressure ΔP and shear stress τ (set to 0 to simulate a fluid-filled crack). The model takes into consideration density layers, weak interfaces, and any external stress field (tectonic or topographic).

The dike propagation is modeled by adding an elementary dislocation at the top of the boundary element crack and removing one or more dislocations at the bottom. The pressure profile is re-evaluated and the new equilibrium configuration is computed for each iteration. The direction of the new dislocation is the one that maximises the amount of the total energy release, given as the sum of the strain energy and the gravitational energy. The propagation is allowed if the energy overcomes a threshold value required to break the new surface.

Davis, Bagnardi, et al. (2021) extended this approach to three dimensions. As shown in fig. 2.6, they discretized the modelled intrusion into triangular elements (Nikkhoo and Walter, 2015). For every triangular dislocation element on the tip-line of the crack, K/K_c is calculated (see section 1.1). At each iteration, the tip-line is advanced in proportion to the ratio $\frac{K}{K_c}$ (Paris law). Dependency on magma buoyancy is also considered, following the expression:

$$(\rho_{rocks} - \rho_{magma}) g \, sin(\beta), \tag{2.11}$$

ρ_{rocks} and ρ_{magma} being the density of rocks and magma respectively, and β being the angle between the crack line and the plumb line: if β is zero (and therefore the intrusion is flat), the sill cannot be buoyant. The propagation direction of the crack results from the competition between external and internal pressure gradients ($\Delta\gamma$).

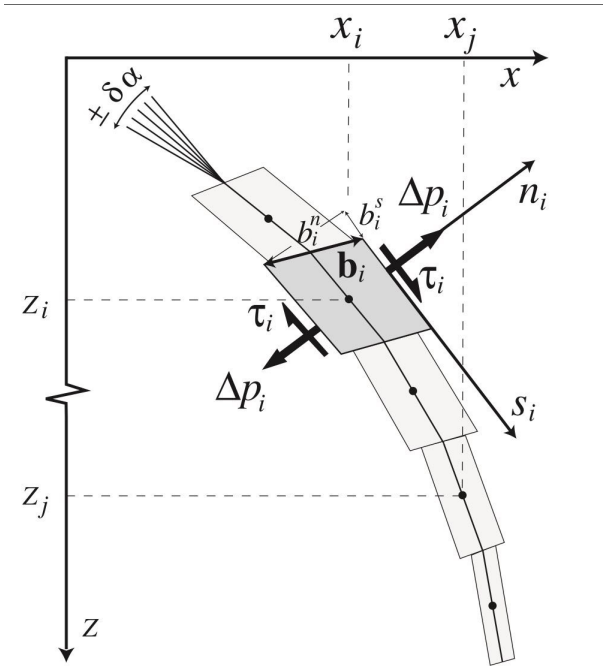

Figure 2.5: Fluid-filled crack modelling by Maccaferri, Bonafede, and Eleonora Rivalta (2011).

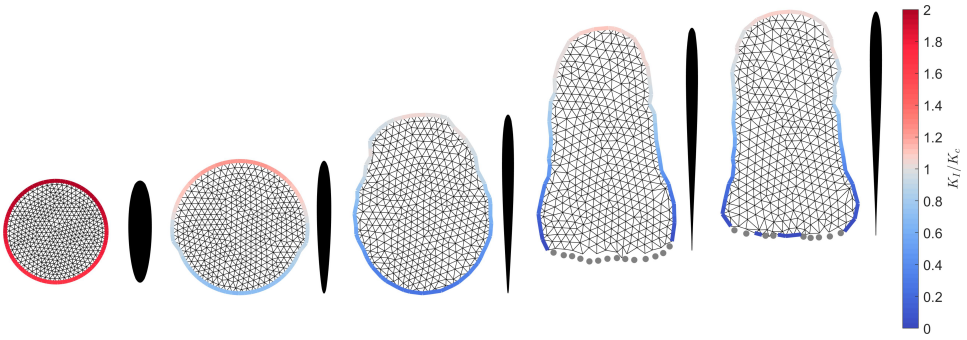

Figure 2.6: Numerical simulation of crack propagation (from left to right), looking at the fractures' face (left) and cross section (right). Grey points are edges that closed in the previous iteration. From: Davis, Eleonora Rivalta, and Dahm (2020).

2.6.1 SAM: Simplified Analytical Model

SAM, which stands for *Simplified Analytical Model* (Mantiloni, Eleonora Rivalta, and Davis, 2023), is a simple 3-D dike propagation model providing streamlines perpendicular to σ_3. Dikes are modeled as propagating tensile penny-shaped cracks, with **fixed radius c**, defined by the coordinates of the central point and a dip angle, which identifies the

plane where the penny lies. The penny inclination is given by the direction perpendicular to σ_3. In order to find the direction of advance and simulate propagation, the penny border are dotted with Observation Points, where the **stress intensity factor** $\boldsymbol{K}$ is computed, as:

$$K = \frac{4}{3\pi}(\Delta\gamma c\sqrt{\pi c}) \tag{2.12}$$

In 2.12, $\Delta\gamma$ is the **pressure gradient**, accounting for the buoyancy force, and, in its turn, computed as:

$$\Delta\gamma_i = \frac{(\sigma_3^i - \sigma_3^j)}{2c} - \rho_m g\frac{(z_O^i - z_O^j)}{2c} \tag{2.13}$$

where ρ_m is magma density and z_O^i, z_O^j are the vertical components of antipodal observation points along the penny's border.

Given these quantities, the penny propagates towards the direction given by the biggest K_i. The Observation point providing that direction is established as the center of the new penny. The procedure is then repeated for the next pennies, until a penny reaches the free surface or the maximum-proximity point to free surface (in case of boundary-element usage). fig. 2.7 shows the selection of observation points on the penny and the propagation of SAM in the direction perpendicular to σ_3.

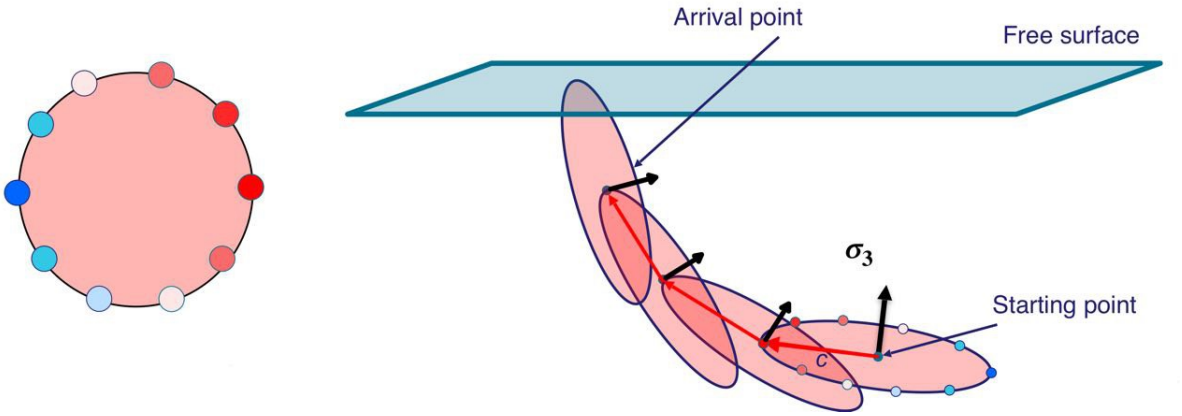

Figure 2.7: Representation of the penny shaped crack of the SAM code. The observation points will be evaluated according to the stress intensity factor. The candidate point for propagation is the one with the largest value of $\frac{K_I}{K_c}$ (Modified from a figure by Eleonora Rivalta).

Chapter 3

Computing the state of stress of a volcano edifice

As mentioned earlier (see section 2.1), calculating subsurface stress in the neighbourhood of a volcanic edifice involves not only considering the loading of the edifice itself, but a variety of other factors.

In this chapter, I will first describe how I created an optimal axisymmetric edifice approximation to simulate volcanic edifices, and how I calculated the stress due to this loading. Subsequently, I will modify this simple model by varying the topography and by adding a tectonic stress according to different assumptions. Furthermore, I will propose a simple model for stress homogenization below the edifice.

3.1 Edifice approximation

For my research, I choose to use axisymmetric topographies approximated by Gaussian or double-Gaussian functions. This choice is justified by the shapes of real shield and shield-like volcano topographies around the world. In figure 3.1 I show some examples of volcano profiles (acquired with GeomapApp, by Ryan (2009)) and how they can be optimally approximated through a Gaussian function.

As shown in picture 3.1, a Gaussian shape is a good approximation for many shield volcanoes; Gaussian approximation of volcano edifices, however, is not always appropriate, especially for steeper flanks (as shown for instance for Mount Fuji). Some volcanoes are better approximated by a "double" Gaussian function:

$$y = A_1 e^{A_2 x^2} + B_1 e^{B_2 x^2}, \tag{3.1}$$

where A_1, A_2, B_1, B_2 are constants determined through fitting the shape of the considered volcano.

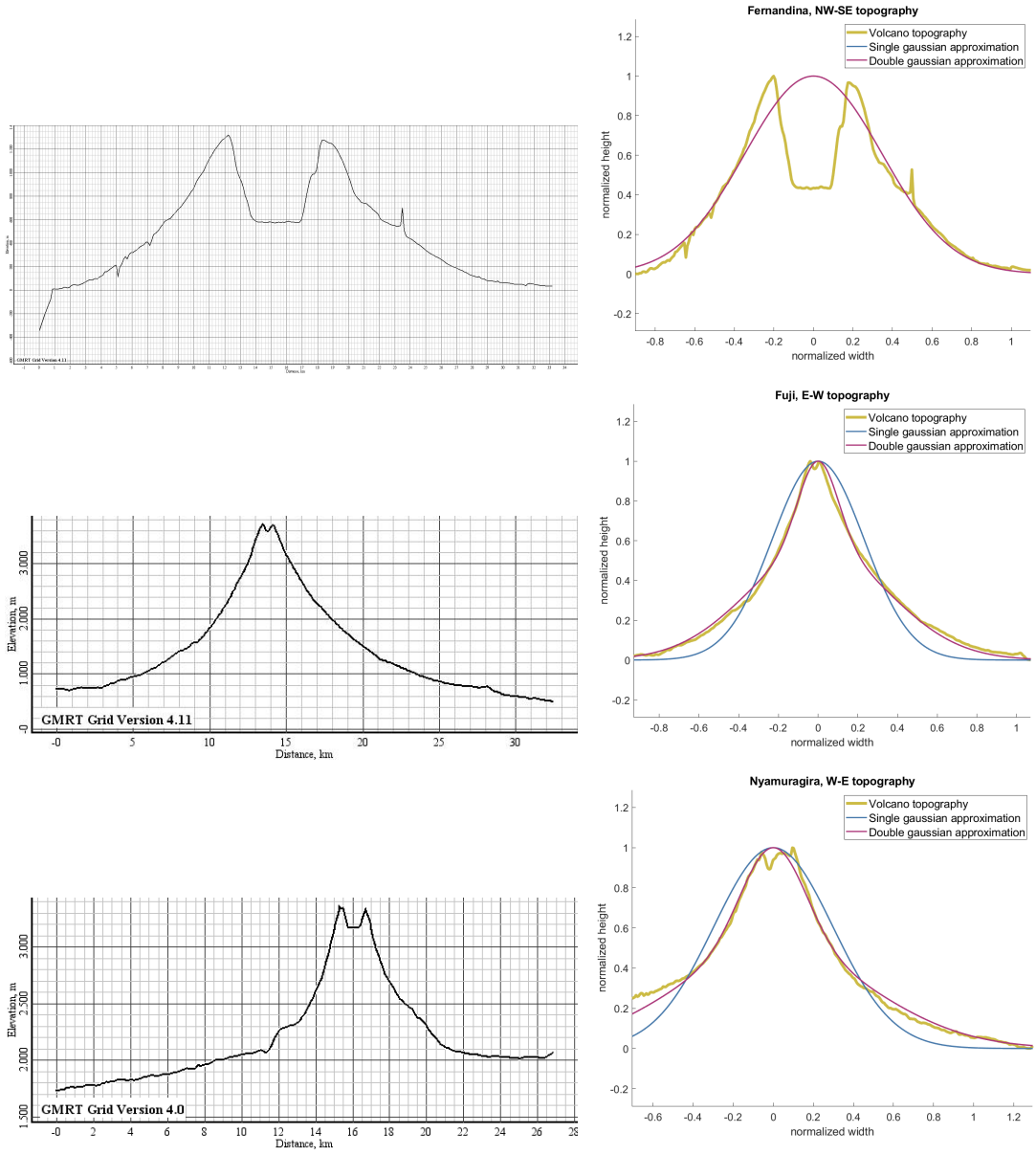

Figure 3.1: In this figure various edifice profiles, together with their Gaussian approximations, are shown. In contrast to the NyiraSE model and the approximations shown in 3.5, these topography profiles are not symmetrized.

I obtained volcano topography profiles through the GeomapApp profile tool (Ryan, 2009). An example is given in fig. 3.2, where the acquisition of the NW-SE profile of Nyiragongo is shown.

To trim the edges of the volcano profile while avoiding excluding part of the edifice, I implemented a code with a user interface: the code shows a plot of the volcano profile (fig. 3.3), and asks the user to click on the points that they consider as the endpoints of the left plateau and the beginning of the right plateau (indicated by the magenta dots in the figure). Points that fall outside the two margins provided as input are discarded, and the highland is subtracted, assigning the plateau height to zero.

The code then either provides the summit of the volcano (if it does not have a caldera) or the midpoint of the caldera, which will be considered the summit. An important note is that in my model the presence of a caldera and the resulting unloading is not included in the final approximation, but it would be a relevant addition to the model in the future. The residual topography is then split along the line identified by the apex point, and then symmetrized in two new topographies for each profile, mirroring the left and right flanks.

I approximated the new obtained symmetric topographies by minimizing the distance between the double (or single) Gaussian and the symmetric topography, using the *fminsearch* Matlab function. The full code for the procedure is given in Appendix A. As shown in fig. 3.5, some volcano edifices are better fit by a double Gaussian, especially when having steep flanks (like Mount Fuji or Etna) while other edifices are well-fitted by a single Gaussian (like Nyiragongo). Some other edifice I tested (like Nyamuragira) show a mixed shape, depending on the considered flank. All things considered, a symmetrical representation by means of a double Gaussian function is preferable to a single Gaussian, since it can be very helpful both in representing steeper volcanoes and in highlighting the Break-In-Slope area, which, as pointed out by Kervyn et al. (2009) and already discussed in sec. 1.3, is a significant hotbed for the opening of new eruptive vents. The values of the coefficients used for the approximation of axisymmetric edifice shown here are shown in table 3.1 for the A factor of the single Gaussian approximation functions, and in table 3.2 for the four factors of the double-Gaussian approximation functions.

As covered in sec. 2.5.1, the A parameter is fixed at the value of 1 by D. F. Mc Tigue (1987), but I have obtained greater A values with my topography approximation functions for a Gaussian-like topography. Even for a double Gaussian, the values for A_2 and B_2 (see 3.1) were greater than 1, especially for very steep flanks, which is a source of problems for the general solution of stresses. I underline that, though not specified by D. F. Mc Tigue (1987), the factor A and the aspect ratio are correlated variables.

The symmetrized S-E profile of Nyiragongo will be taken as a reference model to show further plots of subsequent analysis. For brevity, we will conventionally call this model **'NyiraSE'.** The choice of this profile as a template is justified by two factors:

- Its gentle topography and the absence of irregularities along the flank, which allows

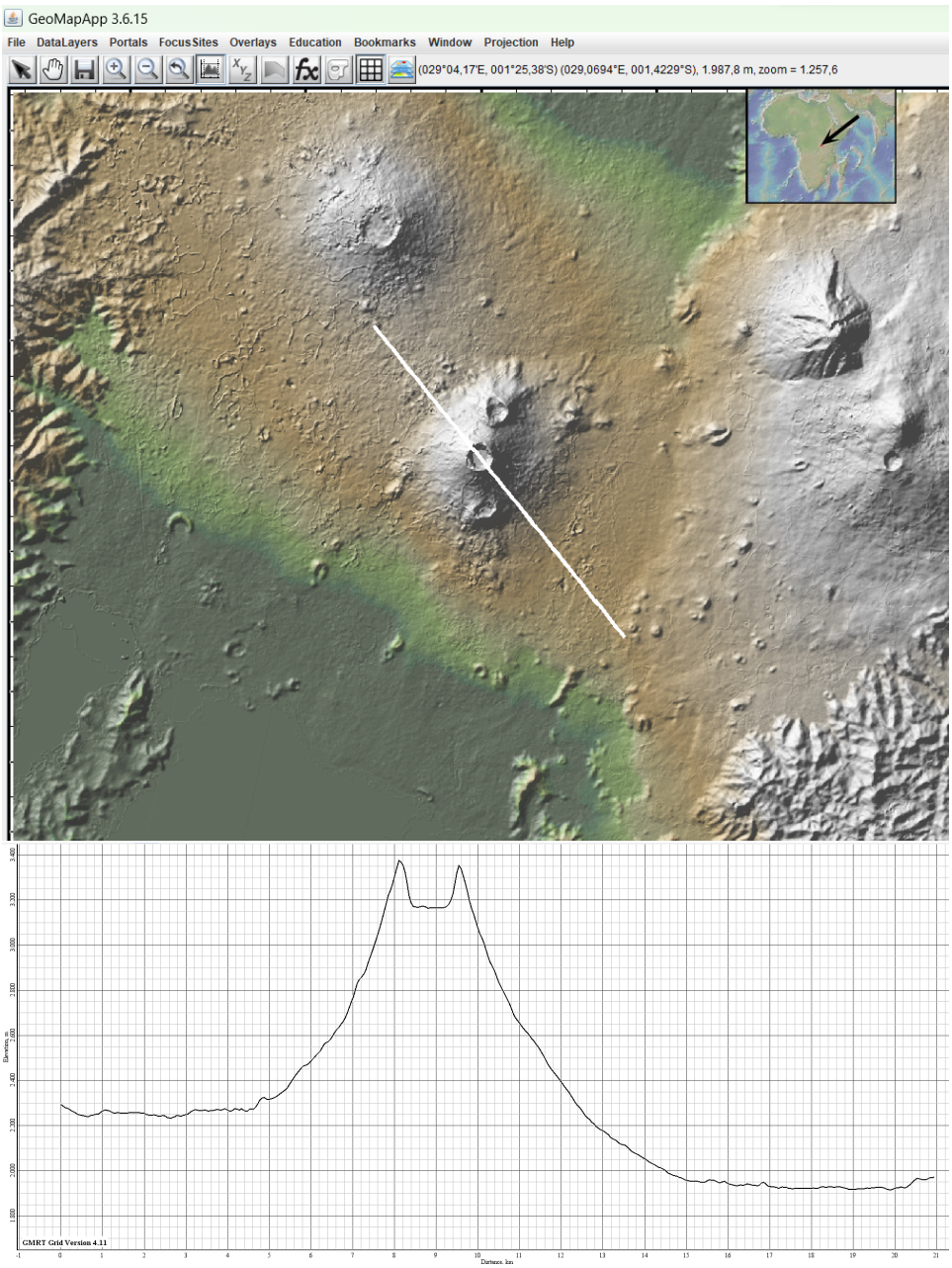

Figure 3.2: Nyiragongo NW-SE topography profile acquired with GeomapApp, Map view with the profile tool line and corresponding profile data (Ryan, 2009).

Gaussian factor	A
Nyiragongo NW	3.4
Nyiragongo SE	4.2
Fuji N	5.51
Fuji S	9.64
Etna NW	11.4
Etna SE	6.1

Table 3.1: Table summarizing the A factors for the single Gaussian approximation obtained for three case studies.

Double Gaussian factors	A_1	B_1	A_2	B_2
Nyiragongo NW	0.43	0.57	3.4	3.4
NyiraSE	0.26	0.74	11.9	3.1
Fuji N	0.21	0.79	38.7	4.05
Fuji S	0.51	0.49	55.7	2.92
Etna NW	0.57	0.43	56.13	2.6
Etna SE	0.40	0.60	86.6	2.6

Table 3.2: Table summarizing the four factors required for the double-Gaussian approximation obtained for three case studies. The symmetrized SE flank profile of Nyiragongo is chosen as reference model, and called NyiraSE.

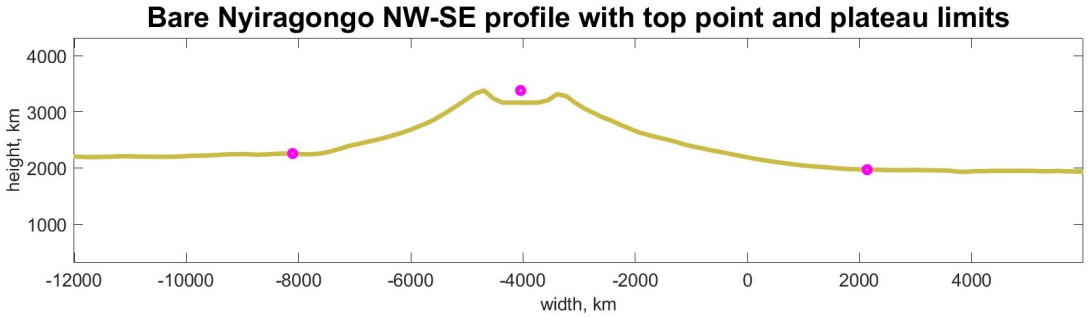

Figure 3.3: NW-SE topographic profile of Nyiragongo (DR Congo). Data obtained through the GeomapApp profile tool (Ryan, 2009). As a first step in constructing an axisymmetric topography, the user is asked to identify the start and end points of the edifice, i.e., where the plateau begins. In the figure, these points are highlighted in magenta, as is the apex of the volcano: the apex is identified as the point of maximum topographic height when the volcano does not have a caldera, while it is calculated as the midpoint between the two apexes if the volcano has a caldera.

for a good representation with a symmetrized double Gaussian;

- The special interest in the stress state below the S-E flank, in light of the eruptive events occurred in 2021 (See section 1.5.1)

3.2 Stress computing and dike propagation

3.2.1 Mesh generation

Numerical methods are achievable thanks to mesh building methods, which allow the creation and mapping of boundary elements. The meshing method used in this work is the Persson's meshing generation for implicit geometries (Persson, 2005). The code is open source and user-friendly, and based on the concept of the truss structure. Iteration after iteration, forces act on the points (nodes of the truss) while the topology (the edges of the truss) is adjusted by the Delaunay triangulation algorithm. A configuration is sought that balances a set of forces between the nodes of the mesh. This guarantees that the triangles building the mesh are as equilateral as possibile.

The shape of the mesh can be defined and modified thanks to a distance function $d(x, y)$; if, after the iterations, any node falls outside the desired geometry, it is removed. The remaining nodes will be the vertices of the mesh triangles. Corresponding edges,

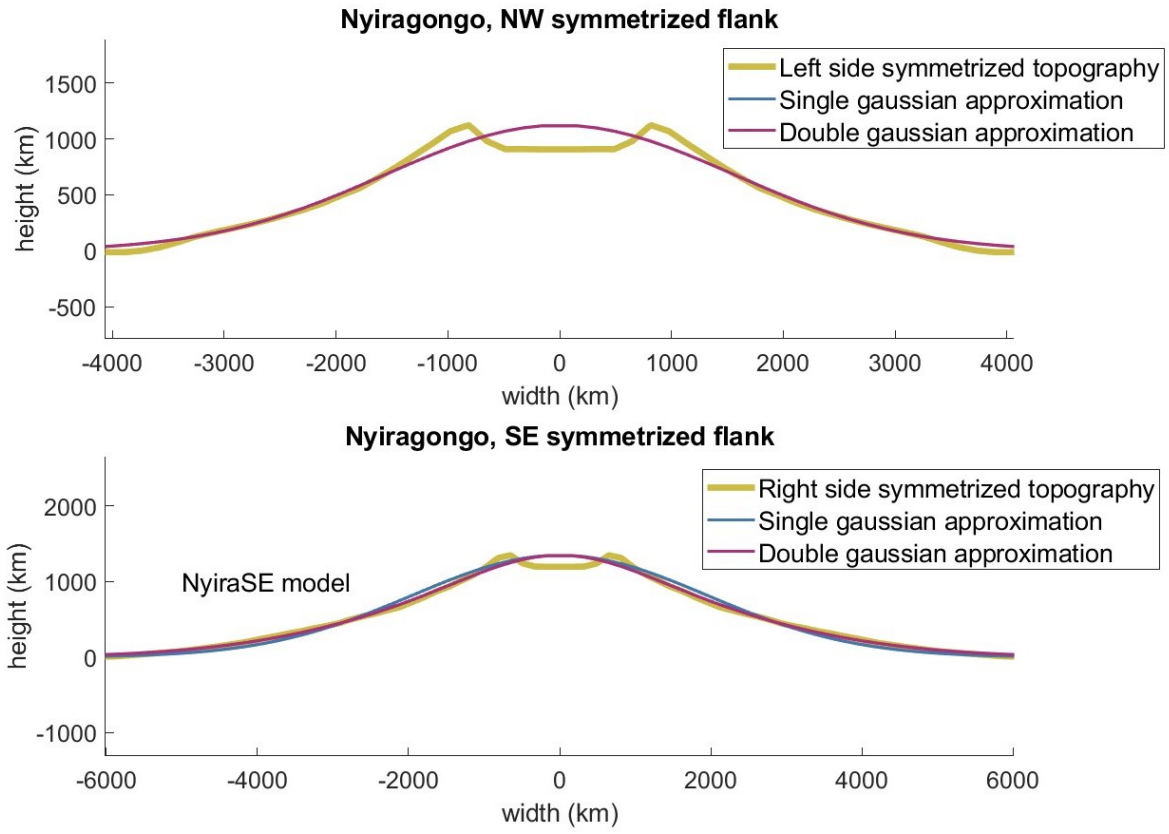

Figure 3.4: Nyiragongo (DR Congo) edifice, NW and SE symmetrized profiles, with Gaussian (blue) and double Gaussian (purple) approximation. Though the double Gaussian approximation seems to better fit the topography, even the single-Gaussian is acceptable for both flanks. We choose the second symmetrized and approximated topography in the figure as the reference model for further plots, naming it NyiraSE.

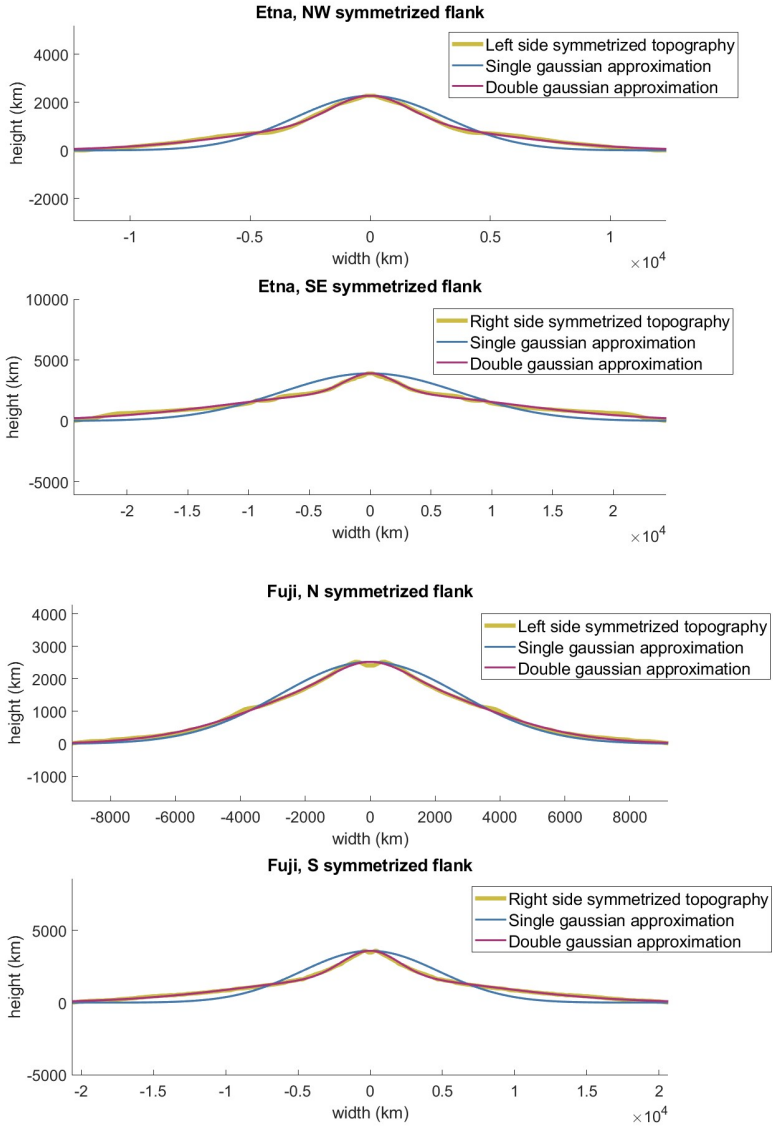

Figure 3.5: Etna (Italy) edifice, N-W and S-E symmetrized flanks, and Fuji (Japan) edifice, North and South symmetrized flanks. Approximations are Gaussian (blue) and double Gaussian (purple). For both the edifices, the single Gaussian function fails in approximating the symmetrized topography. This is probably due to Etna and Fuji great steepness. The double Gaussian approximations are though more accurate.

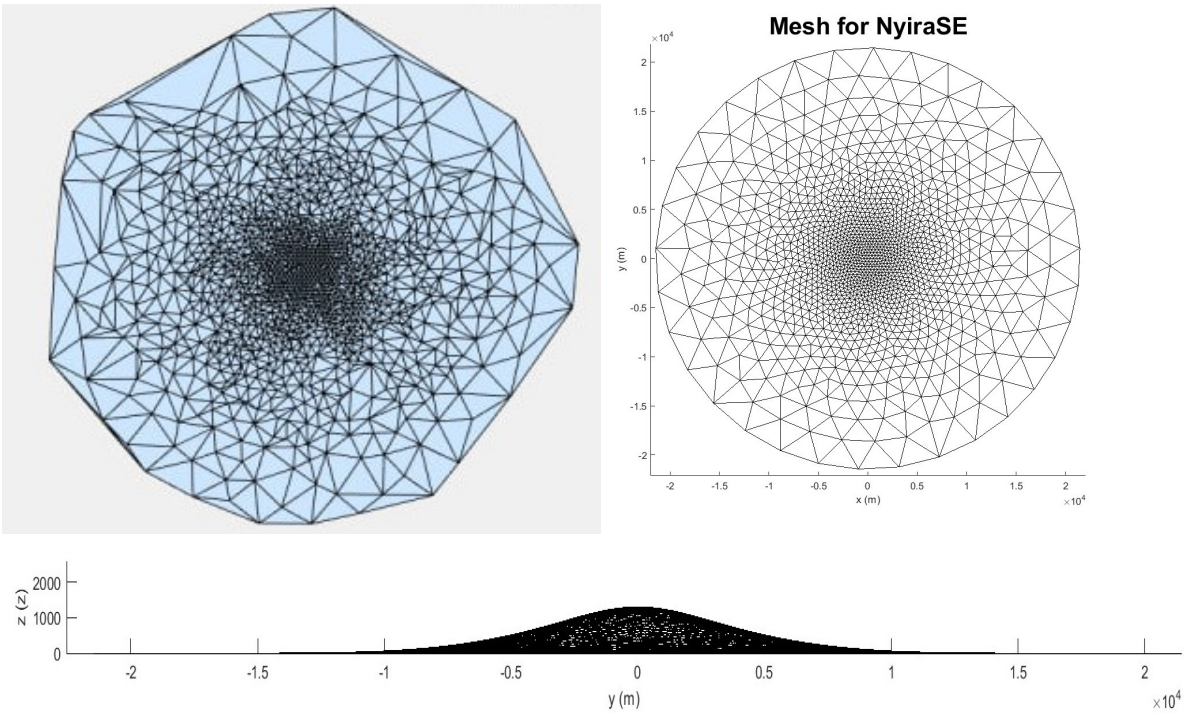

Figure 3.6: An example of one of the meshes used to compute stresses for NyiraSE, obtained thanks to the Davis (2021) Matlab package 'Cut and Displace'. The side of the triangles covering the central part of the volcano measure 300 m approximately. In the first panel, I show the appearance of the mesh at the beginning of the calculation, during triangle adjustment.

represented by couples of nodes, are stored; duplicates are removed. One of the used mesh for the NyiraSE model is represented in fig. 3.6.

3.2.2 Numerical stress solution

The numerical stress solution was obtained through the Cut & Displace Matlab package (Davis, 2017). This code is based on the analytical solutions for triangular dislocations by Nikkhoo and Walter (2015); it uses the Boundary Element Method (BEM), specifically the Displacement Discontinuity Method (DDM), and assumes the material is isotropic, linear elastic and that infinitesimal deformation applies. The half-space formulation is based on S. Martel and J. Muller (2000) (discussed in section 2.5.2). The 2D boundary element segments of that method become here the triangles of a 3D truss structure, constructed through Persson's mesh method. The stress due to loading is imposed, and displacements of the mesh elements (the triangular dislocations) are calculated in order

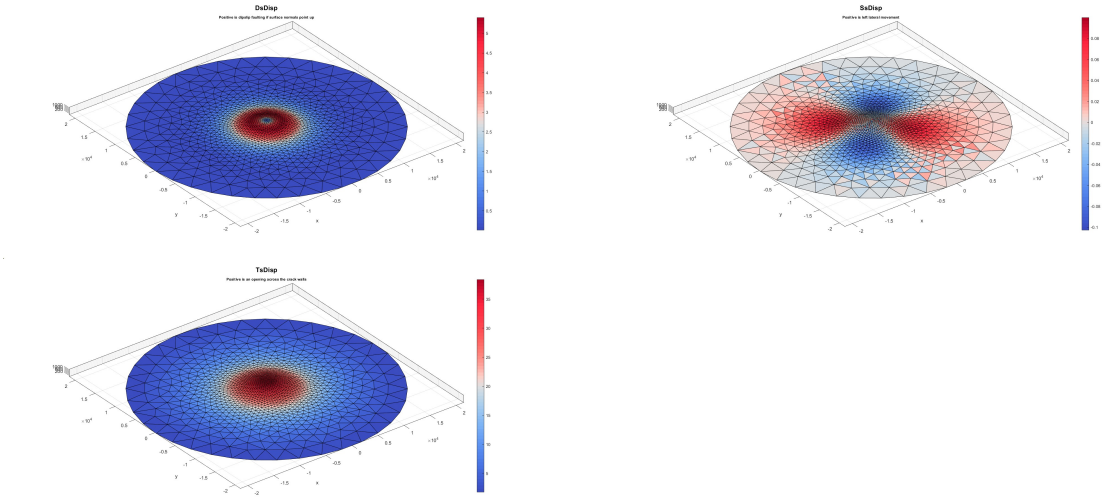

Figure 3.7: Isometric view of the three displacements directions for the NyiraSE model, obtained thanks to the Cut and Displace Matlab package (Davis, 2017), through the implementation of the meshing method by Persson (2005). In order to impose topographic loading while maintaining the free surface condition, the boundary elements by which the mesh is formed must displace to impose, on the crack, a stress that nullifies the tensile stress in the edifice. Here the three components of displacement are shown, respectively: dip-slip, strike-slip, opening (normal displacement with respect to the single boundary element plane).

to nullify the value of the stress on the free surface. An example of displacement of the mesh elements is shown in fig. 3.7. Each panel shows a displacement direction resulting from the application of the free surface boundary condition, respectively: Dip-Slip, Strike-Slip, and Normal to the boundary element surfaces.

3.2.3 Numerical solution validation

First, I compared my solution to the McTigue and Mei's solution, in order to validate the stress values obtained through the numerical method. The numerical solution for the stresses can be computed with both stress states:

- Completely lithostatic stress;
- Laterally confined stress.

The McTigue and Mei model, however, is defined just for the laterally confined case. (see eq. 2.5). The validation, achieved with the following standard values:

- $a = 1$ (exponent value in Eq. 2.6);

Magma density	2300 kg/m^3
Rock density	2850 kg/m^3
Poisson Ratio (ν)	0.25
Shear modulus (μ)	6x10^9 Pa

Table 3.3: Magma and encasing rock parameters.

- $\epsilon = \frac{h}{r} = 0.1$;
- $k = 0$ (Laterally confined case).

is shown in section components in fig. 3.9.

Oscillation near the free surface are due to the proximity of the observation points to the edges of the triangles which are my boundary elements. (see section 2.5.2)

3.3 SAM dike orientation and propagation

In this section I show how different imposed conditions for the stress field affects the propagation of SAM dikes.

SAM takes as input the stress and the topography shape, assuming homogeneous elastic parameters, and provides the trajectories of the dikes as output. The rock and magma parameters are summarised in table 3.3. I used SAM to create two types of plots: snapshots that show the starting configurations of a grid of pennies distributed within the edifice, and entire propagation trajectories of a few pennies. The first type of plot is a simple way to show the orientation of principal stress axes in the edifice: the pennies always lie, by definition, on the plane perpendicular to σ_3. The second type of plot adds information regarding the gradients of σ_3, which is what 'pushes'the pennies in one direction or another, together with the buoyancy effect. In this type of plot, by convention, I consider to be erupted all the dikes that reach a depth below the surface equal to or less than the sides of the triangles that make up the mesh. In the case of the meshes used in the following plots, this size is about 300 m.

3.3.1 Loading

As the simplest case of study, I present a state of lithostatic stress disturbed by a loading due to volcano topography. To do so I built an axisymmetric volcano shaped as the SE flank of Niyragongo: NyiraSE.

In fig. 3.10, I show the stress values for this case with the lithostatic stress contribution removed. The top of the volcano has the most intense stress because what is shown is only the stress exerted by the boundary elements on the edifice below. This stress is what holds the edifice together by compensating for the tensile stress resulting from the

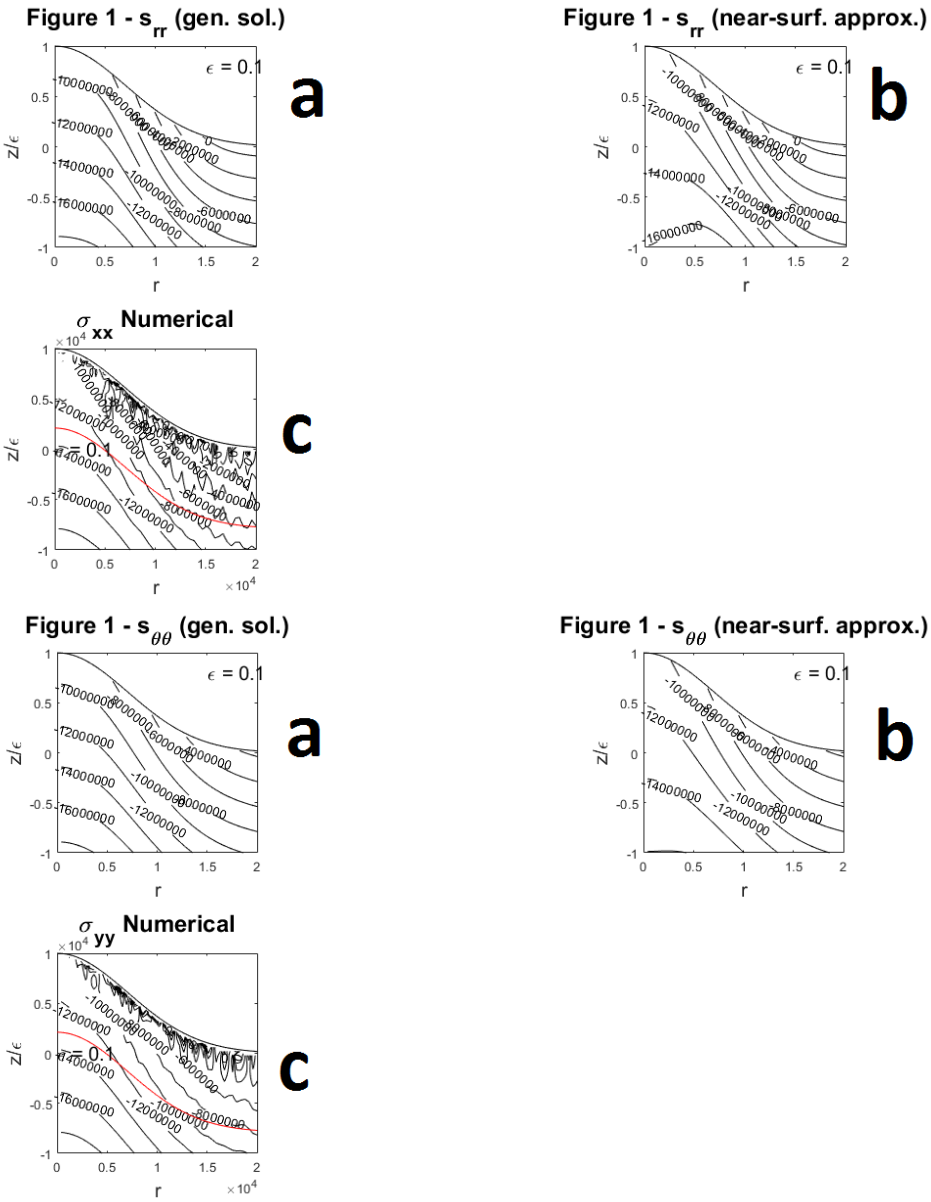

Figure 3.8: x-z plane sections showing values for the σ_{xx} and the σ_{yy} stress components. McTigue and Mei method gives two outputs: one for the Analytical solution (a), and another one for the near-surface approximation (b). The third output shows the numerical solution (c). In (c), values at depth match the values at depth in (a). The oscillations near the free surface can be then replaced with near surface values given by (b).

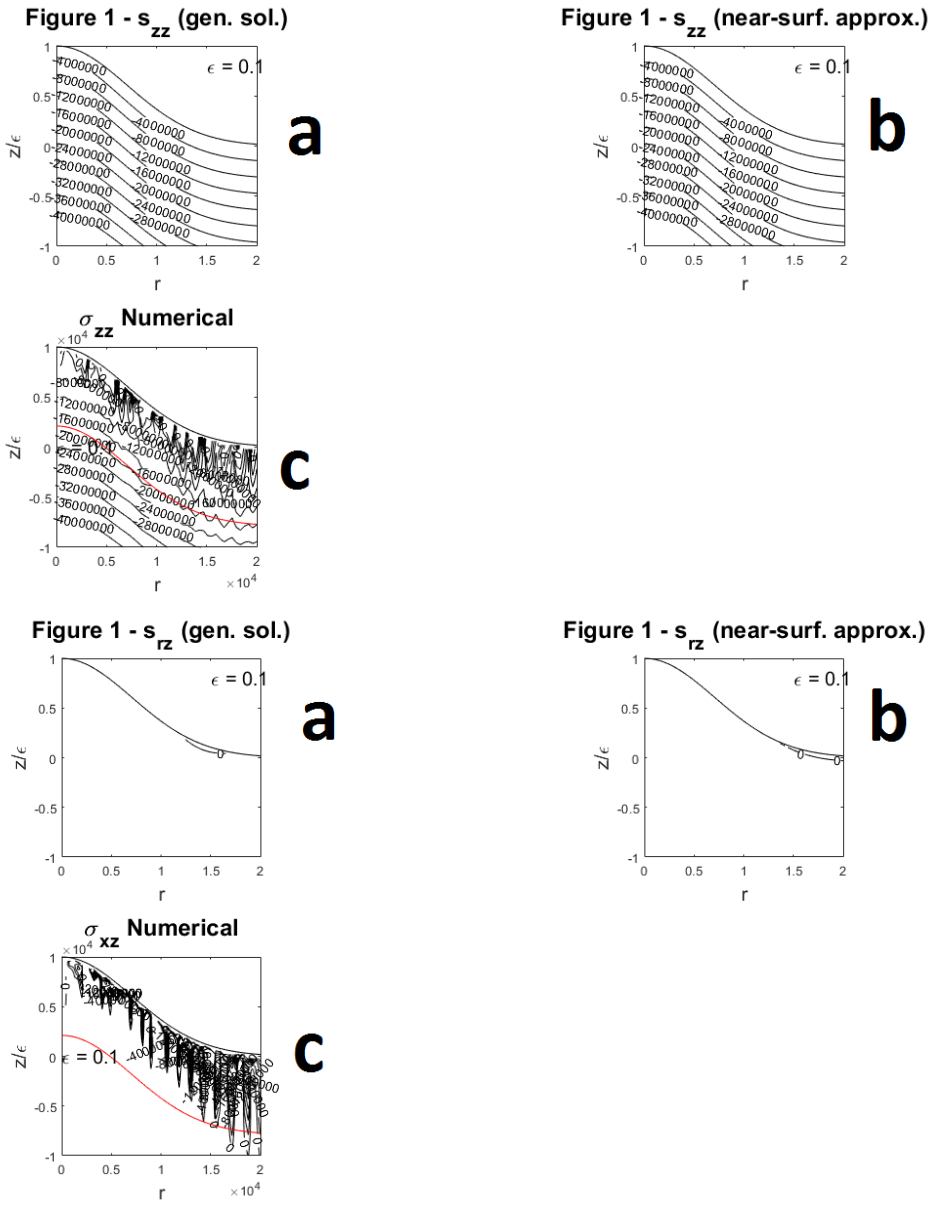

Figure 3.9: x-z plane sections showing values for σ_{zz} and σ_{xz} stress components. McTigue and Mei method gives two outputs: one for the Analytical solution (a), and another one for the near-surface approximation (b). The third output shows the numerical solution (c). In (c), values at depth match the values at depth in (a). The oscillations near the free surface can be then replaced with near surface values given by (b).

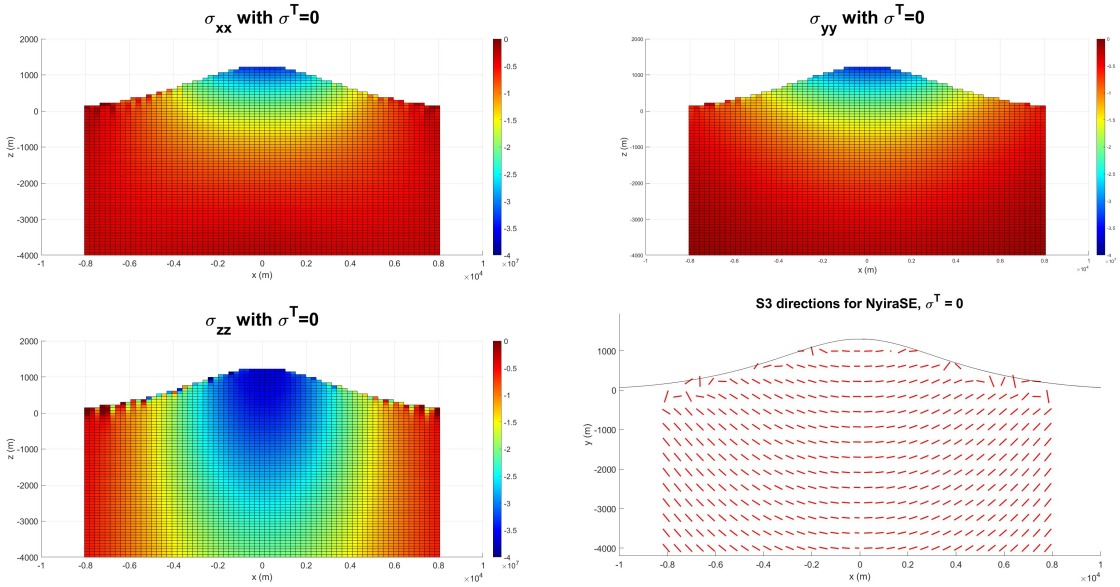

Figure 3.10: NyiraSE model, σ_{xx}, σ_{yy}, σ_{zz} components due to a topographic loading, plotted for NyiraSE. Note: The the stresses shown are without the contribution of lithostatic stress. The last panel is a representation of the directions of σ_3.

(not shown) lithostatic stress (see section 2.5.2 for more details on the method). The orientation of σ_3 is unchanged if lithostatic stresses are removed. In fact, the lithostatic stress is isotropic, so its removal results in an isotropic variation of σ_3, not affecting its orientation.

In figure 3.11 I show the orientation of the SAM pennies, which reveal the orientation of σ_3. From the figure, it is evident that these dikes are arranged circumferentially around the edifice, and not radially, as we would expect from other studies (Valerio Acocella (2006), Chadwick Jr and J. Dieterich (1995)). I would like to point out that σ_{xx} and σ_{yy} are similar in intensity. This means that the displayed dike orientation may be changed easily if an additional contribution to stress becomes active.

In figure 3.12 and 3.13 I show the propagation of SAM dikes for the case of stress due to loading, for the model NyiraSE, respectively starting from a depth z = 500 m and z = -5000 m. The dikes are arranged circumferentially, as already shown through the orientation of the SAM pennies within the edifice. Dike starting inside the edifice and then propagating downward stop propagating at a z absolute value comparable to the volcano height. Dike propagating upward from below the edifice tend to be attracted by the edifice, as previously found by J. R. Muller, Ito, and S. J. Martel (2001) and then confirmed by Maccaferri, Bonafede, and Eleonora Rivalta (2011).

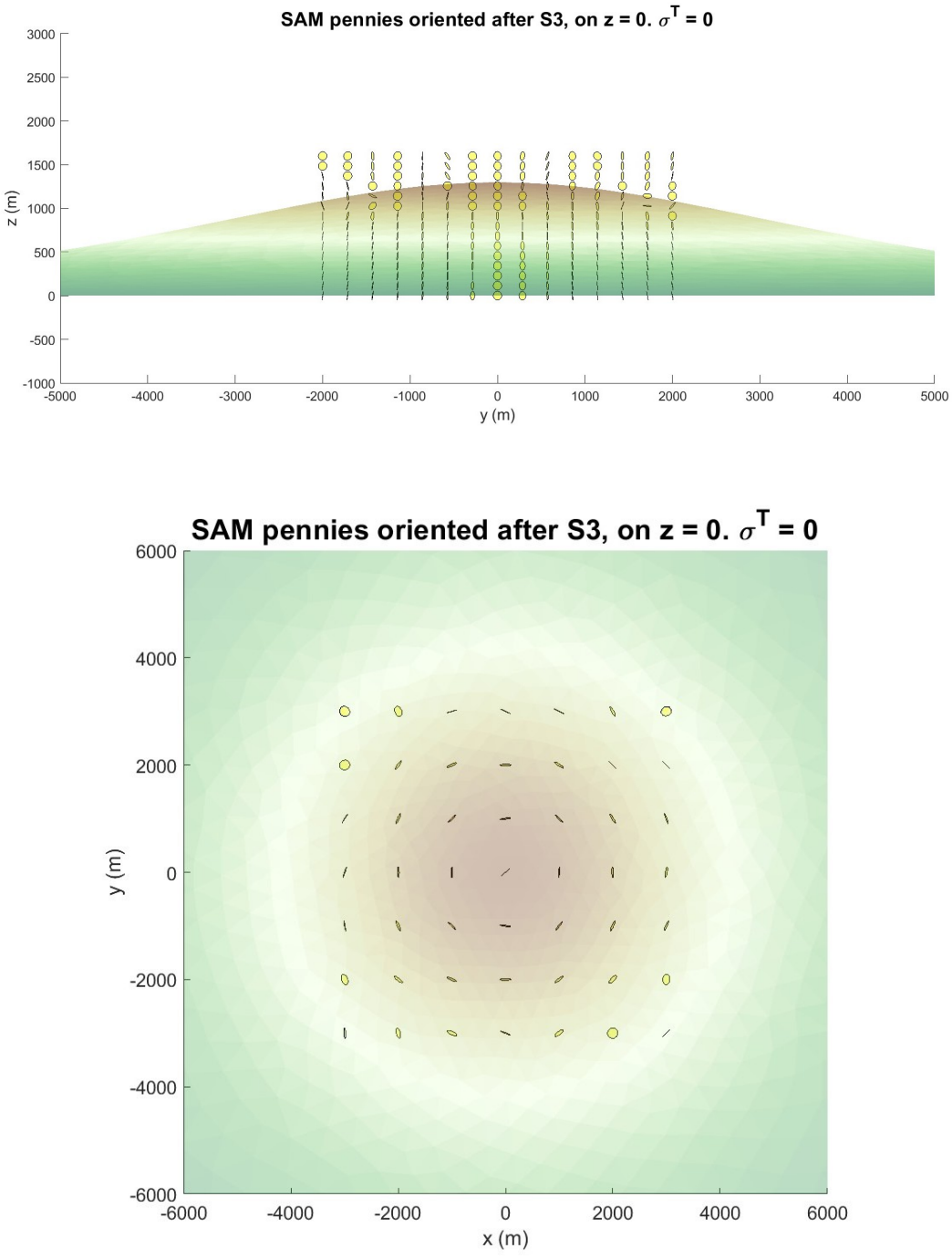

Figure 3.11: SAM pennies oriented perpendicular to $\sigma 3$, side view and view from above of the NyiraSE model.

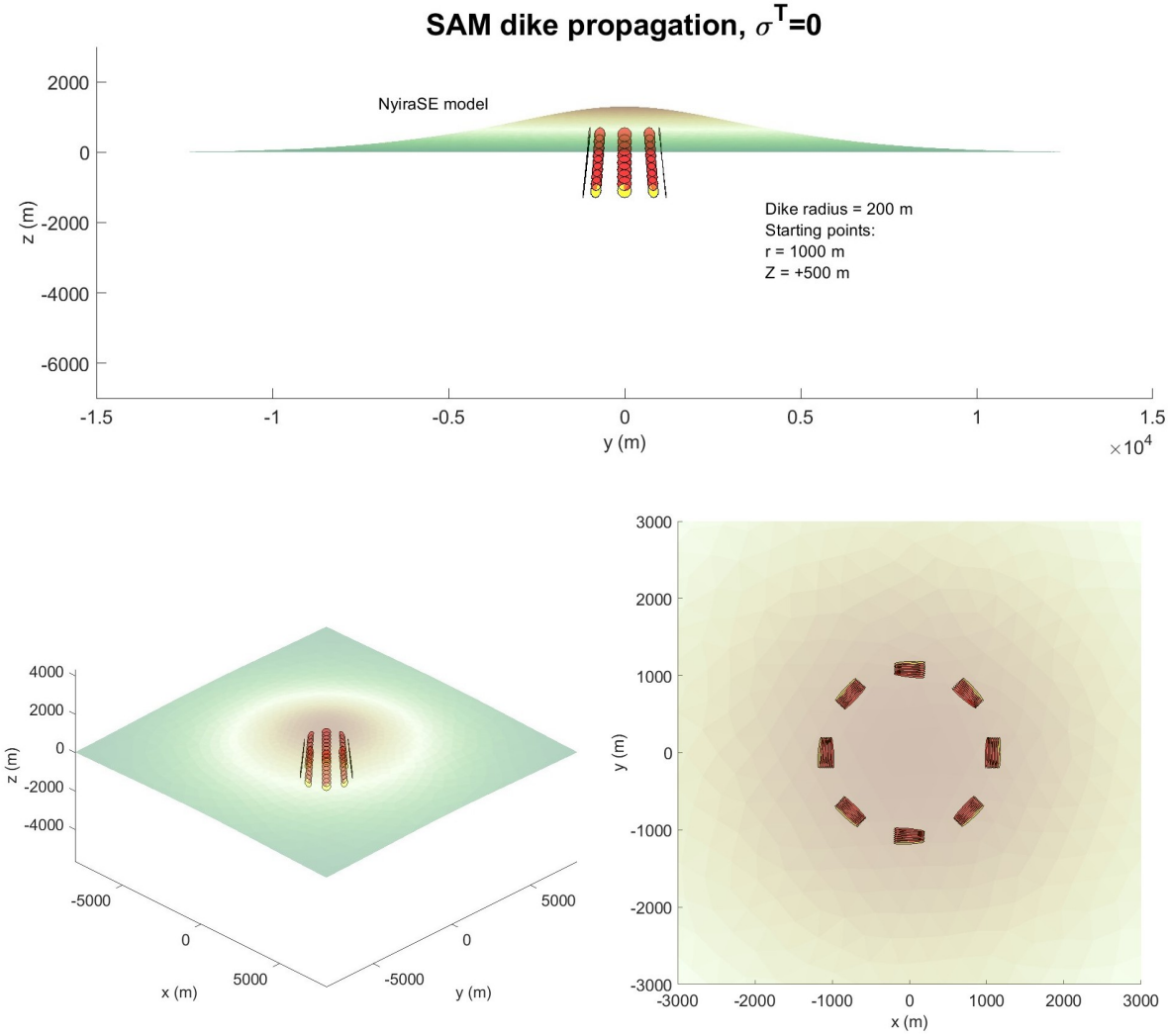

Figure 3.12: NyiraSE model, propagation of SAM dikes starting inside the edifice at z = +500 m. The final penny is coloured yellow. The dikes propagate downward driven by the stress due to loading. They show a circumferential orientation.

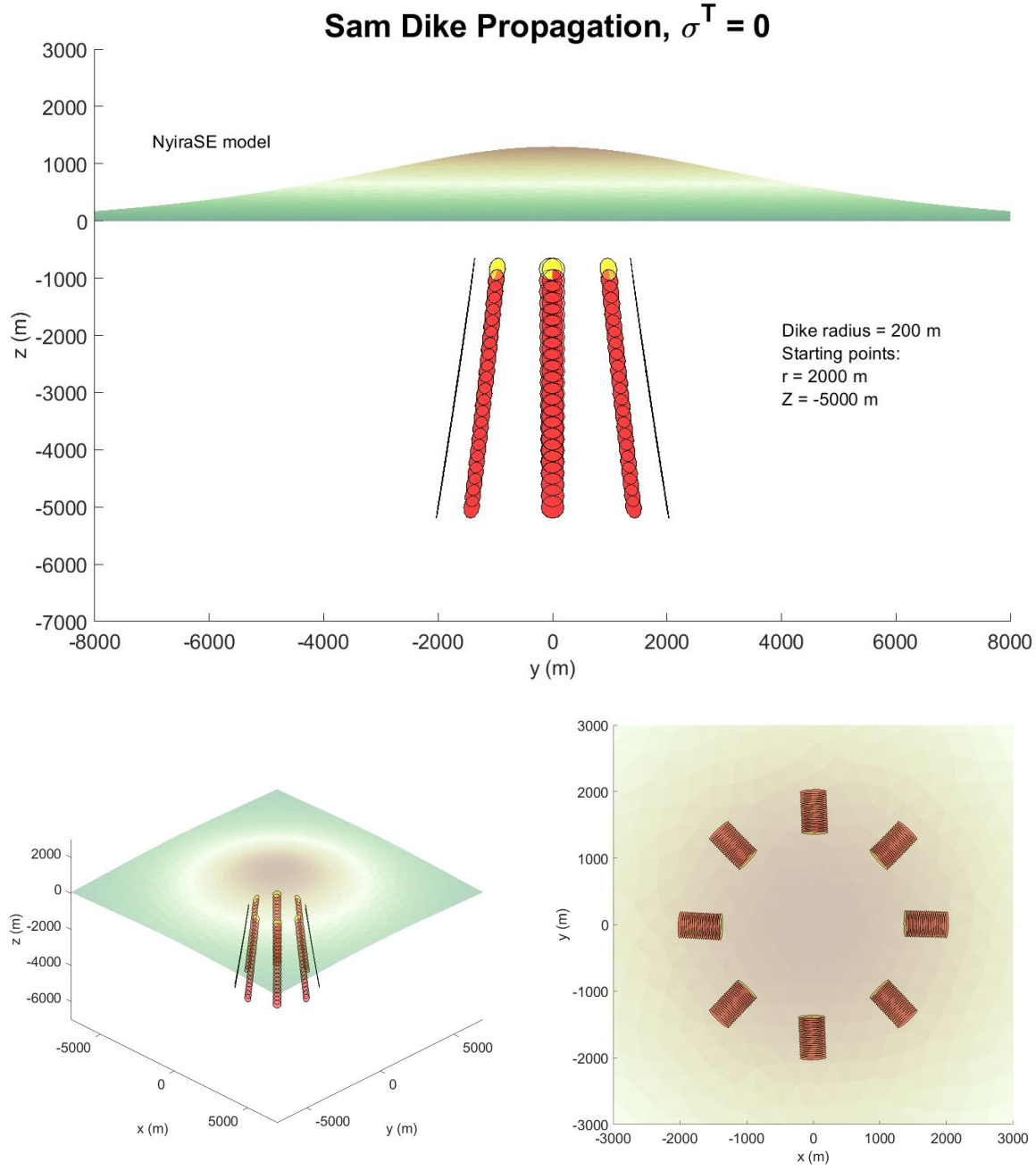

Figure 3.13: NyiraSE model, propagation of SAM dikes starting below the edifice at at z = -5000 m. The final penny is coloured yellow. The dikes propagate towards the edifice, attracted by the loading, but then halt about at z=-1000 m. The dikes show a circumferential orientation.

3.3.2 Adding the tectonic stress

In order to make the simulation more realistic, I added the tectonic stress factor to the equation:

$$\sigma^{Tot} = \sigma^{Background} + \sigma^{Loading} + \sigma^{Tectonic} \tag{3.2}$$

Specifically, I worked with a tectonic stress of 5MPa, along the x direction. The tectonic stress must be imposed together with the loading, imposing the tectonic stress after the numerical model calculations would violate the free-surface condition below the mesh.

In fig. 3.14, plots of the x component of the stress in the Y-Z plane, before and after the application of a stress equal to 5MPa along the x axis, are compared for the NyiraSE model. Upon application of tectonic stress, the reduction of the value of the compressive stress in the x-direction is evident. Again, these plots are deprived of the background lithostatic stress, to better show the influence of loading and of tectonic stress.

In fig. 3.15 are the SAM pennies. The strong influence of tectonic stress causes all the pennies to align perpendicular to the x-axis, the direction on which tectonic stress is applied.

In figures 3.17 and 3.16 I show the propagation of SAM dikes in the stress field influenced by loading and tectonic stress, with propagation starting from z = 500 m and z = -5 km, respectively. In both cases, the dikes head to the surface with a nearly vertical dip angle. At a z absolute coordinate value comparable to the edifice height, they deflect toward the base of the volcano. When dikes are propagated from inside the edifice, they propagate downward, but then deviate to return to the surface again, and erupt at the base of the volcano flanks. The deviation from their initial trajectory probably occurs because, at a certain depth with respect to the origin (in our case about equal to the height of the volcano), the influence of loading on the stress field becomes weaker, and the dikes will therefore tend to sense regional stress, and their buoyancy will be more efficient in leading them towards the surface. In both cases, the dike orientation is almost exclusively determined by the orientation of the tensile tectonic stress.

3.3.3 Making stress isotropic

As already discussed, stress tends to become more and more homogeneous and isotropic under volcanic edifices as intrusions repeatedly cut through the edifice and are emplaced. To properly account for this, I used a function to make the stress closer to an isotropic state. Since the vertical stress must be equal to the overburden, then the isotropic part of the stress will be a diagonal tensor with the overburden on the diagonal elements. Thus, given the total stress as eq. 3.2, I decompose the total stress tensor in two addends:

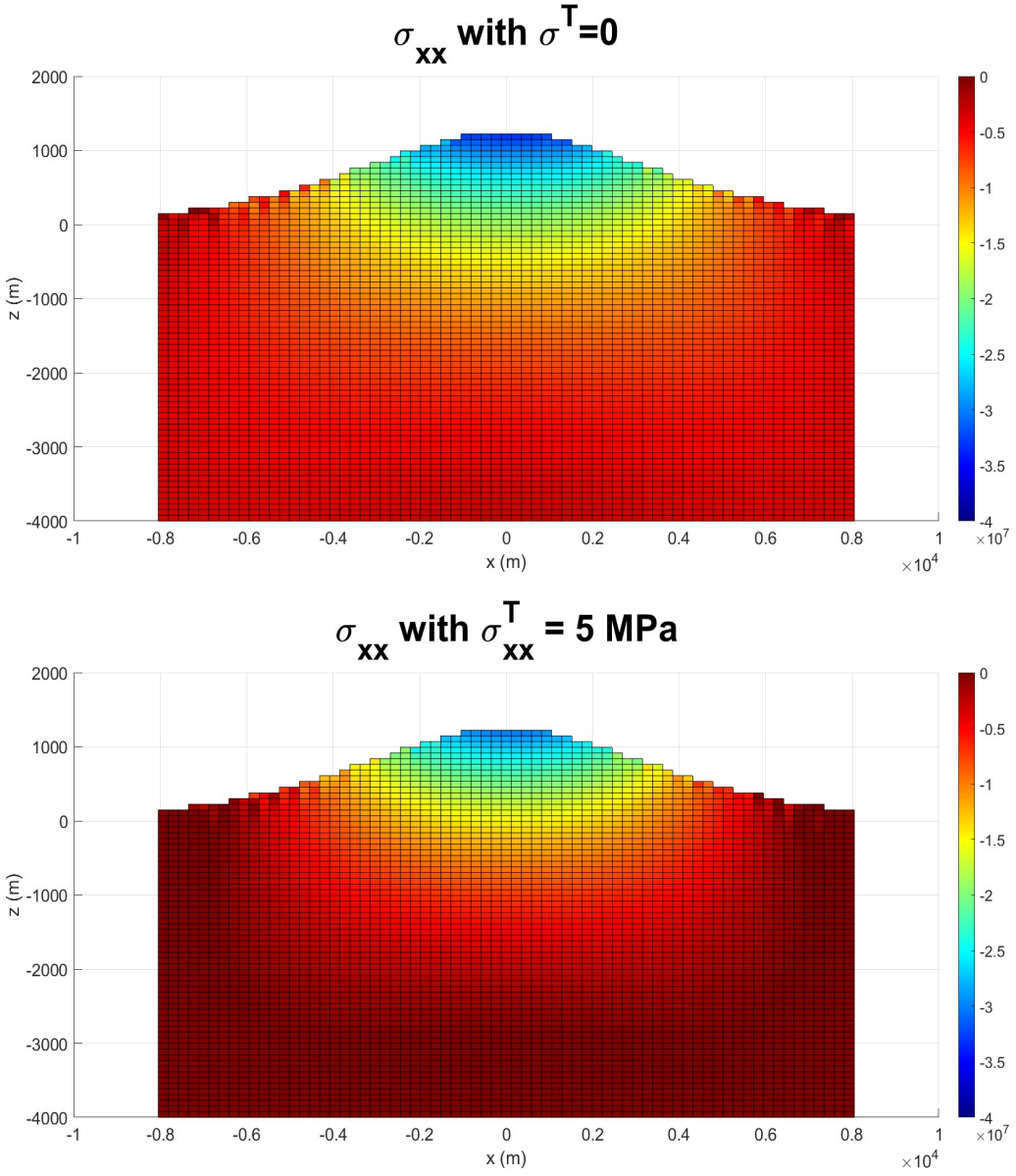

Figure 3.14: NyiraSE model, σ_{xx} component shown without and with the application of a tectonic stress acting along the x-axis, equal to 5 MPa. Note: The the stresses shown are without the contribution of lithostatic stress to highlight the effect of loading and tectonic stress.

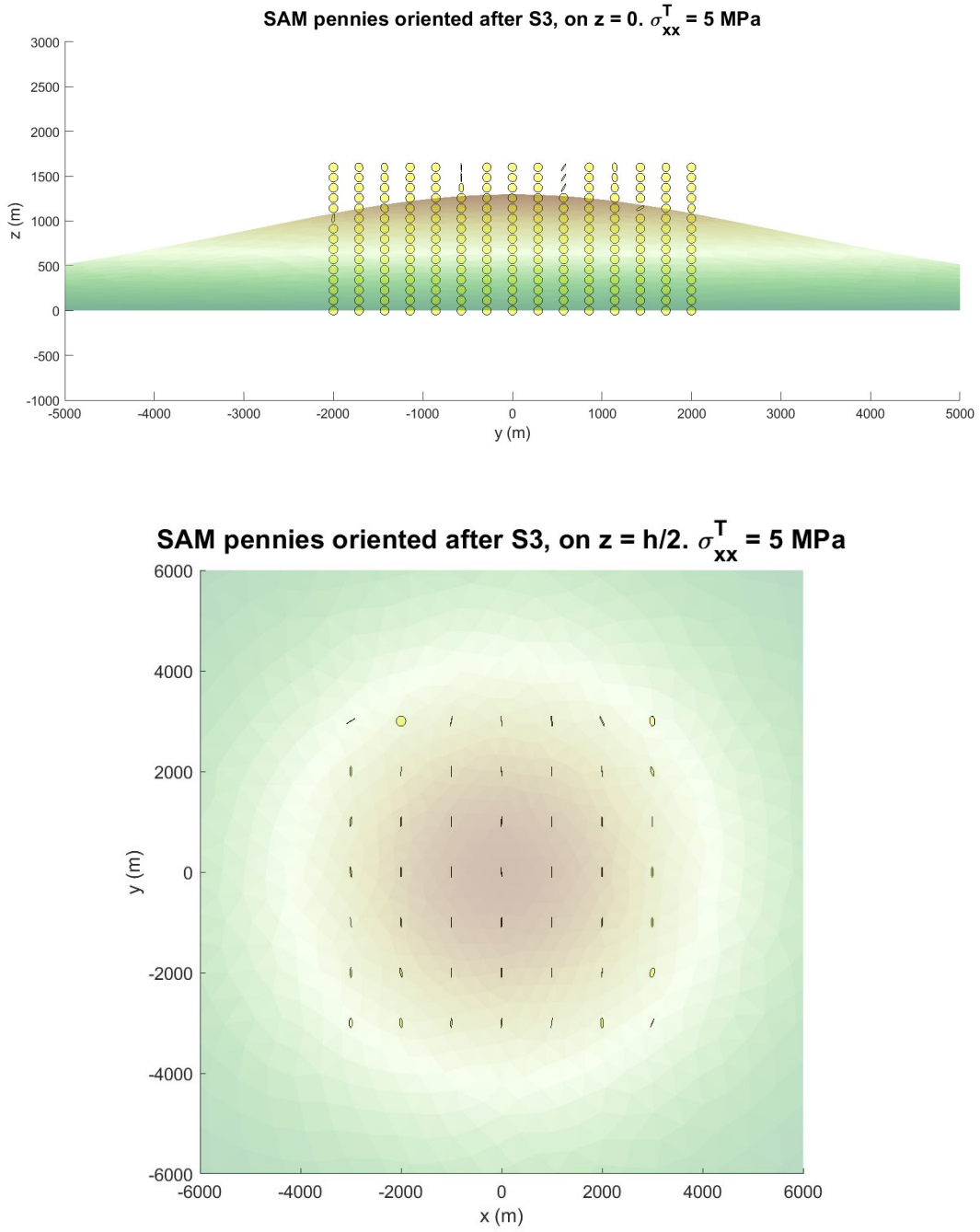

Figure 3.15: SAM pennies, side view and view from above of the NyiraSE model, with a tectonic stress of 5 MPa applied along the x direction.

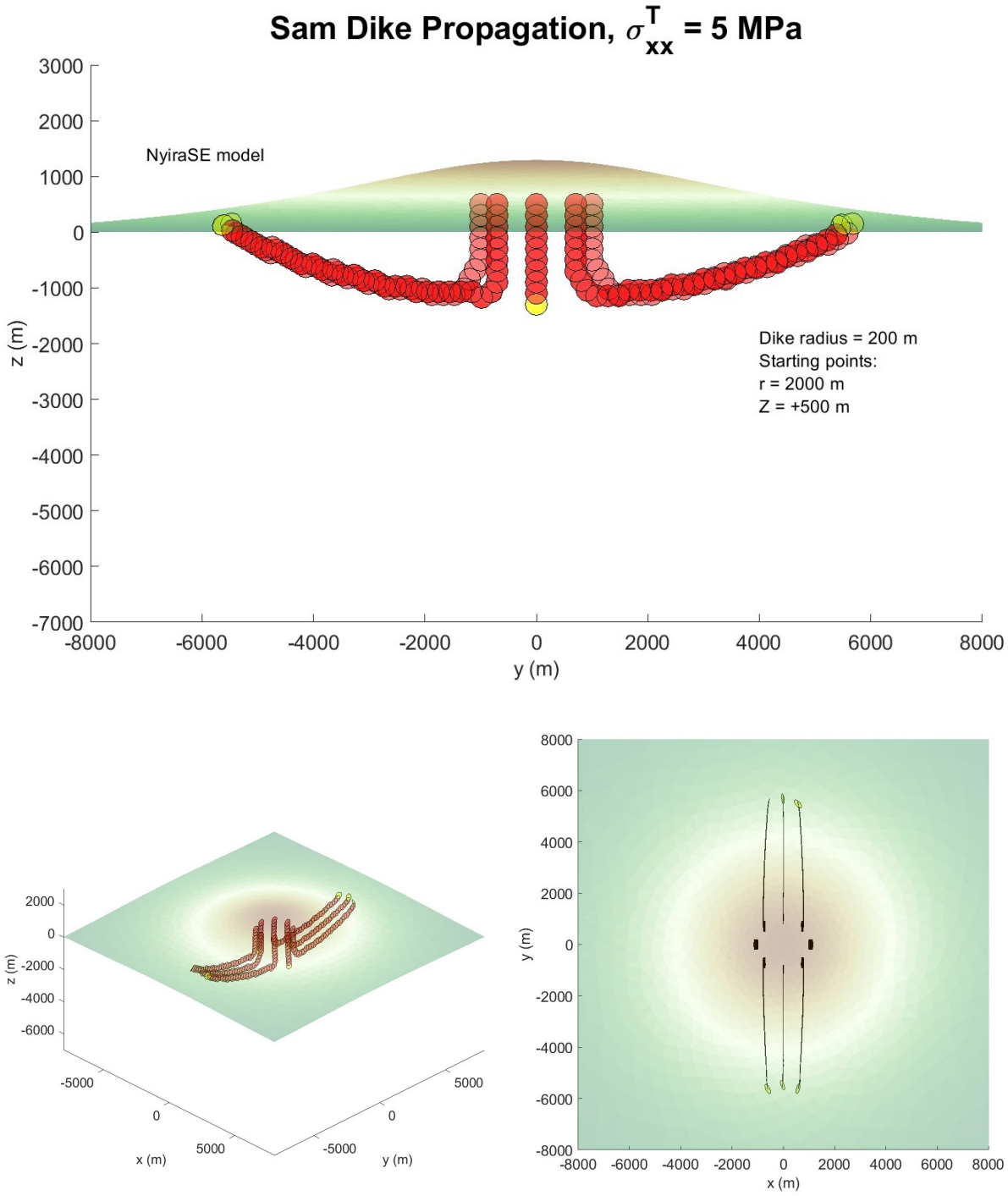

Figure 3.16: NyiraSE model, propagation of SAM dikes starting inside the edifice at z = +500 m. The final penny is coloured yellow. The dikes orient perpendicularly to the tectonic stress tensile stress and propagate downward driven by the edifice loading. Then they drift up again toward the less steep part of the flanks.

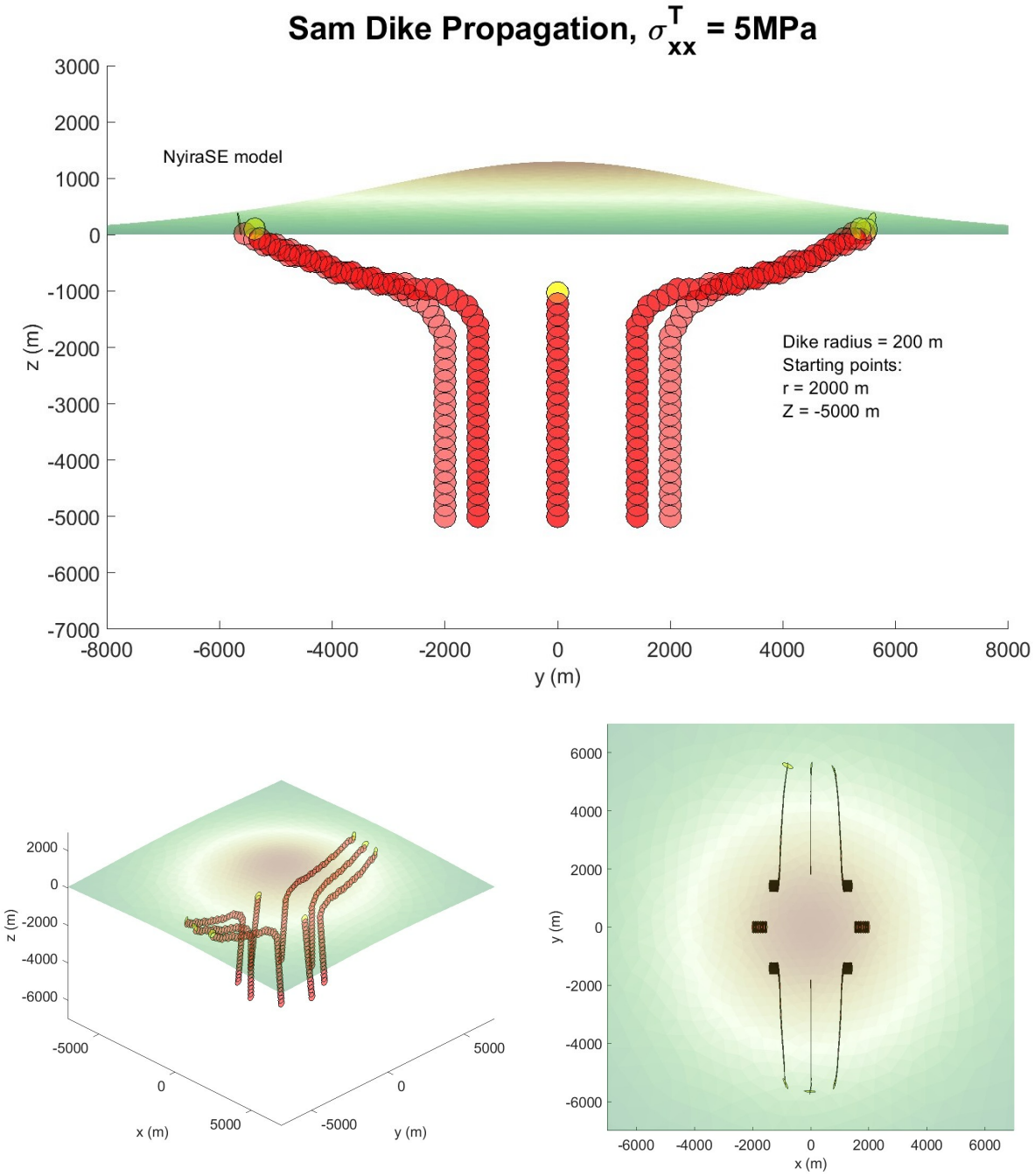

Figure 3.17: NyiraSE model, propagation of SAM dikes starting below the edifice at z = -5000 m. The final penny is coloured yellow. The dikes propagate upward and then drift toward the less steep part of the flanks. In their whole path, they orient perpendicularly to the tectonic tensile stress.

$$\begin{pmatrix} \sigma_{xx} & \sigma_{xy} & \sigma_{xz} \\ \sigma_{yx} & \sigma_{yy} & \sigma_{yz} \\ \sigma_{zx} & \sigma_{zy} & \sigma_{zz} \end{pmatrix} = \begin{pmatrix} \sigma_{zz} & 0 & 0 \\ 0 & \sigma_{zz} & 0 \\ 0 & 0 & \sigma_{zz} \end{pmatrix} + \begin{pmatrix} \sigma_{xx} - \sigma_{zz} & \sigma_{xy} & \sigma_{xz} \\ \sigma_{xy} & \sigma_{yy} - \sigma_{zz} & \sigma_{yz} \\ \sigma_{zx} & \sigma_{zy} & 0 \end{pmatrix} \tag{3.3}$$

Where $\sigma_{xy} = \sigma_{yx}$, $\sigma_{xz} = \sigma_{zx}$ and $\sigma_{yz} = \sigma_{zy}$. Multiplying the second addend by a factor k_2, the degree of isotropization can be controlled, obtaining a new, isotropized, stress tensor σ_{ij}^{iso}:

$$\begin{pmatrix} \sigma_{xx}^{iso} & \sigma_{xy}^{iso} & \sigma_{xz}^{iso} \\ \sigma_{yx}^{iso} & \sigma_{yy}^{iso} & \sigma_{yz}^{iso} \\ \sigma_{zx}^{iso} & \sigma_{zy}^{iso} & \sigma_{zz}^{iso} \end{pmatrix} = \begin{pmatrix} \sigma_{zz} & 0 & 0 \\ 0 & \sigma_{zz} & 0 \\ 0 & 0 & \sigma_{zz} \end{pmatrix} + k_2 \begin{pmatrix} \sigma_{xx} - \sigma_{zz} & \sigma_{xy} & \sigma_{xz} \\ \sigma_{xy} & \sigma_{yy} - \sigma_{zz} & \sigma_{yz} \\ \sigma_{zx} & \sigma_{zy} & 0 \end{pmatrix} \tag{3.4}$$

In this way:

- for $k_2 = 0$, the stress is completely isotropic;
- for $k_2 = 1$, the stress is laterally confined;
- for $0 < k_2 < 1$, the stress takes intermediate values between the two endpoints.

I apply the procedure just described to a case with tectonic stress, with $k_2 = 0.5$. Exactly as in the case of tectonic stress application, the dikes are oriented perpendicular to the x-axis (axis of tectonic stress application). If propagated within the edifice (with a starting point $z > 0$), they move downward, as shown in fig. 3.18, and upward if propagated from depth (with a starting point $z < 0$), as in fig. 3.19. In both cases, they deflect their trajectory to head toward the surface to erupt at the base of the volcano. A slight difference lies in the turning point z coordinate, which is shallower in the case of dikes propagated inside the edifice (see fig. 3.16), while the ascent seems gentler for the case of dikes propagated from deeper levels.

3.4 The case of the elongated edifice

Subsequently, I investigate the case of an edifice with an elliptical base. The purpose of creating such a case is to investigate whether the circumferential orientation of the dikes found for an axisyemmtric edifice can be modified by this shape variation. For this case I only show, in fig. 3.20, the plots for σ_3, along with the propagations of the dikes starting inside the edifice ($z > 0$) and at depth ($z < 0$). Indeed, we find that the edifice shape influences the orientation of the SAM pennies. Although tectonic stress has not been imposed, the pennies tend to orient perpendicularly to the major axis of the elliptic edifice.

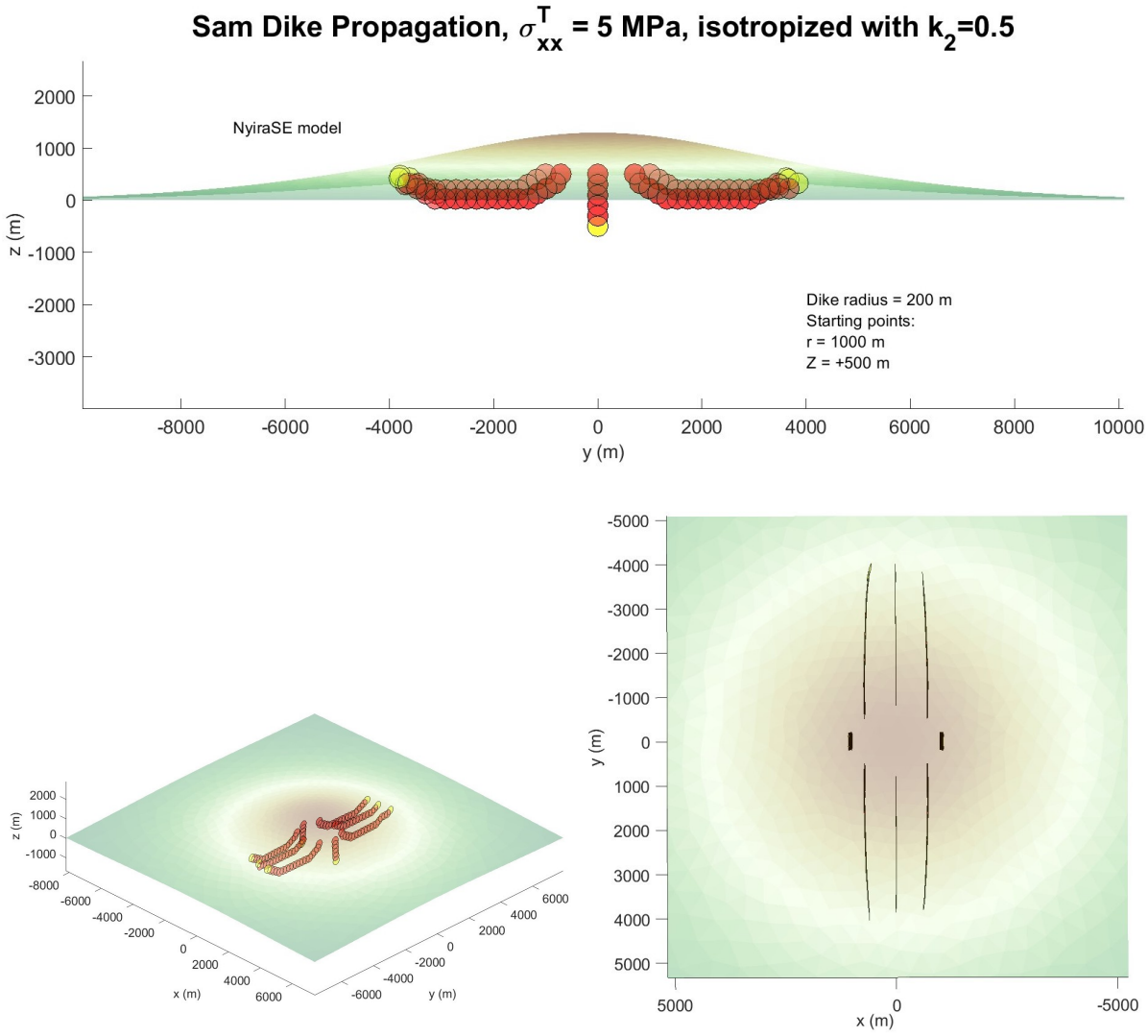

Figure 3.18: SAM dike propagation for an isotropized state of stress including loading and tensile tectonic stress, the latter applied along the x axis. When dikes are propagated from inside the edifice (z=500m) they migrate downward and then turn to erupt at the volcano base. The difference between this propagation and the one seen for non-isotropized tectonic stress is that, in this case, dikes turn their path at a shallower depth, inferior to the volcano height.

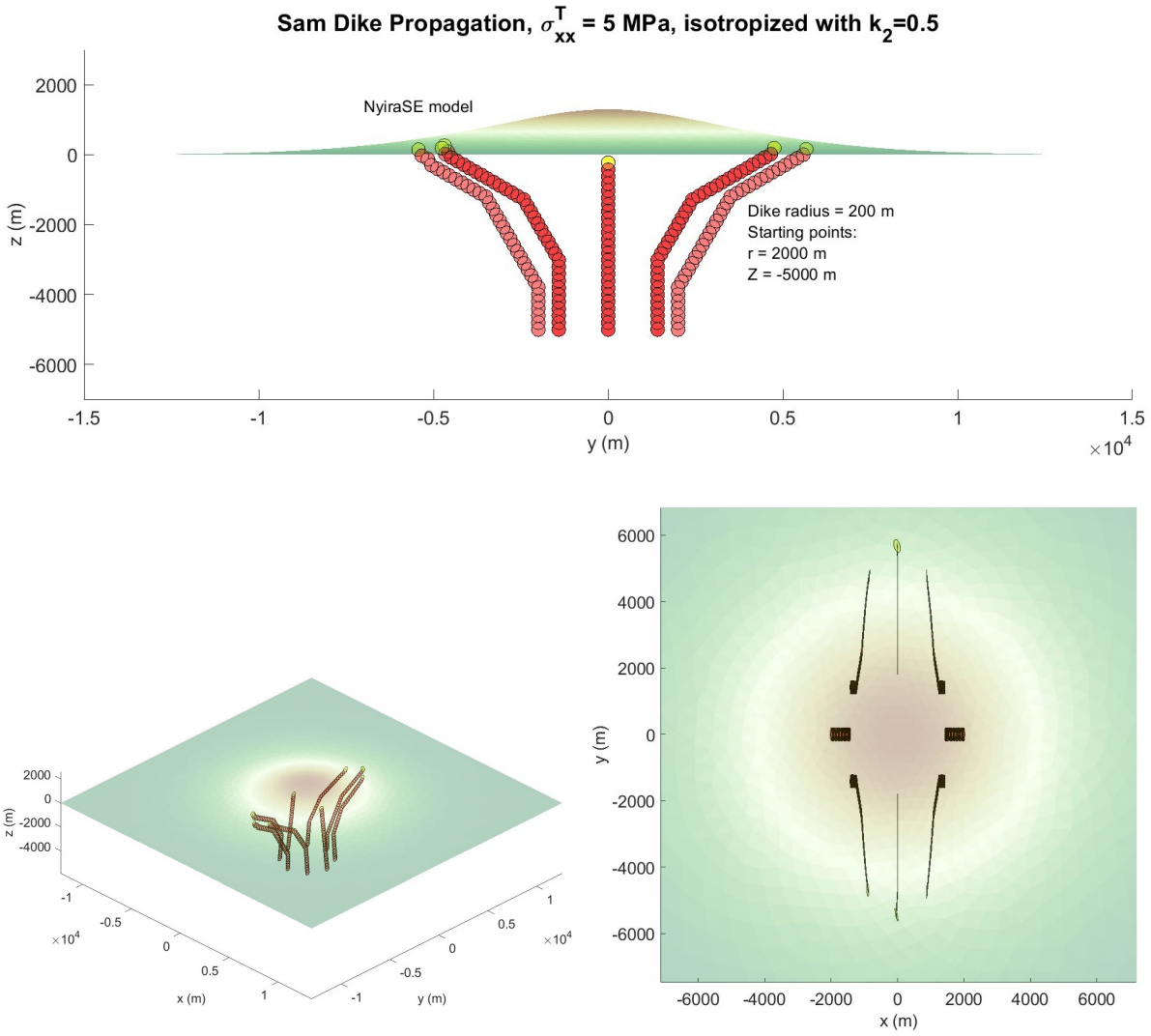

Figure 3.19: SAM dike propagation for an isotropized state of stress including loading and tensile tectonic stress, the latter applied along the x axis. When dikes are propagated below the edifice (z = 500 m) they migrate perpendicularly to the surface, but then turn to erupt at the volcano base. The difference between this propagation and the one seen for non-isotropized tectonic stress is that, in this case, dikes present a less inclined pathway.

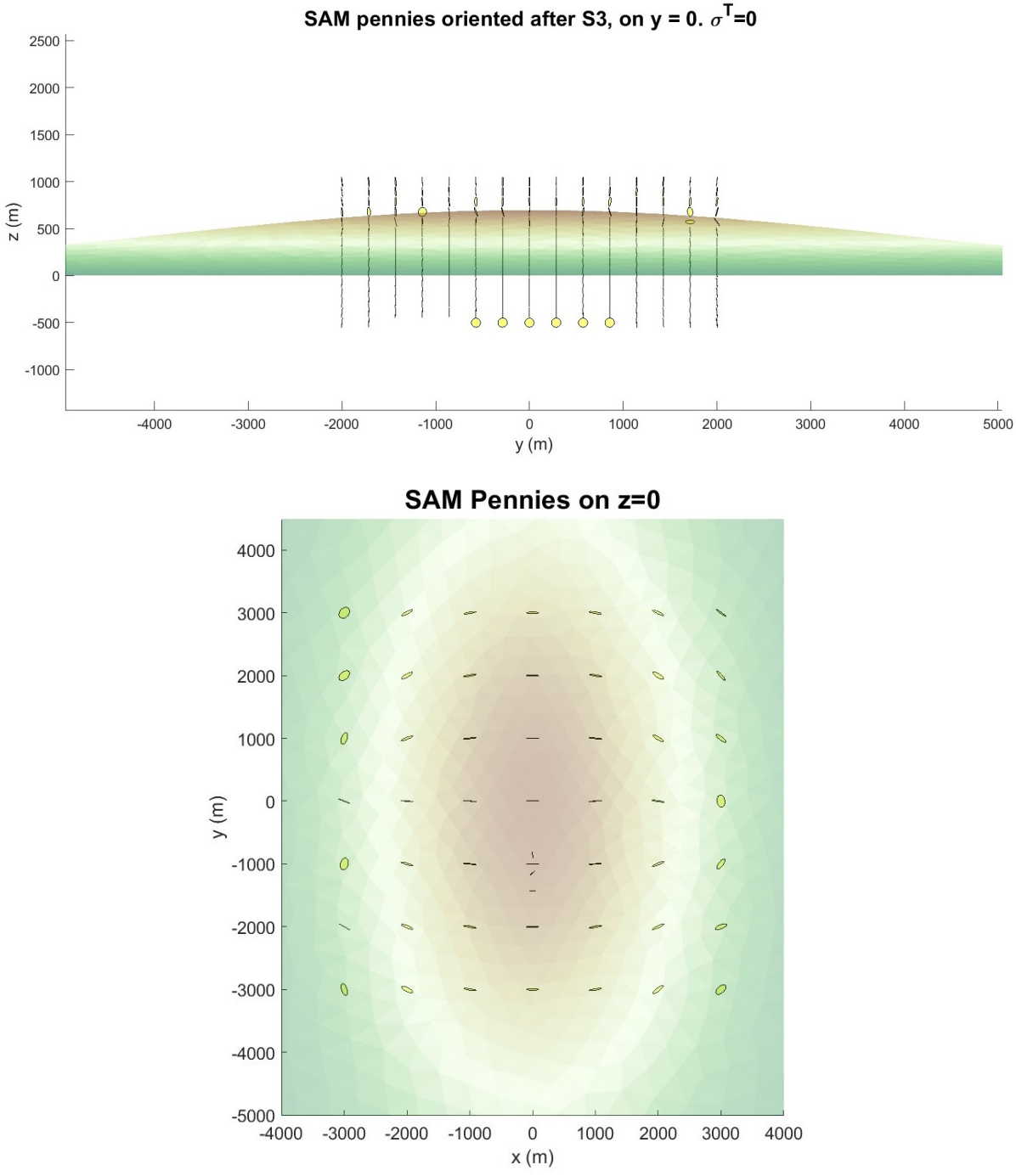

Figure 3.20: SAM pennies arranged in the y=0 and z=h/2 planes are shown in the figure. For this oblate geometry, which is different from the axisymmetric case, the pennies are oriented perpendicularly to the major axis of the ellipse.

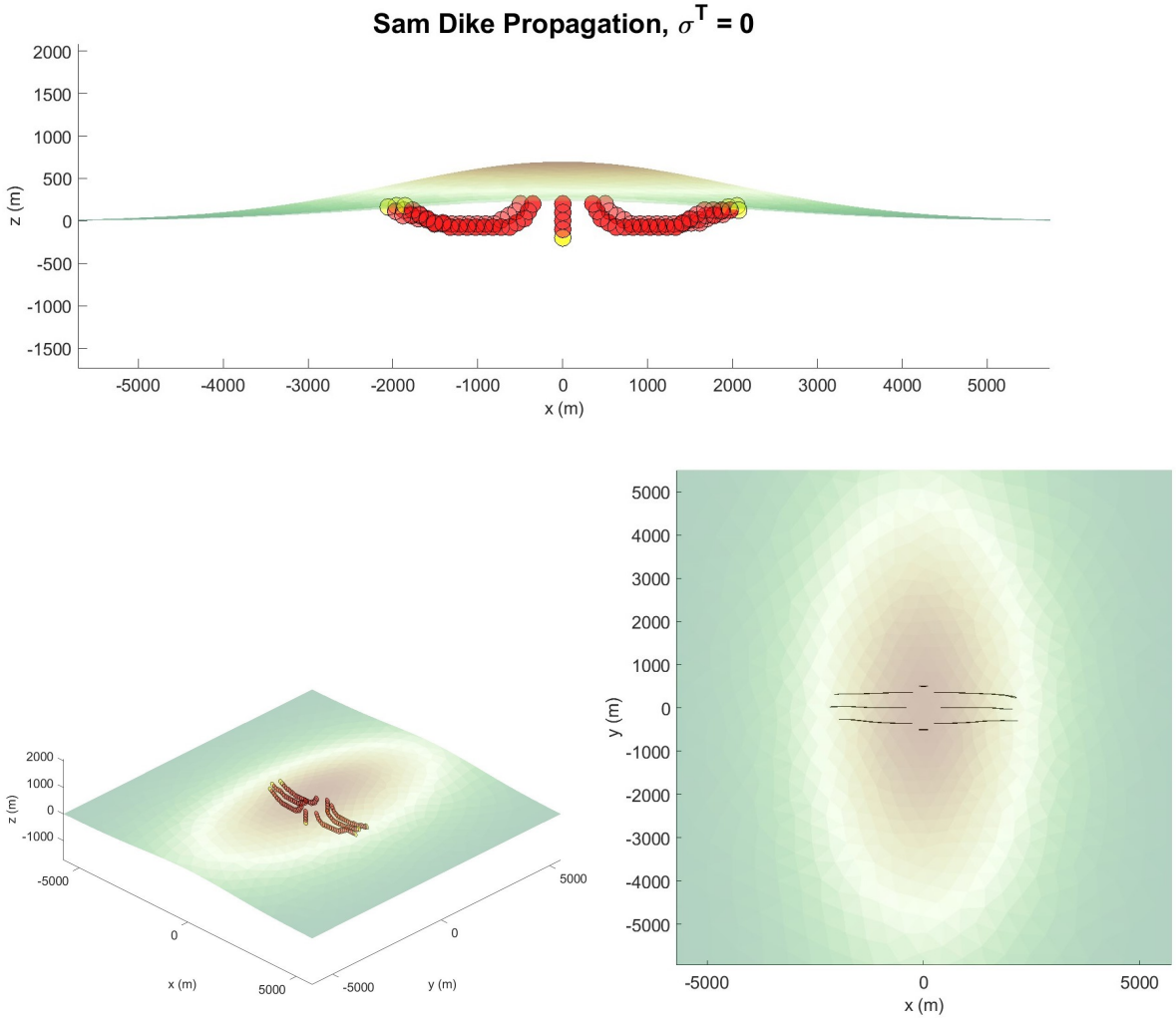

Figure 3.21: SAM dikes propagating from inside the oblate edifice. The dikes tend to propagate downward, but then turn their trajectory to erupt at the base of the flanks. The reached z level before the turning point is equal to the absolute value of the height of the volcano.

3.5 Changing the background state of stress

Next, I tested the behavior of SAM dikes in the presence of an intermediate background stress, between lithostatic and laterally confined. I used a multiplicative factor for determining the laterally confined and lithostatic conditions as in 2.5:

$$f = k + (1 - k)\frac{\nu}{1 - \nu} \tag{3.5}$$

where **f** is the multiplicative factor to apply to my stress components. In this case, for k=1 (lithostatic case), **f** will be equal to 1; for k=0, on the other hand (laterally confined case), **f** takes a value equal to the quantity $\frac{\nu}{1-nu}$, where ν is the Poisson's ratio. In this work, the value of ν was set at 0.25, so the multiplicative factor would have a value of 0.33 (thus, $\frac{1}{3}$ is the ratio between horizontal and vertical stress in a laterally confined case).

I imposed a value of k equal to 0.34 (shown in fig. 3.22 and 3.23) to investigate how an intermediate background state value would affect the dike propagation. When propagating from z=500 m , SAM dikes are outward dipping near the top of the volcano and show circumferential orientation, while they show radial orientation at depth. The dikes propagate downward without stopping. If starting from below the edifice (z=-5000 m in this case), they do not ascend, as in purely lithostatic cases, but propagate downward. An important note is that the dikes would continue to propagate downward indefinitely if they were not given the command to stop at a maximum depth (set at z=-6000 m). Even with the application of tectonic stress, the dikes do not turn their trajectory to erupt, as I observed for the purely lithostatic case: they continue to proceed downward.

In fig. 3.24, I compare a fully laterally confined background stress state (k=0), and two intermediate situations, for k=0.34 and k=0.85, respectively. In each of these cases, dike start circumferential immediately after departure, but become radial thereafter. As the value of k increases, the depth at which the dikes turn from circumferential to radial also increases.

In fully laterally confined conditions, the horizontal stresses are 1/3 of the vertical stress. At the same time, the magma remains in a condition of hydrostatic stress, making the dikes extremely anti-buoyant. As highlighted in fig. 3.24, for the magma and rock density values I used, dikes propagate as anti-buoyant even when applying intermediate stress conditions between lithostatic and laterally confined.

3.6 A preliminary application to a DEM topography

In this section, I discuss a preliminary application of Digital Elevation Models (DEMS) to propagate SAM dikes within real topographies. To do this, I have considered the

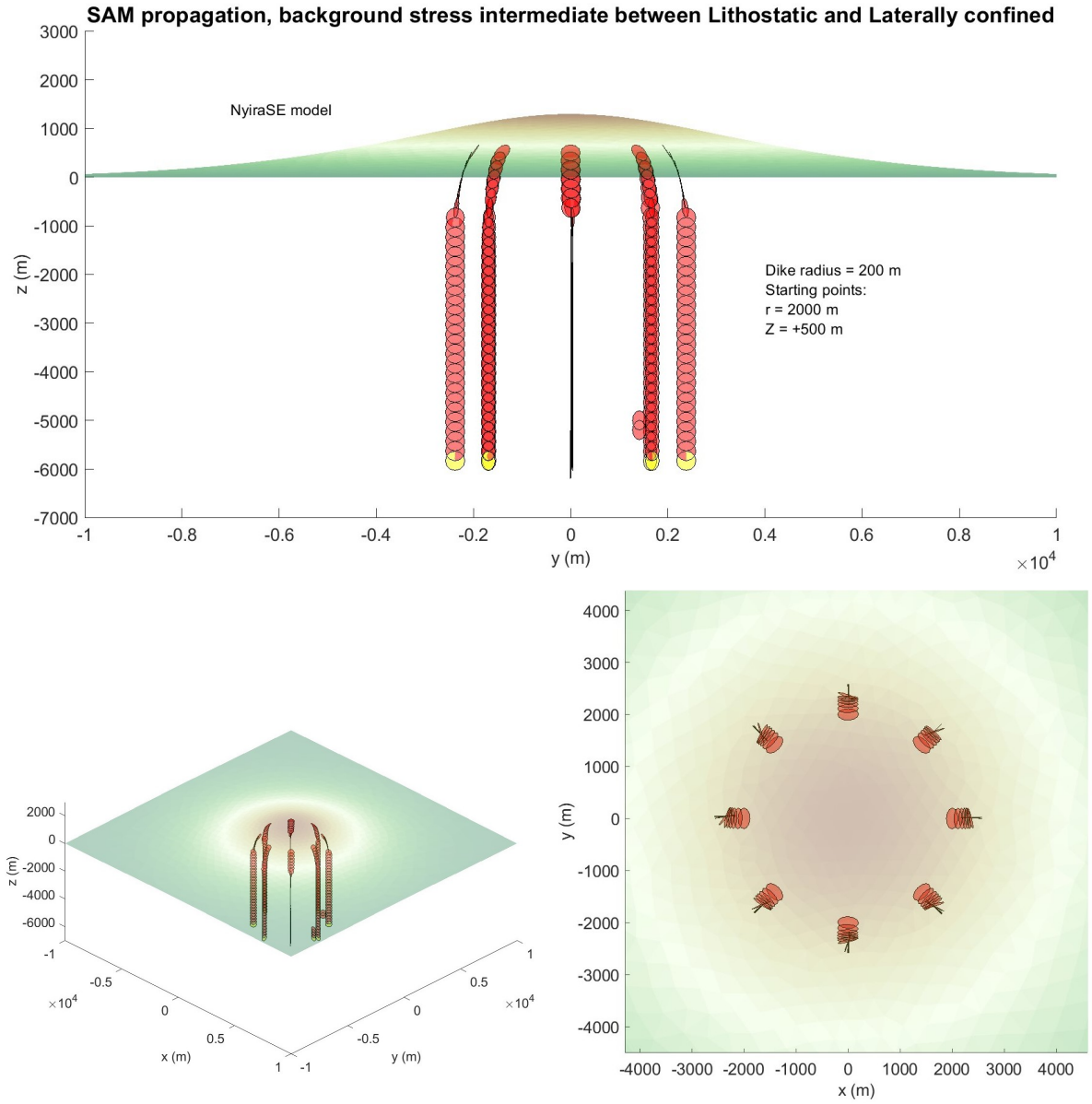

Figure 3.22: SAM dikes with the application of an intermediate background stress between the totally lithostatic and the fully laterally confined case (k = 0.34). No tectonic stress is applied. Dikes tend to orient circumferentially closer to the volcano summit and to turn into radial getting closer to the volcano base.

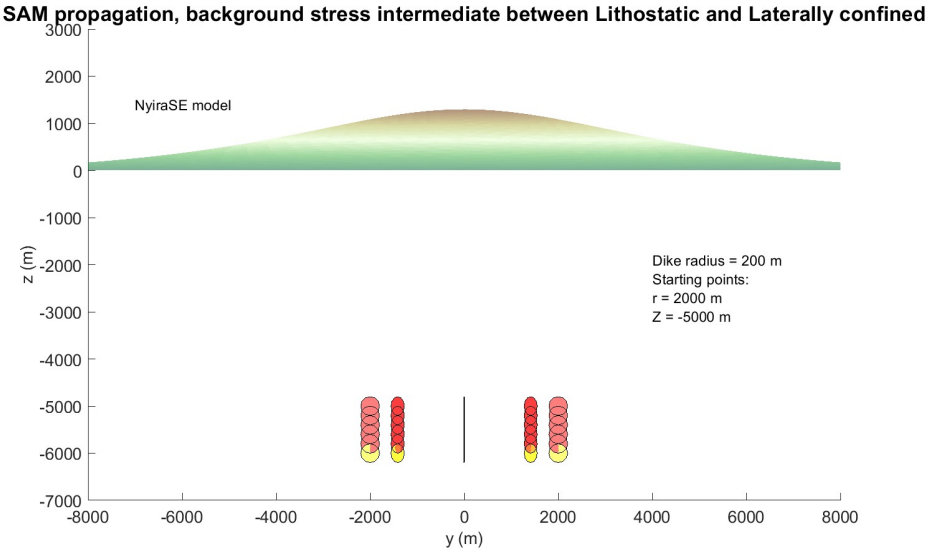

Figure 3.23: SAM dikes starting at at z=-5000 m, for an intermediate background condition between the totally lithostatic and the fully laterally confined case (k=0.34). Dikes propagate downward in a radial orientation.

case of Nyiragongo (fig. 1.10). I obtained the DEM data through the U.S. Geological Survey. The data were acquired by the Shuttle Radar Topography Mission (Farr and Kobrick, 2000). I used these data to build the free-surface mesh in a way analogous to the previous cases.(3.25). Nyiragongo is very interesting because it is near to another volcano, Nyamuragira, and to Lake Kivu. The distribution of these loads could have an impact on dike propagation.

I introduce only a simple case in which I did not subtract the highland from the volcano topography.

In fig. 3.26 I show the orientation of the SAM pennies in order to understand the structure of σ_3. Pennies orient perpendicularly to the y axis, even though a regional stress is not applied. This could be due to the shape of Nyiragongo, which overlaps with other two craters of older volcanoes: Baruta in the north and Shaheru in the south (Komorowski et al., 2002), as shown in fig. 1.10. The resulting shape may be due to Nyiragongo having an appriximately elliptical edifice, with the major axis directed in the N-S direction. Thus, the stress pattern may be similar to the one I observed for an elliptical edifice.

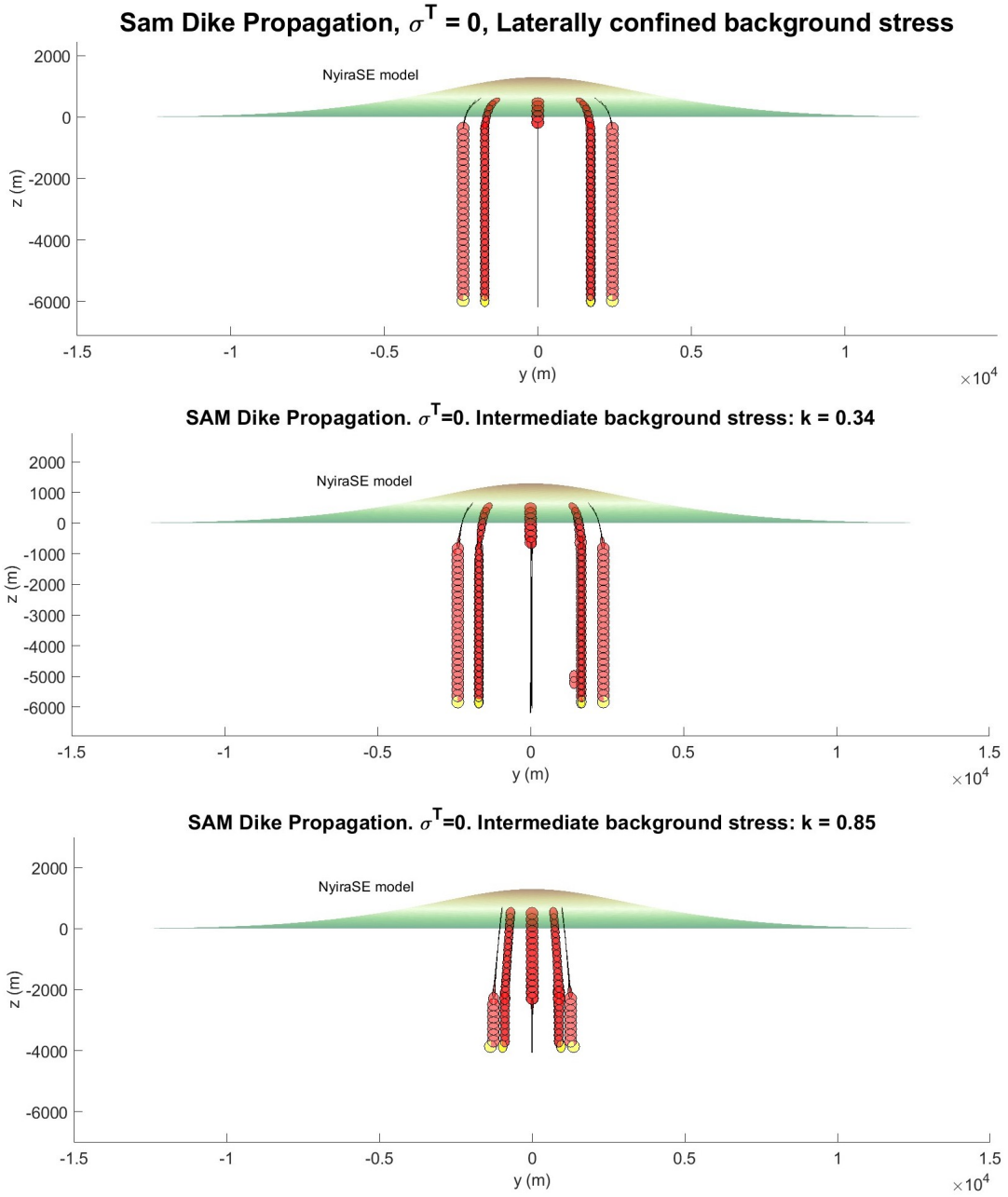

Figure 3.24: Comparison between dike propagation under NyiraSE model, respectively undergoing fully laterally confined background stress and intermediate situation with coefficient k=0.34, and k=0.85. I observed that dikes tend to change their orientation from circumferential to radial at a depth that increases as the k factor increases. Dikes propagate downward indefinitely (here they stop due to a condition I set).

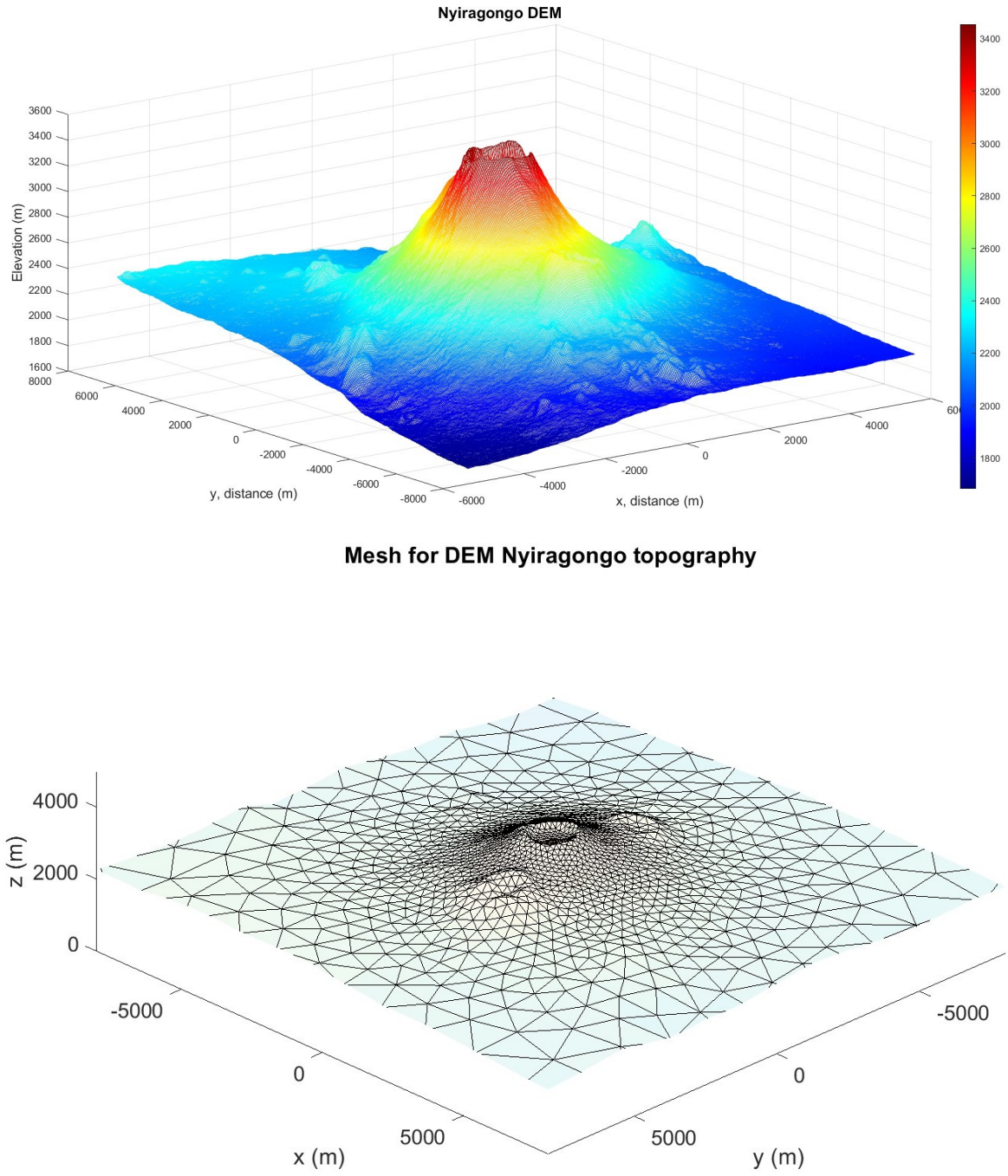

Figure 3.25: SRTM DEM (Farr and Kobrick, 2000) and Mesh obtained through by method from the SRTM DEM for Nyiragongo. The highland was not subtracted from the data.

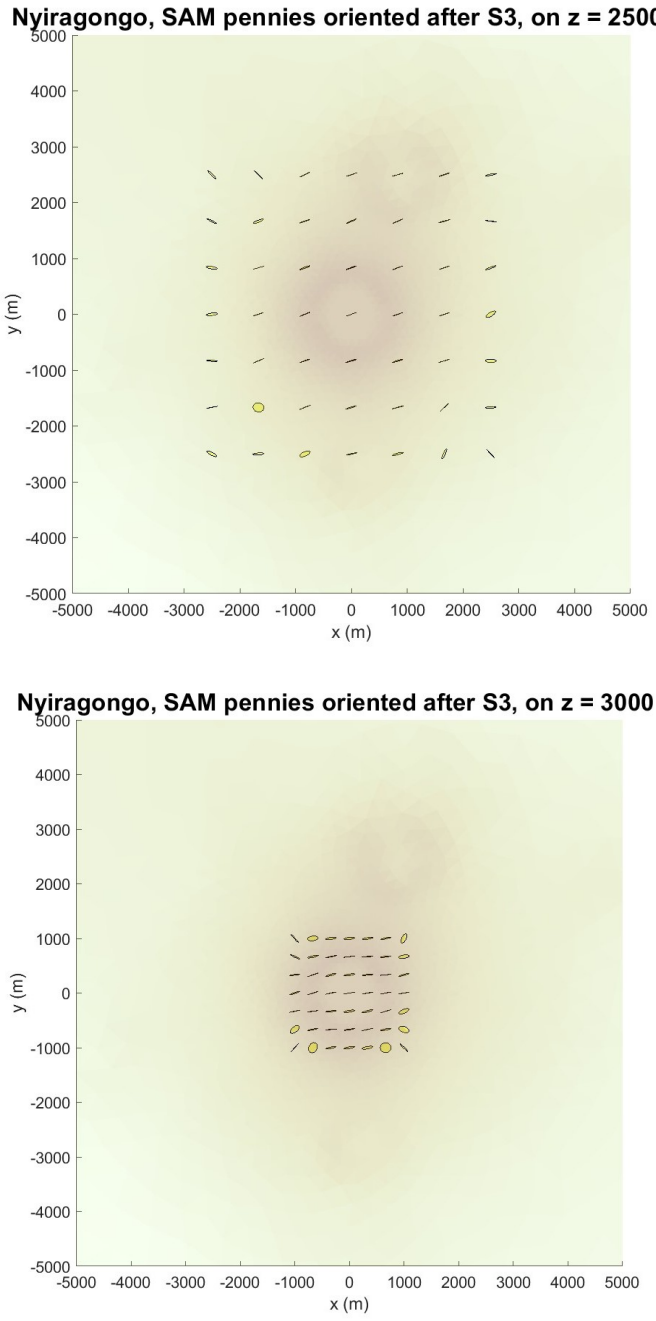

Figure 3.26: Penny SAM orienting perpendicularly to σ_3, for a DEM topography, at a height of z=2500 m and z=3000 m respectively. The stress applied is only due to loading. The highland was not subtracted from the data.

Chapter 4

Discussion

4.1 An overview on the whole project

My project has focused on on the state of stress within volcanic edifices, with the ultimate purpose of clarifying the mechanisms controlling the location where magma will breach the Earth's surface during effusive volcanic eruptions. Observations show that eruptions can occur from established vents, from newly opened vents at the summit, on the flanks of the volcano, or even far from the volcanic edifice. To better understand these complex scenarios, I created models that included stress due to loading (sec 3.3.1) and regional tectonic stress (sec. 3.3.2), while also taking into account stress isotropisation effects due to repeated intrusions into the edifice (sec. 3.3.3). Using the Simplified Analytical Model for dike propagation (sec. 2.6.1), I simulated dike propagation at axisymmetric volcano edifices (sec. 3.3). I also studied the stress in an edifice with an elliptical base (sec. 3.4), the case of the background stress intermediate between lithostatic and laterally confined (sec. 3.5), and a preliminary work with Digital Elevation Models (3.6).

4.2 Discussing the results

As shown by the examples in figure 3.1, real shield and shield-like volcano edifices can often be well-represented through Gaussian or double-Gaussian shapes. For milder edifice flanks, the single Gaussian function is a good approximation while a double-Gaussian shape is a good choice to approximate steeper flanks, and better portrays edifice features of interest such as the Break-In-Slope.

Through the Simplified Analytical model (Mantiloni, Eleonora Rivalta, and Davis, 2023) I simulated dike propagation and observed how it is influenced by various factors, including background stress, stress due to loading, tectonic stress and geometric factors, and I proposed a method to simulate the stress isotropization observed in volcanic areas due to repeated magma intrusions (sec. 3.3.3).

In the case where the applied stress was only that due to loading (along with background stress), for an axisymmetric edifice, the dikes are oriented circumferentially instead of radially (see fig. 3.11). According to observations of real volcanoes where regional stress is not dominant (Valerio Acocella, 2006), I would have expected a radial pattern. A laterally confined background stress results in a radial pattern (fig 3.24). The problem with the laterally confined configuration is that the dikes do not erupt, but tend to move downward, as they are effectively anti-buoyant (see sec. 3.5). This anti-buoyant behaviour persists when applying an intermediate situation between the condition of pure lateral confinement and purely lithostatic stress state. In contrast, purely lithostatic stress state before the application of the load leads dikes to erupt but to circumferential arrangement of the dikes. To summarise, none of the background stress conditions analysed are completely satisfying.

A possibility, not explored in this thesis, could be to increase the buoyancy of the magma. However, we already use a comparatively low magma density of $\rho_m = 2300\,\mathrm{kg\,m^{-3}}$, considering that for the encasing rock we have $\rho_m = 2850\,\mathrm{kg\,m^{-3}}$. Thus, I exclude this as the fundamental reason why the models are not fully consistent with observations.

One more reason why dikes show a circumferential orientation could be the absence of a magma reservoir. As analyzed in section 2.2, loading has been accounted as the main reason for causing the stress pattern that leads to circumferential intrusions (Roman and Jaupart, 2014), but other studies highlight the importance not only of the presence of a magma chamber, but also of its shape (Chadwick Jr and J. Dieterich, 1995).

In order to simulate the isotropization due to repeated intrusions occurring in volcanic areas, I created a function to homogenize the stress, subtracting σ_{zz} from the diagonal of the stress tensor and multiplying that matrix for a factor k_2 whose value I chose as equal to 0.5 (see sec. 3.3.3). This is only one of the ways in which this effect can be accounted for; another way might be, for example, to have many intrusions propagate, one after the other, taking into account the effect of crack opening generated by them. In fact, I did not consider the stress modifications imparted by the emplacement of the dikes I propagated. In the future it would be worth investigating whether this procedure would lead to a stress model closer to observations.

An additional way to homogenize stress inside an edifice is to make the regional stress decay in proximity of the Earth's surface. In fact, the shallowest rock layers are often composed by sediments or poorly consolidated eruptive products and are unlikely to store much stress. A tectonic stress decay function within the edifice could be applied, such that it assumes the full value at the base of the volcano (or deeper) and decays, with an arbitrary curve, to a zero value at the surface.

In my propagation models for axisymmetric edifices, I observed the occurrence of eruptions at the base of the volcano only in the presence of tectonic stress; in my convention, I consider the eruption to occur when the dike reaches a distance from the surface equal to the size of the triangle sides that compose the mesh. In the absence

of tectonic stress, the circumferentially oriented dikes are attracted by the loading of the edifice, but then they tend to get arrested below it and do not continue toward the surface (fig. 3.13). This is in accordance with the results of Dahm (2000), J. R. Muller, Ito, and S. J. Martel (2001) and Maccaferri, Bonafede, and Eleonora Rivalta (2011). Similarly, when dikes are propagated from inside the edifice, they propagate downward (fig. 3.12). When tectonic stress comes into play, on the other hand, the dikes, oriented perpendicular to that stress, propagate toward the center of the edifice starting at $z < 0$, and downward when starting from the inside of the edifice ($z > 0$). In both cases, however, they deflect to head toward the surface and erupt at the base of the volcano (fig. 3.17 and 3.17). The turning point is around z=-1000 m at depth, a distance similar to the height of the reference topography NyiraSE. Here, I did not explore the effect of increasing or decreasing the size of the volcano or change its aspect ratio. All these factors deserve to be explored in the future.

A particular case amongst the others, highlighting the relevance of the edifice geometry in determining dike propagation, is the elongated edifice. The elliptical edifice displays an interesting pattern of dikes: they are arranged perpendicular to the major axis of the ellipse, even though no tectonic stress has been applied. This result reveals the importance of the edifice shape in determining the dike orientation. The map in fig. 1.4 of the Erta Ale volcano (from Valerio Acocella (2006)) shows that the dikes are actually arranged perpendicular to the minor axis of the edifice. However, these two cases cannot be compared directly, because Erta Ale is situated on a developing Mid Ocean Ridge and subject to tectonic extension. From my cases with tectonic stress, I see that this is able to overprint the circumferential arrangement and it is likely it would work in this case too.

SAM dikes for an elongated edifice propagate with a pattern similar to that observed for asymmetric edifices in the presence of tectonic stress: they propagate downwards and then reverse their trajectory to erupt at the base of the volcano. The turning point in their trajectory occurs, even in this case, at a comparable absolute value of z to the height of the edifice.

To summarise, the geometry of the loading volcano evidently influences the propagation of dikes, although an oblate case like the one I observed is difficult to find in nature. In this simulation, in fact, only the stress due to loading was adopted, while real elongated edifices tend to form predominantly in rift zones or where the tectonic stress is dominating, and where even dikes tend to propagate parallel to the major axis of the volcano because of regional stress dominance.

In the case of the preliminary study on Nyiragongo, the SAM pennies are arranged perpendicular to the y axis, as in the case of the elliptical edifice. The shape of Nyiragongo is not elliptical, but has two large craters located north and south of the main crater, derived from old volcanoes (Komorowski et al., 2002). My hypotesis is that their loading may have influenced the stress state in the edifice, making it similar to the case of the oblate edifice, and influencing the dikes to orient perpendicularly to the axis pass-

ing by the three craters. No tectonic stress has been applied here, and a more accurate analysis of this case should take into account the Nyiragongo geographical location in the East African Rift, and the influence of the resulting tectonic stress on the area. Other aspects to be considered for this model are the neighbourhood of Nyiragongo to Nyamuragira volcano (see fig. 1.10), which may influence Nyiragongo stress field through the loading due to its weight or through its intrusions, and the proximity to Lake Kivu.

4.3 Limitations and perspectives

My models are very simple and neglect many factors present in real volcanoes.

A relevant factor in determining how dike propagate, turn their trajectories or halt, is rock layering. Rock layering implies changes in rock density and/or rigidity, conditioning dike pathways. Amongst others, Maccaferri, Bonafede, and Eleonora Rivalta (2010) used a boundary element method coupled with analytical solutions to identify dike behaviours in a rigidity layered material. They observed that when dikes are distant from the rigidity transition, they propagate straight; when they reach the boundary between a stiff and compliant layer, they deviate toward the vertical direction; when they approach a stiffer medium, they deviate toward the horizontal direction. A stratified model was not used in simulations in my thesis, but it could be an interesting starting point for a future project.

One more important point not touched upon in this thesis, is the influence of unloading due to caldera on the propagation of dikes. Corbi et al. (2015), studied stress field for a volcano (specifically Fernandina, Galàpagos) undergoing a stress variation due to caldera unloading. The presence of a caldera results in a strong influence for the stress field, competing with tectonic stress and magma buoyancy forces in controlling the conditions of dike orientation emplacement. By taking into account the decompression due to the caldera formation, they developed two models: an isotropically-stressed volcano and a gravitationally loaded volcano. In the former case, unloading due to the caldera formation showed a complex rotation of the stress axes; in the latter, the edifice sagging under its own weight is found to have a stronger influence on the stress field compared to the unloading of the caldera. A correlation between the last intrusions at Fernandina volcano and the unloading due to its caldera collapse is found.

For a case like Fernandina volcano, the stress due to caldera unloading cannot be ignored, because of the large size of the caldera geometry (see fig. 3.1). Caldera unloading could be an interesting feature to add to the presented models, and could provide the missing piece for a more accurate representation of particular edifices with this peculiarity (Mantiloni, Eleonora Rivalta, and Davis, 2023).

The layer-by-layer load growth, highlighted by Chadwick Jr and J. Dieterich (1995), could be an important factor in determining load influence on stress underground. Unfortunately, it is not straightforward to take this factor into account, since, in my models,

the whole volcanic edifice is treated as a single, gravitationally loaded unit. A significant future challenge in dike propagation modelling would be to construct a comprehensive volcano-growth model that consider the stress modification caused by incremental addition of lava layers upon the volcano edifice, eruption after eruption. Such a model could quantify the homogenization of the underground stress caused by the repeated intrusion emplacements, accompanying the eruptions. Developing such a model would have important implications in the field of dike propagation modelling, deepening our understanding on how the stress in a volcano is built up through time.

As already mentioned, the k value for the state of stress is still an issue in geophysics. SAM could be an interesting tool to be used in trying to provide a constraining method to find the best k value for the state of local stress in the proximity of a topographic relief, such as the one originated by a volcano edifice. Here I would like to provide a potential recipe for future works which aim seeking to constrain the k value through SAM dike propagation, by means of an inversion procedure similar to the one employed by Maccaferri, Richter, and Walter (2017). This requires the collection of specific data for the targeted volcano, such as InSAR (Interferometric Synthetic Aperture Radar) data for ground displacements to locate dike trajectories within the volcano, geological vent location maps, or erupted dike maps. Next, the state of stress must be built up under different assumptions based on the geological history of the volcano or on reasonable hypotheses about its stress state. The SAM code can then be used to propagate dikes; the results can then be compared to real emplaced dikes in the area of interest. The k value and initial stress conditions can be adjusted until there is a correspondence between SAM and the actual dike emplacements. This process must be iterated while considering different hypotheses and different k values. It is worth noting that the model can only be validated when a new intrusion occurs, at which point it could be updated accordingly. This undertaking presents a significant challenge, as it requires a deep understanding of the complex interplay between different factors influencing dike propagation. However, successfully addressing this challenge could have significant implications for our understanding of magma migration through dikes and our ability to forecast future vent openings.

Chapter 5

Conclusions

In conclusion, my thesis aimed to improve our understanding of magma transport in volcanic edifices and the mechanisms controlling the location of new vent openings. Through the use of the Simplified Analytical Model for dike propagation (Mantiloni, Eleonora Rivalta, and Davis, 2023), I have analyzed the influence of various factors on underground stress and dike propagation, focusing particularly on the role of topographic loading. The findings presented in this study open more questions than they answer about the complex processes of volcanic eruptions, aiming to lay the groundwork for new scientific challenges.

After presenting an in-depth analysis of magma propagation in axysimmetric volcanic edifices, it is important to summarise the key findings and results of my study. This will provide a concise overview of the research presented in the thesis, highlighting the main contributions and implications for the field. The results of my research showed that the orientation of dikes is influenced by tectonic stress (sec. 3.3.2), background stress (3.5), and edifice geometry (sec. 3.4). In each configuration I observed that loading acts as a point of attraction for propagating dikes starting at depth, except for cases where the background stress was laterally confined or intermediate (in those cases the dikes always tended to move downward, away from the edifice). At the same time, dikes departing from inside the edifice always tend to propagate downward, driven by the influence of loading. In my simulations, dikes could reach the surface only for cases where tectonic stress was present (sec. 3.3.2), or for the case of a non-axisymmetric edifice (sec. 3.4). In both cases, dikes erupt at the base of the volcano or away from the summit, in agreement with Kervyn et al. (2009). In the case of tectonic stress, the dikes tend to lie perpendicular to the axis of minimum stress, while in the case of the oblate edifice, the dikes lie perpendicular to the major axis of that edifice. When this happens, the turning points of the trajectories, which at first point downward, then toward the surface, are at a depth comparable to the height of the edifice. In contrast, when the tectonic stress is subjected to the isotropization process, the depth of the turning point is smaller than the edifice height. In comparison with real-world scenarios, my results

showed good agreement with maps of realistic vent locations. However, further research is needed to account for the effect of crack opening generated by repeated intrusions and to investigate the role of caldera unloading and pressurized magma chamber shape on dike orientation.

I would like to emphasize the significant advancement on dike propagation modelling of the recent years. Until a few years ago, propagating dikes with computational models was only possible in 2 dimensions (Corbi et al., 2015), whereas now we have powerful means such as the SAM, the Simplified Analytical model or TIM, the Three-dimensional Intrusion Model (Mantiloni, Eleonora Rivalta, and Davis, 2023) for dike propagation in 3D. These advances in computational modelling may pave the way for new breakthroughs in this field of study, leading to deepen our understanding on magma transport.

With all the limitations of a study as this one, my thesis remains a novel numerical investigation of stresses in volcanic edifices, where several shapes and different assumptions on stress are studied and compared with each other. There are many points that are still unclear, and a long and careful work would be required to better understand the relation between all the contributing factors and the distribution of new vents. To conclude, I believe an interesting avenue for future research could lie in using the methods I presented here to investigate how stress-modifying processes interact with one another, and how their cumulative contribution affects the propagation of magma within volcanic edifices.

Appendix A

Matlab code for topography approximation

Here I show my Matlab code I used to perform topography approximation as a double Gaussian topography. In the following you will find:

1. The main code;
2. The functions to split the volcano profile in two halves and create two new symmetric profiles: **aspect_ratio_left.m, aspect_ratio_right.m**;
3. The functions performing a Gaussian and double Gaussian approximation minimizing the difference with the symmetrical topographies: **gauss_minsquare.m , double_gauss.m**;
4. The functions providing a Gaussian and double-Gaussian function avaliable with user parameters: **,**app_topography.m, doublegauss_topography.m.

A.1 Topography approximation - Main

```
clear;
close all;
clc;

%Uploading files and converting to arrays

volc = readtable('profiloNW_SE.txt');
%Fuji_N_S.txt  Etna_NW_SE.txt profiloNW_SE.txt
volcano = table2array(volc);
```

```
%Erase Lat and Lon (columns 1 and 2) and substitute with Distance
%(km) and Elevation (m)
volcano(:,1) = volcano(:,3);
volcano(:,2) = volcano(:,4);
volcano(:,4) = [];
volcano(:,3) = [];


%Converting distance from km to m
volcano(:,1) = volcano(:,1)*10^3;


%% Here I plot the volcano profile
fig_bareprofile = figure(1)

plot(volcano(:,1),volcano(:,2),"LineWidth",4,"Color", "#CCBB44")
axi = gca;
axi.FontSize = 16;
axis equal
hold on
title('Bare profile with top point and plateau limits','FontSize', 25);

xlabel('width, km','FontSize',16)
ylabel('height, km','FontSize',16)

% Activate the data cursor mode to identify the plateau by
%clicking on the image
dcm = datacursormode(fig_bareprofile);
dcm.Enable = 'on';
dcm.DisplayStyle = 'window';

% Wait until the user has clicked
disp('Click on the volcano profile point you identify as the ...
plateau point of the left flank! Then press "Return", please.')
pause
% Export cursor to workspace
pl_l=getCursorInfo(dcm);
plateau_left = pl_l.Position;
plateau_left(3) = pl_l.DataIndex;
```

```
disp('<Thanks! Now, do the same for the right flank, please! ...
Then press "Return".')
pause
% Export cursor to workspace
pl_r=getCursorInfo(dcm);
plateau_right = pl_r.Position;
plateau_right(3) = pl_r.DataIndex;

%% Aspect ratio + Data normalization through my h and r values

%Here I compute the aspect ratio for the left part (output of this function)
    caldera = 1; %Boolean variable: 1 = yes caldera. 0 = no caldera
[left_aspect,left_hr,left_res_volcano] = aspect_ratio_left(volcano(:,1),...
volcano(:,2),caldera,plateau_left);
plot(left_hr(1)+plateau_left(1),left_hr(2)+plateau_left(2),...
"o magenta","LineWidth",4);
%Here I compute the aspect ratio for the right part
%(output of this function)
[right_aspect,right_hr,right_res_volcano] = ...
aspect_ratio_right(volcano(:,1),volcano(:,2),...
caldera,plateau_right);%plat_imposto);%

%Here I plot the beginning and end of the plateau
plot(plateau_left(1),plateau_left(2),"o magenta","LineWidth",4)
plot(plateau_right(1),plateau_right(2),"o magenta","LineWidth",4)

hold off


%% Gaussian approximation

% Guess parameters
x(1) = 0.6; %A1
x(2) = 7; %A2
x(3) = 4; %B2
y = 7;

% Calling the Gaussian approximation functions
leftsingle_bestx = gauss_minsquare(left_res_volcano(:,1),...
left_res_volcano(:,2),y);
rightsingle_bestx = gauss_minsquare(right_res_volcano(:,1),...
```

```
right_res_volcano(:,2),y);

% Calling the double-Gaussian approximation functions
left_bestx = double_gauss(left_res_volcano(:,1),...
left_res_volcano(:,2),x);
right_bestx = double_gauss(right_res_volcano(:,1),...
right_res_volcano(:,2),x);


%% Create a handle for the plot function
left_fit_func = @(arr) doublegauss_topography(arr,...
left_res_volcano(:,1));
right_fit_func = @(arr) doublegauss_topography(arr,...
right_res_volcano(:,1));

leftsingle_fit_func = @(sca) app_topography(sca,...
left_res_volcano(:,1));
rightsingle_fit_func = @(sca) app_topography(sca,...
right_res_volcano(:,1));


%% Rescaled topography and approximation plot with different coefficients.
figure(2)
%Plot of topography:
subplot(2,1,1)
hold on
axis equal
title("Nyiragongo, NW symmetrized flank","FontSize", 25);
%plot the rescaled and symmetrized topography
plot(left_hr(1)*left_res_volcano(:,1),...
left_hr(2)*left_res_volcano(:,2),"LineWidth",4,"Color", "#CCBB44")
ax1 = gca;
ax1.FontSize = 15;
%Plot of approximation functions
 %plot(left_res_volcano(:,1),left_fit_func(x),...
 "LineWidth",2,"Color", "#66CCEE") %plot guess fit, cyan

plot(left_hr(1)*left_res_volcano(:,1),...
left_hr(2)*leftsingle_fit_func(leftsingle_bestx),...
"LineWidth",2,"Color", "#4477AA")
```

```
plot(left_hr(1)*left_res_volcano(:,1),...
left_hr(2)*left_fit_func(left_bestx),...
"LineWidth",2,"Color", "#AA3377")

lg1 = legend("Left side symmetrized topography","Single Gaussian...
approximation","Double Gaussian approximation")
lg1.FontSize = 16;
xlabel('width (km)','FontSize',16)
ylabel('height (km)','FontSize',16)
 %Same but fot the right approximation
hold off

%Plot of topography:
subplot(2,1,2)
hold on
title("Nyiragongo, SE symmetrized flank","FontSize", 25);
axis equal
plot(right_hr(1)*right_res_volcano(:,1),...
right_hr(2)*right_res_volcano(:,2),"LineWidth",4,"Color","#CCBB44")
txt = 'NyiraSE model';
%text(-5000,1000,txt,'FontSize',16);

ax2 = gca;
ax2.FontSize = 15;
%Plot of approximation functions

plot(right_hr(1)*right_res_volcano(:,1),...
right_hr(2)*rightsingle_fit_func(rightsingle_bestx),...
"LineWidth",2,"Color", "#4477AA")

plot(right_hr(1)*right_res_volcano(:,1),...
right_hr(2)*right_fit_func(right_bestx),...
"LineWidth",2,"Color", "#AA3377")
 %plot fit from "double_gauss" function
lg2 = legend("Right side symmetrized topography",...
"Single Gaussian approximation","Double Gaussian approximation")
lg2.FontSize = 16;
xlabel('width (km)','FontSize',16)
ylabel('height (km)','FontSize',16)
 hold off
```

A.2 aspect_ratio_left.m and aspect_ratio_right.m

The functions split the volcano profile in two halves and create two new symmetric profiles.

A.2.1 aspect_ratio_left.m

```
%Function to calculate the aspect ratio of a volcano edifice: E = h/r.
%The function requires a boolean variable used as a switch: with 1,
%it provides aspect ratio for a volcano with a caldera, and without one with 0.

%For a caldera-equipped volcano, the function calculates the midpoint
%between the two maxima and assign it to r, and takes the height of the
%lower maximum as h.

%For a no-caldera volcano, r and h are just the peak x and y


function [aspect,values_hr,res_data] = ...
aspect_ratio_left(xdata,ydata,boolean,plat)

    %Checking which function to use
    switch boolean
        case 1 %Edifice with a caldera

        %Here I find the topography peaks and their locations in
        %data tables
        [peaks,peaks_where] = findpeaks(ydata);
        %Here I spot the two maximum values within the peaks
        [maxval,maxpos] = maxk(peaks,2);
        %Here I locate all the data between the two max peaks
        max_volcano = peaks_where(maxpos);
        %Here I find the equidistant x point between them
        middle = (xdata(max_volcano(2))+xdata(max_volcano(1)))/2;
        discrepancy = abs(middle-xdata);
        [x_center,x_center_pos] = min(discrepancy);
        r = xdata(x_center_pos)-plat(1); %x value for the peak
        r_pos = x_center_pos - plat(3);

        %Here I find the plateau to my data
```

```
     %Here I locate the height of the approximation
     h = (ydata(min(max_volcano)))-plat(2); %y value for the
     %peak

     %Here I compute the aspect ratio (output of this function)
     aspect = h/r;
    %With two variables for the output, the function will give
    %r, h in a
    %two-elements vector.
    values_hr(1) = r;
    values_hr(2) = h;

    case 0 %Edifice without a caldera
        [h,hpos] = max(ydata);
        r = xdata(hpos)-plat(1);
        h = h-plat(2);
        aspect = h/r;
        values_hr(1) = r;
        values_hr(2) = h;
        r_pos = hpos - plat(3);
        x_center_pos = r_pos;
    otherwise
        display("aspect_ratio: Retry providing a third...
        variable with value 1 if your topography shows a ...
        caldera and 0 if not")
end

%Here I assign the new data
new_data(:,1) = xdata;
new_data(:,2) = ydata;

new_data(1:plat(3),:) = [];
new_data(:,1) = new_data(:,1)-plat(1);
new_data(:,2) = new_data(:,2)-plat(2);

%Here I assign the rescaled data

%First half
res_data1(:,1) = new_data(1:r_pos,1)/r;
res_data1(:,2) = new_data(1:r_pos,2)/h;
```

```
    %I create and concatenate arrays for the second half
    %To obtain symmetric rescaled data

    res_data2(:,1) = res_data1(:,1);
    res_data1(:,1) = flip(res_data1(:,1));
    res_data1(:,1) = -res_data1(:,1);

    res_data2(:,2) = flip(res_data1(:,2));
    res_data = [res_data1; res_data2];
```

A.2.2 aspect_ratio_right.m

```
%Function to calculate the aspect ratio of a volcano edifice: E = h/r.
%The function requires a boolean variable used as a switch: with 1,
%it provides aspect ratio for a volcano with a caldera, and without one with 0.

%For a volcano with a caldera, the function calculates the midpoint
%between the two maxima and assign it to r, and takes the height
%of the lower maximum as h.

%For a no-caldera volcano, r and h are just the peak x and y.


    function [aspect,values_hr,res_data] = ...
    aspect_ratio_right(xdata_,ydata_,boolean,plat)
%
%     %assigning the data
     ydata = ydata_;
     xdata = xdata_;

%Checking which function to use
    switch boolean
        case 1 %Edifice with a caldera

        %Here I find the topography peaks and their locations in data tables
        [peaks,peaks_where] = findpeaks(ydata);
        %Here I spot the two maximum values within the peaks
        [maxval,maxpos] = maxk(peaks,2);
        %Here I locate all the data between the two max peaks
        max_volcano = peaks_where(maxpos);
        %Here I find the equidistant x point between them
```

```
    middle = (xdata(max_volcano(2))+xdata(max_volcano(1)))/2;
    discrepancy = abs(middle-xdata);
    [x_center,x_center_pos] = min(discrepancy);
    r = -xdata(x_center_pos)+plat(1); %x value for the peak
    r_pos = plat(3)-x_center_pos;

    %Here I find the plateau to my data

     %Here I locate the height of the approximation
     h =((ydata(max(max_volcano)))-plat(2)); %y peak value

     %Here I compute the aspect ratio (output of this function)
     aspect = h/r;
    %With two variables for the output, the function will give
    %r, h in a
    %two-elements vector.
    values_hr(1) = r;
    values_hr(2) = h;

    case 0 %Edifice without a caldera
        [h,hpos] = max(ydata);
        r = -xdata(hpos)+plat(1);
        h = (h-plat(2));
        aspect = h/r;
        values_hr(1) = r;
        values_hr(2) = h;
        r_pos = -hpos + plat(3);
        x_center_pos = hpos;

    otherwise
        display("aspect_ratio: Retry providing a third...
        variable with value 1 if your topography shows a ...
        caldera and 0 if not")
end

%Here I flip and assign the new data

new_data(:,1) = xdata;
new_data(:,2) = ydata;

new_data(plat(3):end,:) = [];
```

```
    new_data(1:x_center_pos,:) = [];
    new_data(:,1) = flip(-new_data(:,1)+plat(1));
    new_data(:,2) = new_data(:,2)-plat(2);

    %First half

    res_data2(:,1) = new_data(:,1)./r;
    res_data2(:,2) = new_data(:,2)./(h);


    %I create and concatenate arrays for the second half
    %To obtain symmetric rescaled data

    res_data1(:,1) = flip(-res_data2(:,1));

    res_data1(:,2) = flip(res_data2(:,2));
    res_data = [res_data1; res_data2];
```

A.3 gauss_minsquare.m and double_gauss.m

These functions perform a Gaussian and double Gaussian approximation minimizing the analytical functions difference to make them match with the symmetrical topographies.

A.3.1 gauss_minsquare.m

```
%Defining a function to use fminsearch as an optimizer.

% This function provides a Gaussian function to approximate a volcano
% edifice topography using fminsearch.
%
% ------------------------------------------------------------------
%
% INPUT:
%
% xdata_ -> for now rescaled between [-1,1]
% ydata_ -> topography normalized data
%
% ------------------------------------------------------------------
%
```

```
% OUTPUT:
%
% best_x -> best value for double Gaussian parameters.
%   Provide them to the "app_topography" function in order to plot the data
%   approximation obtained.
%
% ------------------------------------------------------------------

function bestx = gauss_minsquare(xdata_, ydata_, param)

    switch nargin
        case 2
            x = 5;
        otherwise
            x = param;

     end

    xdata = xdata_;
    ydata = ydata_;

    g = @(xdata,ydata,x) sum((ydata - (exp(-x*(xdata).^2))).^2);
    one_val_g = @(x) g(xdata,ydata,x);
%     x0(1) = 0.4;
%     x0(2) = 7;
%     x0(3) = 5;
    x0 = x;
    bestx = fminsearch(one_val_g,x0);

end
```

A.4 double_gauss.m

```
%Defining a function to use fminsearch as an optimizer.

% This function provides a Gaussian function to approximate a volcano
% edifice topography using fminsearch.
%
```

```
% ------------------------------------------------------------------
%
% INPUT:
%
% xdata_ -> for now rescaled between [-1,1]
% ydata_ -> topography normalized data
%
% ------------------------------------------------------------------
%
% OUTPUT:
%
% best_x -> best value for double Gaussian parameters.
%   Provide them to the "app_topography" function in order to plot the data
%   approximation obtained.
%
% ------------------------------------------------------------------

function bestx = double_gauss(xdata_, ydata_, param)

     switch nargin
         case 2
             x(1) = 0.6;
             x(2) = 1;
             x(3) = 9;
             x(4) = 1-x(1);
         otherwise
             x = param;
             x(4) = 1-x(1);
     end

    xdata = xdata_;
    ydata = ydata_;

    g = @(xdata,ydata,x) sum((ydata - ...
    (x(1)*exp(-x(2)*(xdata).^2) + (1- ...
    x(1))*exp(-x(3)*xdata).^2))).^2);
    one_val_g = @(x) g(xdata,ydata,x);

    x0 = x;
    bestx = fminsearch(one_val_g,x0);
    bestx(4) = 1-bestx(1);
```

A.5 app_topography.m and doublegauss_topography.m

The functions providing a Gaussian and double-Gaussian function avaliable with user parameters

A.5.1 app_topography.m

```
% Double Gaussian function for normalized data
%
% INPUT:
%
% par -> scalar, single guess-values array, containing:
% param(2) -> A2, x-multiplication coefficient for the Gaussian
%
% xdata -> horizontal data for your topography
% (already rescaled within [-1,1])
%
% -------------------------------------------------------------------
%
% OUTPUT:
%
% g -> Call the function depending on provided parameters

function g = app_topography(par,xdata)

    param = par;

  g = exp(-param*(xdata).^2);
```

A.5.2 doublegauss_topography.m

```
% Double Gaussian function for normalized data
%
```

```
% INPUT:
%
% par -> 4 guess-values array, containing:
%   param(1) -> A1, coefficient for the first Gaussian
% (the coeff B1, for the second Gaussian, is given by 1-A1)
%   param(2) -> A2, x-multiplication coefficient for the first
% Gaussian
%   param(3) -> B2, x-multiplication coefficient for the second
% Gaussian
%
% xdata -> horizontal data for your topography (already rescaled
% within [-1,1])
%
% ------------------------------------------------------------------%
% OUTPUT:
%
% g -> Call the function depending on provided parameters

function g = doublegauss_topography(par,xdata)%,h_)
%
% switch nargin
%     case 3
%         h = h_;
%     case 2
%         h = 1;
% end
    param = par;

  g = param(1)*exp(-param(2)*(xdata).^2) + ((1-...
  param(1))/1)*exp(-param(3)*(xdata).^2);
```

Aknowledgments

Today I could not be happier to have achieved this goal. That is also why I want to use this space to say that if I made it, it is because I am privileged. Graduating, in my country, is still an economic and psychological privilege. For this reason, I want to thank my parents, in the first place, who have been supporting me both ways during all these years. I could not be here today without your aid. I hope that in the future things will change, that the right, rather than the privilege, to study will be guaranteed, and all those who wish to will have the opportunity to study thanks to an accessible, substantial and accountable support from the institutions.

The path through the final result has been long and winding, and I feel extremely lucky to have worked with Eleonora, who has been a true mentor for me. I have witnessed her precious ability to create a healthy environment around her, based on listening, trust, and a deep understanding of the science she works with. She taught me science is not far from telling a story, as long as you have the right tools, and she made me believe that a future in this work, and being a woman in science, is possible.

My work owes so much to Lorenzo, whose proficiency, dedication and support has been crucial in helping me during the whole path. I wish one day I could be able to help someone in the effective way he helped me. I hope your passion and kindness will always be your lead!

This thesis was at first inspired by a 2021 work by Delphine, who has been a patient listener and wise interlocutor to me. Thanks for your time and advice, I wish you the best on your path.

Thanks to all my loved ones:

Thanks to Daniele, who believed in me and supported me as my biggest fan, for taking care of me when I needed it most, and for helping me with image editing, teaching me how to use Gimp and forcing me to drop Paint.

Thanks to Alessia for recommending useful language tools; special thanks to Gaia for looking after me by providing me with her company, support and a place to write the thesis in the last days before submission; thanks to both of them, together with Benedetta, for our shared study sessions, for our ritual Monday dinner and for making

my last year in Bologna the best year ever.

Thanks to my brother Gioele and to my friends from Marche, Juri, Luca, Martina, Martina, who made me feel home whenever I went back home, and to Marco, who migrated to keep working in science, and whose words of affirmation are always heart warming.

Bibliography

Acocella, V and M Neri (2009). "Dike propagation in volcanic edifices: overview and possible developments". In: *Tectonophysics* 471(1-2), pp. 67–77.

Acocella, Valerio (2006). "Regional and local tectonics at Erta Ale caldera, Afar (Ethiopia)". In: *Journal of Structural Geology* 28(10), pp. 1808–1820.

Anderson, EM (1936). "Dynamics of formation of cone-sheets, ring-dikes, and cauldron subsidences: Royal Society of Edinburgh Proceedings, v. 56". In.

Bagnardi, Marco, Falk Amelung, and Michael P Poland (2013). "A new model for the growth of basaltic shields based on deformation of Fernandina volcano, Galápagos Islands". In: *Earth and Planetary Science Letters* 377, pp. 358–366.

Borgia, Andrea and Benjamin van Wyk de Vries (2003). "The volcano-tectonic evolution of Concepción, Nicaragua". In: *Bulletin of Volcanology* 65, pp. 248–266.

British Geological Survey, website (2023). *Types of volcanoes*. URL: https://www.bgs.ac.uk/discovering-geology/earth-hazards/volcanoes/how-volcanoes-form/.

Chadwick Jr, WW and JH Dieterich (1995). "Mechanical modeling of circumferential and radial dike intrusion on Galapagos volcanoes". In: *Journal of Volcanology and Geothermal Research* 66(1-4), pp. 37–52.

Chestler, Shelley R and Eric B Grosfils (2013). "Using numerical modeling to explore the origin of intrusion patterns on Fernandina volcano, Galapagos Islands, Ecuador". In: *Geophysical research letters* 40(17), pp. 4565–4569.

Corbi, Fabio et al. (2015). "How caldera collapse shapes the shallow emplacement and transfer of magma in active volcanoes". In: *Earth and Planetary Science Letters* 431, pp. 287–293.

Crouch, S.L. and A. M. Starfield (1983). *Boundary Element Methods in Solid Mechanics: With Applications in Rock Mechanics and Geological Engineering*. Allen & Unwin. ISBN: 9780046200107. URL: https://books.google.it/books?id=l-6uQgAACAAJ.

D. F. Mc Tigue, C. C. Mei (1987). "Gravity-induced stresses near axisymmetric topography of small slope". In: *International journal for numerical and analytical methods in geomechanics* 11, pp. 257–268. ISSN: 0363-9061.

Dahm, Torsten (2000). "Numerical simulations of the propagation path and the arrest of fluid-filled fractures in the Earth". In: *Geophysical Journal International* 141(3), pp. 623–638.

Davis, Timothy (2017). *A new open code boundary element code and its application to geological deformation [electronic resource] : exploring stress concentrations around voids and the effects of corrugation orientation on fault slip in 3D.* URL: https://github.com/Timmmdavis/CutAndDisplace.

Davis, Timothy (2021). "An analytical and numerical analysis of fluid-filled crack propagation in three dimensions". PhD thesis. University of Potsdam.

Davis, Timothy, Marco Bagnardi, et al. (2021). "Extreme curvature of shallow magma pathways controlled by competing stresses: insights from the 2018 Sierra Negra eruption". In: *Geophysical Research Letters* 48(13), e2021GL093038.

Davis, Timothy, Eleonora Rivalta, and Torsten Dahm (2020). "Critical fluid injection volumes for uncontrolled fracture ascent". In: *Geophysical Research Letters* 47(14), e2020GL087774.

Dieterich, James H (1988). "Growth and persistence of Hawaiian volcanic rift zones". In: *Journal of Geophysical Research: Solid Earth* 93(B5), pp. 4258–4270.

Dumont, Quentin et al. (2022). "22 years of satellite imagery reveal a major destabilization structure at Piton de la Fournaise". In: *Nature Communications* 13(1), p. 2649.

Farr, T. G. and M. Kobrick (2000). *Shuttle Radar Topography Mission, 1 Arc-Second Global*.

Gonnermann, Helge and Benoit Taisne (2015). "Chapter 10 - Magma Transport in Dikes". In: *The Encyclopedia of Volcanoes (Second Edition)*. Ed. by Haraldur Sigurdsson. Second Edition. Academic Press: Amsterdam, pp. 215–224. ISBN: 978-0-12-385938-9.

Griffith, Alan Arnold (1921). "VI. The phenomena of rupture and flow in solids". In: *Philosophical transactions of the royal society of london. Series A, containing papers of a mathematical or physical character* 221(582-593), pp. 163–198.

Grosse, Pablo and Matthieu Kervyn (2018). "Morphometry of terrestrial shield volcanoes". In: *Geomorphology* 304, pp. 1–14.

Jaeger, J.C., N.G.W. Cook, and R. Zimmerman (2007). *Fundamentals of Rock Mechanics*. Wiley. ISBN: 9780632057597. URL: https://books.google.it/books?id=FqADDkunVNAC.

Kervyn, M et al. (2009). "Volcano load control on dyke propagation and vent distribution: Insights from analogue modeling". In: *Journal of Geophysical Research: Solid Earth* 114(B3).

Komorowski, JC et al. (2002). "The January 2002 eruption-The January 2002 flank eruption of Nyiragongo Volcano (Democratic Republic of Congo): chronology, evidence for a tectonic rift trigger, and impact of lava flows on the city of Goma". In: *The January 2002 eruption-The January 2002 flank eruption of Nyiragongo Volcano (Democratic Republic of Congo): chronology, evidence for a tectonic rift trigger, and impact of lava flows on the city of Goma*, pp. 1000–1035.

Maccaferri, Francesco, Maurizio Bonafede, and Eleonora Rivalta (2010). "A numerical model of dyke propagation in layered elastic media". In: *Geophysical Journal International* 180(3), pp. 1107–1123.

Maccaferri, Francesco, Maurizio Bonafede, and Eleonora Rivalta (2011). "A quantitative study of the mechanisms governing dike propagation, dike arrest and sill formation". In: *Journal of Volcanology and Geothermal Research* 208(1-2), pp. 39–50.

Maccaferri, Francesco, Nicole Richter, and Thomas R Walter (2017). "The effect of giant lateral collapses on magma pathways and the location of volcanism". In: *Nature communications* 8(1), p. 1097.

Maccaferri, Francesco, Eleonora Rivalta, Derek Keir, et al. (2014). "Off-rift volcanism in rift zones determined by crustal unloading". In: *Nature Geoscience* 7(4), pp. 297–300.

Maccaferri, Francesco, Eleonora Rivalta, Luigi Passarelli, et al. (2016). "On the mechanisms governing dike arrest: Insight from the 2000 Miyakejima dike injection". In: *Earth and Planetary Science Letters* 434, pp. 64–74.

Mantiloni, Lorenzo, Eleonora Rivalta, and Timothy Davis (2023). "Mechanical modeling of pre-eruptive magma propagation scenarios at calderas". In: *Journal of Geophysical Research: Solid Earth* 128(3), e2022JB025956.

Martel, Stephen and J. Muller (Aug. 2000). "A Two-dimensional Boundary Element Method for Calculating Elastic Gravitational Stresses in Slopes". In: *Pure and Applied Geophysics* 157, pp. 989–1007. DOI: 10.1007/s000240050014.

McCarthy, Paul and Eugene Rankey (2020). "Oxford Dictionary of Earth Sciences , edited by Michael". In.

Muller, Jordan R, Garrett Ito, and Stephen J Martel (2001). "Effects of volcano loading on dike propagation in an elastic half-space". In: *Journal of Geophysical Research: Solid Earth* 106(B6), pp. 11101–11113.

National Park Service, website (2023). *Monogenetic Volcanic Fields*. URL: https://www.nps.gov/subjects/volcanoes/types-of-volcanoes.htm.

Nikkhoo, Mehdi and Thomas R Walter (2015). "Triangular dislocation: an analytical, artefact-free solution". In: *Geophysical Journal International* 201(2), pp. 1119–1141.

Odé, Helmer (1957). "Mechanical analysis of the dike pattern of the Spanish Peaks area, Colorado". In: *Geological Society of America Bulletin* 68(5), pp. 567–576.

Persson, Per-Olof (2005). "Mesh generation for implicit geometries". PhD thesis. Massachusetts Institute of Technology.

Pollard, David D and Otto H Muller (1976). "The effect of gradients in regional stress and magma pressure on the form of sheet intrusions in cross section". In: *Journal of Geophysical Research* 81(5), pp. 975–984.

Rivalta, E et al. (2015). "A review of mechanical models of dike propagation: Schools of thought, results and future directions". In: *Tectonophysics* 638, pp. 1–42.

Rivalta, E. et al. (2019). "Stress inversions to forecast magma pathways and eruptive vent location". In: *Science advances* 5(7), eaau9784.

Roman, Alberto and Claude Jaupart (2014). "The impact of a volcanic edifice on intrusive and eruptive activity". In: *Earth and Planetary Science Letters* 408, pp. 1–8.

Ryan, et al. (2009). *GeomapApp*. DOI: 10.1029/2008GC002332. URL: https://www.geomapapp.org/.

Savage, WZ, HS Swolfs, and PS Powers (1985). "Gravitational stresses in long symmetric ridges and valleys". In: 22(5), pp. 291–302.

Smittarello, D et al. (2022). "Precursor-free eruption triggered by edifice rupture at Nyiragongo volcano". In: *Nature* 609(7925), pp. 83–88.

Smittarello, Delphine et al. (2019). "Combining InSAR and GNSS to track magma transport at basaltic volcanoes". In: *Remote Sensing* 11(19), p. 2236.

Vries, Benjamin van Wyk de and Ray Matela (1998). "Styles of volcano-induced deformation: numerical models of substratum flexure, spreading and extrusion". In: *Journal of Volcanology and Geothermal Research* 81(1-2), pp. 1–18.

Weertman, John (1971). "Theory of water-filled crevasses in glaciers applied to vertical magma transport beneath oceanic ridges". In: *Journal of Geophysical Research* 76(5), pp. 1171–1183.

Wyk, de Vries B van (1995). "Tectonics and magma evolution of Nicaraguan volcanic systems." In.

Xiao, HT and ZQ Yue (2011). "A three-dimensional displacement discontinuity method for crack problems in layered rocks". In: *International Journal of Rock Mechanics and Mining Sciences* 48(3), pp. 412–420.

Zhan, Yan et al. (2022). "Earthquakes Indicated Stress Field Change During the 2006 Unrest of Augustine Volcano, Alaska". In: *Geophysical Research Letters* 49(10), e2022GL097958.

List of Figures

List of Tables